Novel considerations in computed tomography for feline lung and hepatic imaging and cholangiography

Joanna Louise Pilton BE(hons) BVSc(hons) PGCVetClinStud MANZCVS (SA med, SA imaging) DipECVDI

Sydney School of Veterinary Science

Faculty of Science

University of Sydney

A thesis submitted in fulfilment of the requirements for the degree of 'Masters of Veterinary Clinical Studies'

December, 2024

Table of Contents:

Statement of Originality:

This is to certify that to the best of my knowledge, the content of this thesis is my own work. This thesis has not been submitted for any degree or other purposes.

I certify that the intellectual content of this thesis is the product of my own work and that all the assistance received in preparing this thesis and sources have been acknowledged.

Signature: Joanna Pilton

Date: 27.12.2024

Author Attribution Statement:

The contents of Section 4 of this thesis are published in:

Publication 1

Authors: Pilton JL, Chau J, Foo TS, Hall EJ, Martinez-Taboada F, Podadera JM, Makara MA.

Title: Hepatic computed tomography and cholangiography by use of gadoxetic acid in healthy cats. Am J Vet Res.

Year of Publication: 2019

Journal: American Journal of Veterinary Research Apr;80(4):385-395.

I co-designed the study, performed the experimental work described in chapter 4 including submitting ethics approval, obtaining a bequest for funding, meeting with the research facility and selecting the cats, assessing the cats with a health screen including obtaining blood samples and assessing health screen results, and co-designing the methodology. I performed the CT scans, positioned patients in the CT scanner, recovered patients and performed husbandry and monitoring of the cats after the study and at the research facility. I performed the objective analysis and MM, JMP and TF performed the visual analysis, I assessed and compiled all the analyses with EH performing statistical analysis, I wrote the manuscript and incorporated feedback by the contributing authors and reviewers of the publication.

Publication 2

Authors: Foo TS, Pilton JL, Hall EJ, Martinez-Taboada F, Makara M.

Title: Effect of body position and time on quantitative computed tomographic measurements of lung volume and attenuation in healthy anesthetized cats.

Year of Publication: 2018

Journal: American Journal of Veterinary Research Aug;79(8):874-883.

I provided input into the study design such as assessing and examining the research cats prior to, including blood sampling and vital parameters, during and after the study. I participated in the experimental work, positioning of the cats described in chapter 4 and assisted in CT scanning. I also assisted in the initial draft and editing the manuscript.

Signature: Joanna Pilton Date: 27.12.2024

As a supervisor for the candidature upon which this thesis is based, to my knowledge, I can confirm that the authorship attribution statements above are correct.

Signature:

Supervisor Name: Marianne D Keller

Date: 27.12.2024

I understand that, if my candidature is successful, my thesis will be lodged with the University Librarian and made available for immediate use.

Signature: Joanna Pilton

Date: 27.12.2024

In my opinion, this thesis: (a) is sufficiently well presented to be examined; and (b) does not exceed the prescribed word limit

Name: Marianne Keller

Date: 27.12.2024

The research reported in this thesis was supported by the award of a Research Training Program Scholarship to the Master's Candidate.

Acknowledgements:

I would like to sincerely thank my supervisor Dr Mariano Makara, and my colleagues Drs Jennifer Chau, Juan Podadera, Fernando Martinez-Taboada, Timothy Foo and Evelyn Hall that assisted me in this research. I would also like to sincerely thank Dr Marianne Keller who guided and supported me in the preparation of this thesis.

I would also like to thank the Faculty of Veterinary Science Bequests 2016 for Canine and Feline Research for $3000 that was received to assist with the CT cholangiography portion of the project.

Abstract:

Cats with respiratory and hepatobiliary disease commonly present to veterinary hospitals with non-specific clinical signs, making a timely diagnosis difficult. Imaging plays an important role in the diagnosis of these diseases to accurately prognosticate and guide therapeutic options to improve the patient's outcome. Computed tomography (CT) is increasingly utilised in veterinary medicine to image the feline thorax and abdomen due to advantages such as having rapid repeatable acquisition, good sensitivity with visualisation of cross-sectional anatomy, good soft tissue contrast and increasing availability. Cats often require anaesthesia for CT imaging of the thorax and abdomen to reduce motion artefact that can interfere with the diagnosis. There is currently no gold standard imaging technique to investigate hepatobiliary disease in cats, and previously reported hepatobiliary contrast media have reported various adverse effects. The use of gadoxetic acid (Gd-EOB-DPTA), a newer hepatobiliary contrast medium has not been reported in cats, although it has the potential to provide both morphologic and functional information of the hepatobiliary tract. Despite CT being the gold standard for thoracic imaging, there is limited information on the effect of different body positions on the quantification of lung volume and attenuation changes over time in cats, as well as the quantification of atelectasis under anaesthesia in healthy cats in different body positions.

The aim of this thesis is to improve feline health and welfare by investigating some novel applications for CT using Gd-EOB-DTPA in hepatic imaging and cholangiography and body position in lung imaging. To evaluate contrast hepatobiliary imaging, three doses of Gd-EOB-DTPA were used for hepatic CT and cholangiography in healthy cats to determine the optimal timing for hepatobiliary image acquisition and to evaluate the contrast-enhanced hepatobiliary anatomy. CT cholangiography and hepatic imaging was performed experimentally in five healthy research cats 0, 5, 25, 45, 65, and 85 minutes (mins) after intravenous (IV) administration of a functional and morphologic contrast medium, Gd-EOB-DTPA at low (0.0125 mmol/kg), medium (0.1 mmol/kg), and high (0.3 mmol/kg) doses. Hepatobiliary enhancement for each dose was objectively assessed over time by measuring the attenuation of the hepatobiliary system in Hounsfield units (HU) and by use of a subjective semiquantitative visual assessment score.

It was proven that Gd-EOB-DTPA was safe to use in healthy cats at a dose of up to 0.3 mmol/kg with no adverse clinical signs, by normal physical examination, complete blood count, serum biochemistry and urinalysis. No contrast related adverse side effects were documented at 0.0125 mmol/kg, 0.1 mmol/kg and 0.3 mmol/kg doses. Using CT, each increase in dose of contrast medium resulted in a significant increase in attenuation measured by HU across the hepatobiliary system including the liver, gall bladder, cystic duct and common bile duct. The liver had a significantly higher attenuation at 45 minutes, with homogenous enhancement at all doses of contrast medium. Contrast-enhanced cystic and bile duct HUs were significantly higher and maximal at 65 mins. Contrast-enhanced gallbladder attenuation did not plateau by 85 mins. Using subjective visualisation scores at a high dose of contrast medium, 12 of 60 (20%) biliary tract scores indicated no enhancement of the gallbladder, cystic duct, bile duct and hepatic ducts (where they were

visible from the porta hepatis to the insertion onto the bile duct), 34 (57%) indicated poor enhancement with ill defined borders, and 14 (23%) indicated moderate enhancement with incomplete delineation of borders. No cat had excellent enhancement of the biliary tract with well defined borders throughout the entire length of the biliary anatomy at any dose of Gd-EOB-DTPA. The optimal time for imaging of the liver parenchyma was 45 mins, whereas the optimal time for imaging of the biliary tract was 65 mins after injection of contrast medium. There was a positive relationship in contrast enhancement with increasing dose of contrast medium. Further research into cats with functional hepatobiliary abnormalities, particularly involving the liver could be considered using Gd-EOB-DTPA.

In a separate study, thoracic CT was used to evaluate and quantify the effect of time and recumbency on CT measurements of lung volume and attenuation in healthy cats under general anaesthesia. A separate group of eight healthy research cats was anaesthetized and positioned in sternal recumbency for 20 mins and then in left, right and left lateral recumbency (40 mins / position). Expiratory helical CT scans of the thorax were performed over set time points in each recumbency. CT measurements of lung volume and attenuation were determined and the extent of lung areas that were hyperaerated (- 1000 to - 901 HU), normoaerated (- 900 to - 501 HU), poorly aerated (- 500 to - 101 HU) or non-aerated (- 100 to + 100 HU) [indicative of atelectasis] was determined.

It was determined that cats in lateral recumbency, have a significantly greater lung attenuation (HU) and lower volume on CT in the dependent lung than the non-dependent lung. Within the dependent lung, there was a significantly higher percentage of poorly aerated lung tissue (- 500 to -101 HU) compared to the non-dependent lung. These changes occurred immediately after positioning in lateral recumbency and remained static with no further significant time related change. The percentage of non-aerated lung (-100 to +100 HU) [true atelectasis] in the healthy cats in the present study was minimal. It was also documented that healthy cats had less poorly aerated lung in sternal recumbency compared to the dependent lung in lateral recumbency. Results of this study may provide a starting point for investigations into the value of quantitative thoracic CT scans obtained from patients in lateral recumbency as a functional tool in cases of feline asthma and air trapping, chronic obstructive pulmonary disease (COPD) and emphysema. Such functional information may prove useful for the diagnosis, prognosis, and treatment monitoring of feline lung diseases.

From this research, we can utilise the effect of body position on healthy anaesthetised cats in lung imaging to prioritise the positioning of cats in sternal recumbency for hepatobiliary imaging and for standard morphologic assessment of lung imaging to reduce the occurrence of true atelectasis or poorly aerated lung tissue potentially masking or mimicking lung pathology. Lateral recumbency may be useful for functional lung imaging to assess the lack of atelectasis that is expected in functional feline lung diseases such as feline asthma. Since the lung changes in the dependent lung occur immediately during anaesthesia and are static, the importance of expedient thoracic scanning is reduced. This is particularly useful since if required, concurrent thoracic imaging cannot typically be

performed immediately during hepatic CT and cholangiography, as an early dynamic phase and a delayed hepatobiliary phase are prioritised. Clinical investigations in feline patients commonly include both thoracic and abdominal CT to evaluate for potential diffuse disease because of their non-specific signs, as well as effectively utilising the time, increased risk and expense of anaesthesia to evaluate both body cavities simultaneously.

Both studies also demonstrated that optimal image quality was obtained without motion artefact, and cross-sectional anatomic morphology was clearly visualised using anaesthesia.

Finally, each of the studies utilised contrast in CT to better evaluate the morphology of the anatomy of the lung (negative contrast - inherent gas) and hepatobiliary tract (positive contrast - Gd-EOB-DTPA). Future research into functional hepatobiliary imaging in cats can be considered using Gd-EOB-DTPA in sternal recumbency, and using lateral recumbency for functional lung imaging.

Section 1 - List of Publications:

Publication 1 and 2 will be found in section 4.

Publication 1

Authors: Pilton, J. L., Chau, J., Foo, T. S., Hall, E. J., Martinez-Taboada, F., Podadera, J. M., & Makara, M. A.

Title: Hepatic computed tomography and cholangiography by use of gadoxetic acid in healthy cats.

Year or Publication: 2019

Journal: American journal of veterinary research 80(4), 385–395.

Publication 2

Authors: Foo, T.S., Pilton, J.L., Hall, E.J., Martinez-Taboada, F., Makara, M.

Title: Effect of body position and time on quantitative computed tomographic measurements of lung volume and attenuation in healthy anesthetized cats.

Year of Publication: 2018

Journal: American journal of veterinary research 79(8), 874-883.

Section 2 - Introduction:

Cats are reported to be the most popular pet in Northern Europe, Canada and the United States of America (USA) (Rodan and Sparkes, 2011). Despite being popular companion animals and living in close association with humans, cats often hide signs of illness (Day, 2016; Rodan and Sparkes, 2011). Since cats often show non-specific clinical signs, they present a diagnostic challenge, and a number of diagnostic tests are often required to determine the aetiology of the illness. This occurs in cats with hepatobiliary disease, that commonly present with non-specific clinical signs referable to the abdomen, a varying clinical time course and non-specific physical examination and biochemical findings. Equally, when cats have respiratory disease, they may only present with malaise noted by their owners and respiratory tract signs may only be noticed by the clinician (Baralf, 2011).

As cats are increasingly important members of the family, particularly indoor cats, and as pet insurance use grows, owners are increasingly willing to spend money on the health of their cats. Despite this, there is reduced literature surrounding feline medicine, including abdominal studies and it is unknown whether this is due to less funding or the lack of association with feline and human diseases (Day, 2016; Rojo Rios et al., 2023).

The purpose of this thesis is to improve feline health and welfare by investigating two novel applications for CT in healthy cats, using Gd-EOB-DTPA in hepatic imaging and cholangiography and body position in lung imaging. In doing so, this thesis will discuss an overview of imaging in feline medicine, feline hepatobiliary and lung imaging, contrast media, hepatobiliary anatomy and diseases and lung anatomy. Specifically, this thesis firstly aims to evaluate hepatobiliary imaging using three doses of Gd-EOB-DPTA for hepatic CT and cholangiography in healthy cats and to determine the optimal timing for hepatobiliary image acquisition and evaluation of the contrast-enhanced hepatobiliary anatomy. We hypothesised that Gd-EOB-DTPA would be safely tolerated in cats at these doses and would provide good hepatobiliary contrast in cats, as in humans and dogs. Secondly, this thesis aims to investigate a novel finding of thoracic CT, by evaluating and quantifying the effect of time and recumbency on CT measurements of lung volume and attenuation in healthy cats under general anaesthesia. We hypothesised that the feline lung would become more atelectatic over time.

2.1 Overview of imaging modalities in feline medicine

2.1.1 Radiography:

In veterinary medicine, radiography has been utilised since the 1920s (Meomartino et al., 2021). Traditionally, with ultrasonography, they are the most commonly utilised diagnostic imaging modalities due to low cost and ready availability (O'brien, 2016; Meomartino et al., 2021).

Thoracic radiography allows good assessment of the intra-thoracic structures due to the contrast provided by air in the lungs (Meomartino et al., 2021). Radiography can be stressful for patients with respiratory tract disease (O'brien, 2016). Veterinary patients also normally require chemical or manual restraint for imaging procedures, and the need for

anaesthesia or deep sedation in critical patients can be a negative factor associated with these modalities (Meomartino et al., 2021; O'brien, 2016). Radiographic interpretation can remain challenging due to the visibility of structures varying with animal size, age and breed and there is an overlap in the appearance of different disease processes (Arruda Bergamaschi et al., 2023). Incorrectly positioned patients and poor exposure protocols can also result in repeat studies and undue radiation exposure (Meomartino et al., 2021). Despite this, radiography remains prevalent in practice due to the availability, rapid execution, relatively low cost, ability for fast interpretation, particularly with the increased availability of specialist interpretation through remote teleradiology services (Meomartino et al., 2021; Rudorf et al., 2008).

2.1.2 Fluoroscopy:

Fluoroscopy uses real time continuous x-ray production (Rudorf et al., 2008). The x-rays leaving the patient are received by an image intensifier and the final output is transmitted to a television screen (Rudorf et al., 2008). The benefits of fluoroscopy are immediate viewing of images and real time investigation of movement for assessment of functional abnormalities so that invasive procedures can be performed quickly under guidance (Rudorf et al., 2008).

2.1.3 Nuclear Medicine:

Nuclear medicine (NM) or scintigraphy, creates images using a radiation detector (gamma camera) after the application of a radiopharmaceutical (Morandi, 2008) and is rarely used in small animal veterinary medicine as it requires careful handling and radiation safety of the radioisotopes and patient waste products as well as having a high cost, heavy regulations and a lack of availability (Greco et al., 2018).

2.1.4 Ultrasonography:

Ultrasonography has also been commonly utilised in veterinary medicine since the 1960s (Meomartino et al., 2021). Thoracic ultrasonography can also complement the radiographic interpretation by allowing concurrent assessment of the heart, pleural space as well as surface lung pathology (O'brien, 2016). The abdomen is typically better assessed using ultrasonography or advanced tomographic techniques due to better contrast resolution of the soft tissues compared to radiography (Meomartino et al., 2021). Despite ultrasonography being common in clinical practice and its ability to provide fast results, the diagnostic utility of ultrasonography results relies heavily on the knowledge of anatomy and pathophysiology of the operator, in order to determine good diagnostic information (Meomartino et al., 2021).

2.1.5 Magnetic Resonance Imaging (MRI):

MRI has been utilised in veterinary medicine since the 1990s. Scanners vary in strength from low field (0.2 - 0.4 Telsa (T)), medium field (0.5 - 1.0 T) and high field (> 1 T) (Greco et al., 2023). Low field scanners are more common in veterinary practice due to their low cost, ease of installation and maintenance, with veterinary-specific software and coils. Low

field MRI has a lower signal to noise ratio resulting in lower spatial and temporal resolution with longer acquisition times (Greco et al., 2023). High field MRI, provides improved image quality and is becoming more common in veterinary practice (Greco et al., 2023). There are limited reports in the literature using MRI in feline thoracic and abdominal imaging, in particular with respect to lung and hepatobiliary imaging (Rivero et al., 2005; Briola C., 2022; Ibrahim et al., 2023; Marolf et al., 2011; Marolf et al., 2013; Newell et al., 2000; Rahmani et al., 2023a; Rahmani et al., 2024). Advantages of MRI include the lack of ionising radiation, highly sensitive and non-invasive techniques that provide accurate and detailed anatomical images with good contrast and spatial resolution and the ability to investigate anatomical and physiological function of body tissues (Assefa, 2018). Compared to CT and radiography, the disadvantages of MRI include the increased time and cost of image acquisition, including the length of anaesthesia, and the presence of artefacts such as susceptibility artefact from metal implants or identification microchips which are common in veterinary medicine (Greco et al., 2018).

2.1.6 Computed Tomography (CT):

CT has only been available in veterinary medicine more recently, with clinical use starting in the 1980s (Greco et al., 2023) and has been reported for use in canine, equine, cattle, goat, sheep, swine, avian and chelonian, other reptiles, rabbit and rodent medicine on various anatomical regions (Greco et al., 2023). Whole body CTs are also commonly performed in oncologic patients (Greco et al., 2023).

CT scanners utilise a narrow beam of x-rays positioned opposite a row of detectors which are assembled in a circular arrangement that rotates around the axis of the patient to produce a transverse planar image (Campos and Diaz, 2018). The attenuation of the X-ray beam is measured by comparing the intensity of the detected x-ray photons compared to the emitted X-ray photons, as they pass through tissues of various densities, allowing the construction of a two-dimensional axial image (Campos and Diaz, 2018; Masseau and Reiner, 2019). The axial images are composed of pixels (‘picture elements’) which represent the tissue density of the region scanned and are the smallest square unit of a digital image, normally arranged in a two-dimensional (2D) grid. The resolution of an image depends on the number of pixels. The slice width of the CT scan enables a 3D image to be formed with voxels (‘volume elements’). Computer software stacks the data into a 3D picture that is composed of voxels. The voxel represents the X-ray attenuation of the tissue in HU and indicates the density of the scanned tissue which is based on an arbitrary scale from - 1000 HU (Air) to + 1000 HU (bone), with water being 0 HU (Campos and Diaz, 2018). The ability to measure the attenuation of different structures within the patient is important, particularly in thoracic and abdominal imaging.

More recent scanners use helical scanning, where the scanner rotates continuously in one direction with the patient moving continuously through the scanner during the tube rotation (Campos and Diaz, 2018). This reduces the scan time, allowing a volume of tissue to be scanned rather than a single discrete slice as in older axial scanners. Multidetector computed tomography (MDCT) scanners have advanced CT acquisition, with up to 640

rows of detectors and have faster tube rotation times allowing for faster coverage of a given volume of tissue with thinner slices (Masseau and Reiner, 2019; Campos and Diaz, 2018; Bertolini and Prokop, 2010). The advantage of these scanners is that large anatomic volumes such as the thorax or abdomen can be imaged during a single breath hold reducing motion artefact and potentially the need for anaesthesia (Campos and Diaz, 2018).

Currently, CT is increasingly available in both specialist and general veterinary practice. CT is a popular imaging modality as it allows more precise characterisation and localisation of lesions (Johnson and Wisner, 2007) due to the advancements in MDCT scanners that allow sub-millimetre collimation and fast scanning speeds (Horton et al., 2009). With excellent multi-planar capabilities and post processing tools including three-dimensional (3D) rendering techniques, there is greatly improved temporal, contrast and spatial resolution with CT, improving the ability to image the body and reducing the need for repeat studies due to poor positioning or exposure factors (Horton et al., 2009; Anderson et al., 2008; Greco et al., 2023; Johnson and Wisner, 2007; O'brien, 2016). CT allows for more precise characterisation and localisation of lesions and is invaluable for guiding interventional diagnostic procedures and sampling, and for surgical planning and procedures (Johnson and Wisner, 2007).

CT also allows real time angiography and is able to provide better evaluation of anatomy compared to radiography, ultrasonography and fluoroscopic imaging techniques (Greco et al., 2023). CT is cheaper and generally more available compared to magnetic resonance imaging (MRI), which continues to be limited by its availability and higher cost (Lusic and Grinstaff, 2012). Some patients may be unable to have an MRI due to implants or microchips in or near the field of view. CT also minimises the risk of personnel radiation, due to the requirement for a patient to be anaesthetised, heavily sedated, or placed within a plexiglass box (“VetMouseTrap(TM)”) (Oliver, 2011).

Despite these rapid advances in CT technology, patient movement remains a clinical concern in veterinary medicine as it can cause streak artefact, motion blurring and reduced image quality, particularly for thoracic scans (Greco et al., 2023; Rudorf, 2008). Therefore, most CT scans rely on pharmacological restraint either through anaesthesia or deep sedation (Greco et al., 2023). Control of mechanical ventilation with general anaesthesia can also improve image quality, particularly of the lungs (Greco et al., 2023; Rudorf, 2008). Studies have also shown that CT has the advantage that it can be performed in sedated animals and therefore does not have the increased risks of general anaesthesia in debilitated animals with minimal to moderate reduction in motion artefact affecting image quality (Shanaman et al., 2012; Oliveira et al., 2011a; Reimegard et al., 2022; Klaengkaew et al., 2021; Hunt and Wallack, 2021). Compared to normal cats, most cats in respiratory distress are more tolerant of being in a perspex device that limits movement and that provides oxygen and visualisation of the patient (O'brien, 2016; Oliveira et al., 2011b). There are mixed reviews in the literature regarding the use of the “VetMouse Trap (TM)” which is designed as an alternative to anaesthesia for cats and other small animals (Greco et al., 2023; Oliveira et al., 2011b; Lin and Lo, 2018). Nevertheless, despite studies

demonstrating the possibility of hepatobiliary imaging under sedation, increased accuracy generally occurs with the utilisation of anaesthesia, in particular, to reduce motion artefact and increase visualisation of small structures and in thoracic CT, anaesthetised patients can utilise inspiratory and expiratory CT scans to assess for dynamic disease (Masseau and Reinero, 2019; Greco et al., 2023).

Although scan times are fast, the procedure of a CT scan can be time consuming and ideally requires technicians, anaesthetists and radiologists and obtaining good quality images is not always easy (Greco et al., 2023). Continued research into CT acquisition and image interpretation, particularly in feline medicine, is required to standardise protocols and to improve the diagnostic utility of CT scans in veterinary medicine.

2.2 Hepatobiliary imaging

It is important to diagnose hepatobiliary disease in a timely manner to prognosticate and accurately guide therapeutic options to improve the patient's outcome. However, the aetiology of hepatobiliary disease can be difficult to definitively diagnose.

Nevertheless, diagnostic imaging is essential to differentiate between medical or surgical hepatobiliary disorders, for pre-surgical evaluation of biliary anatomy (particularly due to the high mortality associated with biliary surgical intervention), investigating the integrity of the biliary tract after trauma, obstructions or abdominal surgery (e.g. tears or strictures), as well as enabling interventional procedures such as sampling including fine needle aspiration (FNA) or tru-cut biopsies (Low and Williams, 2023).

Diagnostic imaging of the feline biliary tract and pancreas is challenging, and there have been many attempts to improve the visualisation of the normal and abnormal anatomy with varying success (Spillmann et al., 2014). Hepatic parenchymal and neoplastic diseases are usually diagnosed by histopathology and many of the biliary disorders require a combination of imaging methods with image guided sampling such as biopsy and cholecystocentesis required to elucidate a diagnosis (Van den Ingh et al., 2006).

Described techniques to image the hepatobiliary system in humans, canines and felines have included radiography, percutaneous transhepatic cholangiocystography, cholangiocystography using oral and IV contrast media, transabdominal ultrasonography, contrast enhanced ultrasonography, hepatobiliary scintigraphy, ERCP, MRI, magnetic resonance cholangiography/cholangiopancreatography (MRC/MRCP), CT cholangiography and drip infusion cholangiography (DIC-CT) (Anderson et al., 2008; Banzato et al., 2020; Bargellini et al., 2018; Bentley et al., 2024; Berent et al., 2015; Berk et al., 1981; Carlisle, 1977; Chau et al., 2017; Constant et al., 2016; Fujita et al., 2023; Gaillot et al., 2007; Gold et al., 1979; Hashimoto et al., 2008; Hayakawa et al., 2018; Hittmair et al., 2001; Hoeffel et al., 2006; Horton et al., 2009; Ji et al., 2015; Kim et al., 2019; Leveille et al., 1996; Maiti et al., 2011; Marks et al., 2013; Marolf et al., 2012; Marolf et al., 2013; Marolf, 2017; Miller, 2014; Newell, 1996; Noguchi et al., 2023; Pasanen et al., 1992; Persson et al., 2006; Rahmani et al., 2023a; Rahmani et al., 2023b; Rahmani et al., 2024; Rishniw et al., 2018; Schmitz et al., 1997a; Schmitz et al., 1997b; Soto et al., 2000;

Spain et al., 2017; Spillman et al., 2005; Spillman et al., 2014; Tanaka et al., 2018; Toft et al., 1997; Uno et al., 2009; Yonetomi et al., 2012).

It is important to understand the benefits and limitations of the different modalities in hepatobiliary imaging to ensure that the optimal information is gained from each test, thereby reducing client expense and the potential mortality and morbidity of the patient.

2.2.1 Radiography:

Abdominal radiography is insensitive and also of limited diagnostic value in the diagnosis of hepatobiliary disease, although if choleliths contain enough calcium bilirubinate or calcium carbonate to be of mineral radio-opacity, they appear as single or multiple radiopaque structures in the cranioventral abdomen on lateral radiographs and in the right cranial abdomen on the ventrodorsal projection (Center, 2009; Neer, 1992; Gaschen, 2009; Ettinger and Feldman, 2010). They can also be present in asymptomatic unobstructed cats (Mayhew, 2002). Abdominal radiographs may show decreased serosal detail consistent with an abdominal effusion, or emphysema of the gallbladder (Ettinger and Feldman, 2010). Thoracic radiographs can commonly show a sternal lymphadenopathy in cases of cholangiohepatitis (Center, 2009). Cholangiography performed in normal cats using IV meglumine iotroxate was investigated by Fujita and Orima (1994) and showed that gallbladder and bile duct visualisation occurred 20 mins after contrast media administration.

2.2.2 Percutaneous cholecystography (PC):

Percutaneous cholecystography using positive contrast and radiographs is now an infrequently used imaging modality due to its invasiveness, with risk of bile peritonitis, gallbladder rupture and hepatic haemorrhage (Kim et al., 2019) and requirement of personal radiation exposure in human imaging, as well as the lack of 3D anatomic assessment. Ultrasonographic contrast media (consisting of microbubbles that contain gas and are stabilised by a shell) has demonstrated the feasibility of percutaneous contrast-enhanced ultrasonographic (CEUS) guided cholecystography which has also been described in dogs to evaluate the patency of the biliary tract (Ji et al., 2015). An important limitation of CEUS is the necessity for specialised contrast-specific ultrasonographic techniques (Ji et al., 2015). Laparoscopic-assisted cholecystocentesis and cholecystocholangiography have also been reported in canines (Maiti et al., 2011) and in each of these procedures there is the disadvantage of not being able to visualise structures distal to the obstruction (Heoffel et al., 2006). Kim et al. (2019) demonstrated ultrasonographic guided percutaneous cholecystography in beagle dogs and CT using iohexol, which opacified the gallbladder, intra and extra hepatic bile ducts. Minor leakage of contrast media was observed temporarily post injection in 30% of dogs without associated clinical signs (Kim et al., 2019).

2.2.3 Hepatobiliary scintigraphy:

Hepatobiliary scintigraphy is the traditional means of evaluating the physiologic function of the gallbladder and is useful in diagnosing intra hepatic cholestasis, and extra hepatic bile

duct obstruction (EHBO) in cats, to assess hepatobiliary function, hepatic morphology, and biliary tract patency and cholecystitis, although it does not give anatomic localisation or information other than that of the biliary tract (Newell et al., 1996; Gaschen, 2009; Heller and Lee, 2005). If the radionucleotide doesn't fill the gallbladder or is delayed in entering the small intestine, a diagnosis of partial or complete obstruction of the extra hepatic biliary system can be confirmed (Ettinger and Feldman, 2010).

2.2.4 Ultrasonography:

Despite advancements in the diagnosis of biliary disease, in practice, ultrasonography continues to be frequently used as the initial diagnostic tool, including in people, because the ultrasonographic features of the normal biliary tract and obstructed biliary tract are well established (Gaillot et al., 2007; Gaschen, 2009; Marolf et al., 2013; Ettinger and Feldman, 2010).

Ultrasound offers rapid assessment of clinical symptoms and can show suspended sediment, choleliths, thickened gallbladder wall, EHBO and emphysema, as well as pericholecystic fluid and adhesions or abdominal effusions (Ettinger and Feldman, 2010).

Similarly, in human patients, ultrasonography is often the primary modality for biliary imaging because it has high sensitivity for the presence of gall stones and enables accurate evaluation of the status of intra and extra hepatic bile ducts and examination can be performed relatively rapidly and at low cost (Leveille et al., 1996). Ultrasonography has been reported to determine a specific level of obstruction in approximately 60% of human patients and the actual cause of obstruction determined in approximately 40% of patients (Leveille et al., 1996). Other studies have reported the sensitivities of ultrasonography in determining the level and cause of obstruction to be 92% to 95% and 71% to 88% respectively (Leveille et al., 1996).

Ultrasonography has a low sensitivity and specificity in cats with diseases such as cholangitis and pancreatitis and correlates poorly with histopathologic diagnoses even in advanced stages of disease (Marolf et al., 2012 and 2013). Ultrasound also does not offer functional information. Ultrasound may also have limited visualisation of certain regions such as the peripheral intra hepatic bile ducts, distal CBD and pancreatic structures due to gastric or bowel gas (Hashimoto et al., 2008; Gaillot et al., 2007; Heller and Lee, 2005), despite the cause of the EHBO being found in 5/7 cases (Brain et al., 2005; Leveille et al., 1996).

Use of IV CEUS has also been used to complement conventional ultrasonography in dogs with suspected gall bladder oedema, necrosis and rupture (Bargellini et al., 2018) and in cats with hepatobiliary neoplasms, although there was poor evidence to distinguish between different primary hepatobiliary neoplasms in cats (Banzato et al., 2020). There are no reports of CEUS to evaluate the biliary system in cats.

2.2.5 ERCP:

ERCP uses endoscopy and fluoroscopy to image the biliary and pancreatic ducts (Gaschen, 2009). It has been considered the optimal minimally invasive treatment modality for diagnosis and therapy of many biliary and exocrine pancreatic tract diseases in adults (Berent et al., 2015). The most common reasons for EHBO in humans is obstructive cholelithiasis, followed by tumours, strictures and obstructive pancreatitis. In comparison, dogs most commonly present for obstructive pancreatitis with associated ascending cholangitis, and cholelithiasis is rarely a primary cause (Berent et al., 2015). Since ERCP is an invasive procedure with radiation exposure and potential complications in humans, such as pancreatitis (1% - 20%), bleeding, perforation and infection (cholangitis) that can lead to longer hospitalisation times, increased morbidity and even mortality (Heller and Lee, 2005; Berent et al., 2015), ERCP is now a therapeutic modality for cholelithiasis, in people rather than a diagnostic modality (Heller and Lee, 2005).

ERCP is also reported to be used successfully in dogs > 10kg and is feasible in healthy cats (Spillmann et al., 2005; Spillmann et al., 2014). In comparison to human ERCP reports, a study evaluating endoscopic retrograde pancreatography (ERP) and ERCP in dogs, found no clinical signs of pancreatitis associated complications (Berent et al., 2015; Spillmann et al., 2014). ERCP can be utilised to detect irregularities in the biliary and pancreatic ducts, enabling identification and biopsy of suspicious lesions, collection of bile samples for evaluation and localising choleliths to facilitate removal (Berent et al., 2015). ERCP cannot visualise above the obstruction (Heoffel et al., 2006) and should only be used for dogs with EHBO secondary to pancreatitis, strictures, tumours or cholelithiasis (Berent et al., 2015). ERCP should not be used for treatment of patients with concurrent biliary mucocoeles and pancreatic or hepatic abscesses, which require surgical debridement (Berent et al., 2015).

2.2.6 MRC/MRCP:

MRC/MRCP is a newer low risk imaging technique in humans that is highly sensitive and specific for the diagnosis of biliary and pancreatic duct disorders as it provides anatomical and morphologic information without the use of ionizing radiation or IV contrast (Marolf et al., 2013; Heller and Lee, 2005). Biliary calculi as small as two millimetres may be detected on MRC (Heller and Lee, 2005). Further studies in dogs and cats may lead to a future hepatobiliary imaging using MRC/MRCP to diagnose hepatobiliary disease in animals (Gaschen, 2009; Marolf et al., 2013).

MRI can also detect changes associated with soft tissue pathology better than with ultrasonography as it detects subtle shifts in cellular water and protons (Marolf et al., 2013). Because of this, inflammatory processes of the hepatobiliary system and pancreas have visible signal differences and changes in contrast enhancement using MRI (Marolf et al., 2013). MRI has been shown to detect changes associated with human pancreatitis including increased or decreased size of the entire gland, pancreatic oedema and inflammation and peri-pancreatic inflammation (Marolf et al., 2013). MRC/MRCP uses specific sequences, that are based on the theory that slow moving fluids are hyperintense

on heavily weighted T2 images, so that bile and pancreatic fluid that is slow moving, will be bright compared to the background tissues (Marolf et al., 2013). The advantages of MRCP over sonography include decreased operator dependence and improved visualisation of biliary and pancreatic ducts, and MRCP combined with MR results in complete anatomic imaging of the ductal and extra ductal disease within the liver and pancreas (Marolf et al., 2013). The Marolf et al. (2013) study found that MRCP provided excellent visualisation of the pancreatic and hepatobiliary systems in cats, and it was advantageous over sonography in visualising the pancreatic duct, although the findings for hepatitis/ cholangitis were non-specific. The group concluded that sonography remains the recommended first imaging modality for feline pancreatic and hepatobiliary disease due to its availability, lower cost and lack of requirement for anaesthesia (Marolf et al., 2013). More recently studies have assessed MRCP and MRC in small animals (cats and dogs) including a comparison of MRI sequences utilised in human MRCP; as well as a comparison of MRI with fluoroscopic assessment of the biliary anatomy, corrosion casting and histopathology, wherein MRCP was found to be useful in visualising the feline biliary tract and pancreatic ducts greater than one millimetre diameter, and had limitations in visualisation of hepatic and pancreatic ducts less than one millimetre (Rahmani et al., 2024; Briola, 2022; Rahmani et al., 2023a; Rahmani et al., 2023b). A disadvantage of MRCP is the lack of functional information it provides.

2.2.7 Computed Tomography:

CT has re-emerged as a technique for visualising biliary pathology in people, with the introduction of IV hepatobiliary contrast media (Heller and Lee, 2005). Chau et al. (2017) reported the use of Gd-EOB-DTPA for CT cholangiography in healthy dogs which showed that doses of 0.3 mmol/kg showed better visualisation of biliary structures than doses of 0.025 mmol/kg at 65 minutes post contrast injection. Noguchi et al. (2023) also described IV administration of meglumine iotroxate using CT cholangiography in a cat with gallbladder agenesis, that showed contrast medium entered the duodenum at 45 mins, with progressive contrast entering the duodenum at 60 minutes and subsequently resulted in sufficient contrast enhancement in the hepatic ducts. No adverse reactions were observed in this case and the study was performed without sedation. The optimal scan time remains unknown given the lack of a gallbladder in this study (Noguchi et al., 2023). CT has also recently been reported to correctly diagnose the lobar origin of hepatic masses in cats in 76% of cases (Bentley et al., 2024).

Studies have also shown that CT is comparable to ultrasonography in its ability to detect biliary obstruction and has a greater ability to predict the level and cause of the biliary obstruction, although controversy still exits (Horton et al., 2009). CT is also good at documenting the presence and extent of biliary tract malignancy and as a general survey tool of the abdomen, particularly for metastasis, as well as diagnosing varying forms of bile duct disease in humans such as strictures (Horton et al., 2009; Anderson et al. 2008).

A limitation of hepatobiliary imaging using CT in humans is the sufficient opacification of bile ducts in patients with reduced hepatobiliary function, such as in severe hepatocellular

disease, intra hepatic biliary obstruction or extra-hepatic biliary obstruction (Heller and Lee, 2005). Cholelithiasis can also be variably detected on CT depending on their composition and density (Soto et al., 2000).

2.2.8 Drip Infusion Computed Tomography:

DIC-CT has also been shown to enable fast and non-invasive volumetric imaging of the bile duct in people (Tanaka et al., 2018). It has been reported to detect obstructive biliary disease, although the risks of adverse reactions with the contrast media are as high as 3.4% in people (Tanaka et al., 2018). A study in cats, used meglumine iotroxate at a dose of 2 ml/kg IV over 30 mins in a conscious animal, with the patient anaesthetised immediately after contrast administration and CT scanning commenced 1 hour (h) after initiation of contrast. The study showed that contrast medium was shown to opacify the gallbladder, cystic duct, hepatic duct, CBD and duodenum with no adverse events (Tanaka et al., 2018). In healthy cats and two cats with hepatobiliary disease (cholelithiasis), DIC-CT was reported to detect the bile duct without significant side effects (Tanaka et al., 2018). A case report in a dog with a biloma from intra hepatic bile leakage used DIC-CT with meglumine iotroxate (100 mg I/kg IV over 30 mins) which showed contrast media filling the intra and extra hepatic bile ducts, CBD and duodenum, except the gallbladder and 10 dogs with gallbladder mucocoeles showed the hepatic ducts, cystic duct, CBD, gallbladder and duodenum opacified with contrast in 9 dogs and incompletely opacified biliary system in one dog with hyperbilirubinaemia due to chronic hepatitis (Hayakawa et al., 2018).

Despite the number of described hepatobiliary imaging techniques, limitations or disadvantages remain with each of these techniques. Currently, in cats there is no gold standard imaging technique to definitively diagnose hepatobiliary tract disease. Therefore, developing a non-invasive test to distinguish between hepatobiliary diseases, particularly with functional and morphologic information, is important in the clinical management of feline hepatobiliary disease (Newell, 1996).

We considered CT to be a potentially excellent imaging modality in veterinary medicine to investigate the feline hepatobiliary system using a gadolinium-based contrast media, Gd-EOB-DTPA.

2.3 Lung imaging with emphasis on atelectasis and lung density

Respiratory signs are common in cats presenting to veterinary hospitals. As therapeutic possibilities have increased in feline medicine, thoracic CT is increasingly utilised in cats with thoracic conditions such as thoracic trauma, pulmonary vascular embolic diseases, including infarction, lung lobe torsion, mediastinal masses, pleural disorders, oesophageal disorders, primary pulmonary pathology and more recently in cardiac disorders (Henninger, 2003; Greco et al., 2023).

Imaging is important in evaluating the anatomy and function of the lungs to establish a diagnosis, monitor disease severity or for screening (Gulati and Balasubramanya, 2024).

Understanding the benefits and limitations of the different thoracic imaging modalities is important to ensure a rapid diagnosis for cats with respiratory tract disease.

2.3.1 Radiography:

Radiographs are typically the first modality utilised in feline respiratory medicine as they can be used to identify the presence and location of a disease, type of lesion, extent of lesion and provide a list of potential or differential diagnoses, suggest additional procedures and document the course of a lesion (Rudorf et al., 2008). It should be noted that thoracic radiographs can be fatal in animals with severe thoracic disease and the benefit of obtaining radiographs should outweigh the risks (Rudorf et al., 2008). Contrast radiography has been used in thoracic imaging including for oesophagography, bronchography (now obsolete) and angiocardiography.

2.3.2 Nuclear medicine:

NM can be used to evaluate ventilation, perfusion or positive emission tomography CT for staging of lesions. It is not commonly used due to a lack of access to technology, high costs and difficulties licensing and handling the radiopharmaceutical and animal waste (Gulati and Balasubramanya, 2024).

2.3.3 Ultrasonography:

Thoracic ultrasonography can also complement thoracic radiographs, as there is normally easy access, portability, relatively high sensitivity and specificity without using ionising radiation or anaesthesia. It can be utilised to examine the lung surface, pleural space, ribs and thoracic wall, as well as for therapeutic procedures such as thoracocentesis and biopsy. Due to the artefact between the soft tissue to gas interface at the lung surface, lesion assessment within the lung lobe is difficult or impossible unless there is a lesion bordering on the pleural lung margin or if there is consolidation of the lung (Mai et al., 2008). Interpretation of the imaging findings also lies with the skill of the user.

2.3.4 Magnetic Resonance Imaging:

MRI is typically used in people when contrast or ionising radiation is not recommended and it is rarely performed to evaluate the lung in animals compared with CT due to inherently low signal from lung and artefacts (Schwarz, 2008).

2.3.5 Computed tomography:

MDCT including CT angiography should be used when thoracic disease is suspected and the cause and extent is not clear on radiographs or ultrasonography, particularly to investigate the airways and lungs including for tracheal collapse, bronchial obstruction, rupture and thickening and peribronchial infiltrates, screening for metastatic lung lesions for oncological staging and presurgical planning, all interstitial lung disease, to determine the exact location, nature and extent of pulmonary masses and bullae, pulmonary thromboembolism, lung lobe torsion, differentiation between collapsed (atelectatic) and consolidated lung lobes (Schwarz, 2008).

Thoracic CT in cats is reported to be more sensitive compared to radiography for detecting pulmonary disease, including when using a conscious techniques and is similar to previous studies of thoracic CT in humans and anaesthetised dogs and cats (Oliveira et al., 2011a; Oliveira et al., 2011b). Nevertheless, as thoracic CT also has a low specificity, biopsies or other sampling techniques such as FNA or bronchoalveolar lavage are required to obtain a final diagnosis (Henninger, 2003).

Thoracic CT is commonly utilised in cats both with and without respiratory signs to evaluate for intra-thoracic disease (Henninger, 2003; Prather et al., 2005; Samii et al., 1998; Lamb and Jones, 2016). Non-clinical cats have also been reported to have a high prevalence (77%) of respiratory tract abnormalities including atelectasis, bronchial disease and pulmonary masses (Lamb and Jones, 2016).

2.3.6 Atelectasis:

The term atelectasis means non-expansion of a terminal space, and as a medical term is defined as an acute or chronic collapse or airless state of the whole lung or parts of it, caused by congenital or acquired conditions (Mai et al., 2008). During anaesthesia, atelectasis occurs in the dependent lungs wherein lung volume reduces, due to collapse of alveolar air spaces and existing air spaces resulting in non-aerated lung (Staffieri, 2007). In CT atelectasis is described as a partial or complete reduction in lung volume resulting in an increase lung density and is expressed in HU (Lamb and Jones, 2016). Although atelectasis occurs in 90% of healthy anaesthetised patients, it causes impairment in gas exchange (Duggan and Kavanagh, 2005). Potential complications from atelectasis can include pneumonia, hyperaemia and respiratory failure (Duggan and Kavanagh, 2005). Atelectasis has been described as the most common abnormality in thoracic CT scans in 41% of cats without respiratory tract signs (Lamb and Jones, 2016). Bronchial disease (24%) and space occupying lesions (21%) were noted in cats without respiratory signs (Lamb and Jones, 2016).

Traditionally, atelectasis is detected through subjective (visual) interpretation of diagnostic imaging modalities. Subjective features of atelectasis include reduced inflation of the lung with reduced lung volume and mediastinal shift, crowding and reorientation of pulmonary blood vessels, crowding of ribs, compensatory hyperinflation of other lung lobes, bronchial rearrangement, cardiac rotation, displacement of inter lobar fissures, displacement of the diaphragm, change in location of abnormal structures and rounded pulmonary margins (Gaschen, 2016).

More recently, objective or quantitative computed tomographic analysis of atelectasis is being investigated (le Roux et al., 2016; Staffieri et al., 2007; Hunt et al., 2021; Henao-Guerrero et al., 2011; Klaengkaew et al., 2021). The quantitive analysis of lung atelectasis is semiautomatic and based on the HU distribution of bone (+ 400 to + 1000 HU); soft tissue (+ 40 to + 80 HU); water (0 HU); fat (- 60 to - 100 HU); lung (- 400 to - 600 HU); air (- 1000 HU). Quantitative lung atelectasis is defined as pixel attenuation values of - 100 to + 100 HU. Lung attenuation analysis has been classified using hyper aerated lung (- 1000

to - 901 HU), normo aerated (- 900 to - 501 HU), poorly aerated (- 500 to - 101 HU) and non-aerated (- 100 to + 100 HU) [true atelectasis] lung tissue (Foo et al., 2018).

Reported factors affecting subjective or objective atelectasis formation include the fraction of inspired oxygen, with a high fraction of inspired oxygen worsening atelectasis during anaesthesia; body habitus; pre-existing pulmonary pathology; position; anaesthetic agents (e.g. IV or inhalation); duration and type of surgery; low Va/Q; decreased tidal volume; and surgical factors (such as thoracic packing, retraction) (Duggan and Kavanagh, 2005).

In anaesthetised dogs and cats, atelectasis has been reported to be minimised by prompt imaging following anaesthetic induction, use of lower inspired oxygen concentrations (40%) and addition of positive end-expiratory pressure (PEEP) (Stafferi et al., 2007; Allison et al., 2017). Jones and Lamb's (2016) study also noted that atelectasis was associated with increasing body weight. The most frequently collapsed lung lobes in Lamb and Jones (2016) study was the right middle and left and right cranial lung lobes. The right middle lung lobe is also reported to be frequently collapsed in cats with bronchial disease because of mucus or exudate obstruction in the airways (Mantis et al., 2008).

Atelectasis is important to understand in addition to the potential medical complications that it can cause, it can also reduce the detection and diagnosis of pulmonary pathology during imaging wherein, the density of the atelectatic tissue is the same soft tissue density or radio-opacity as pathologic tissue causing border effacement. Atelectasis can therefore mask the pathological tissue since there is no gas (negative contrast) surrounding the pathologic tissue and therefore, there is no contrast in the lungs to increase the conspicuity of the pathologic lesions.

Previous research determined that quantitative CT accurately measures lung volume and density (Wandtke et al., 1986). In 2007, Staffieri researched quantitative CT atelectasis in dogs and then in cats in 2010. Quantitative CT was used to compare four ventilatory protocols of thorax in healthy cats (Henao-Guerrero et al., 2012). Choi et al. (2014), also used quantitative CT to evaluate lung volume and density in healthy dogs with relation to body weight, age, sex and breed. Henao-Guerrero et al. (2012) also discussed the tendency for lung atelectasis in anaesthetised cats. In dogs, high inspired pO2 during anaesthesia has been associated with a higher prevalence of atelectasis compared to moderate pO2 (Stafferi et al., 2007). This may also occur in cats, although Lamb and Jones (2016) showed that anaesthetised cats, were no more likely to develop atelectasis than sedated cats. Lamb and Jones (2016) also suspected that cats in ventral or dorsal recumbency would be less affected by atelectasis than those in lateral recumbency.

Knowledge of these factors can assist in the interpretation of radiographs and CT images of the thorax in cats. Currently there are no accepted normal reference ranges in animals to define atelectasis and there is no consensus on the degree of atelectasis over time and the effect of body position.

2.3.7 Lung density:

Previous CT research has documented the density of lung into three components - pulmonary parenchyma, blood and gas (Simon et al., 2005). Lung is essentially composed of air (- 1000 HU) and lung tissue e.g. blood, cells, water (0 HU), so that a region of interest (ROI) on a portion of lung that is approximately - 600 HU would account for lung that is composed of approximately 60% air and 40% lung tissue (Simon et al., 2005). The difference in density between the gas and soft tissue structures, allows the lung tissue, which consists of consists of alveoli, interstitial tissue, bronchial walls and blood to be visualised.

When interpreting radiographic and CT images of the lung, assessment for changes in lung volume and densities is essential. The relative proportions of the components of lung and therefore the lung density differ with changes in lung volume such as during respiration (Masseau and Reiner, 2019). A reduction in lung volume, such as during expiration, cause an increase in physical density and thence increased attenuation (HU) of the lung since there is less gas (Foo et al., 2018; Horton et al., 2009). Conversely, lung is less dense during inspiration when there is more gas in the lung.

Pronounced changes in lung density also occur commonly during anaesthesia, sedation or recumbency, due to atelectasis (Foo et al., 2018). Pathologic changes in the lung also normally involve an increase in lung density as they generally involve cellular infiltration, such as neoplasia, haemorrhage, oedema or inflammation (Horton et al., 2009). Since cats are commonly anaesthetised and positioned in either lateral, dorsal or sternal recumbency for imaging, the increase in the attenuation of the lung due to atelectasis can have important clinical implications by potentially mimicking pathologic lesions or masking evidence of intra-thoracic disease, therefore further complicating the interpretation of thoracic radiographic and CT findings (Morandi et al., 2003; Foo et al., 2018). This is a particular concern as atelectasis is reported as the most prevalent pulmonary abnormality in cats without respiratory tract signs (Lamb and Jones, 2016). A specific diagnoses is often difficult due to the lack of specificity of lung changes and limited literature on the normal and abnormal CT features of feline airways.

Traditionally, increases in lung density are described as alveolar, bronchial, vascular or interstitial (unstructured or structured) patterns (O'brien, 2016). The increase in lung density is caused by an increase in the number of cells such as inflammatory, structural, haemorrhage, infiltration such as tumour or infection; an increase in the amount of blood vessels; decreased volume of air in the alveoli, for example during exhalation, hypoinflation due to obesity or pleural cavity disorders or atelectasis; or replacement of air by fluid or cells in air spaces (Masseau and Reinero, 2019). Often there is a mixed pattern, but usually one lung pattern predominates. The distribution and density of the lung changes are important in prioritising differential diagnoses, and can be assessed by qualitative, visual assessment or quantitative assessment by CT imaging (Campos and Diaz, 2018). Qualitative data has been shown to correlate with corresponding pathologic

data, and it is reported to be subject to high intra or inter observer variability (Campos and Diaz, 2018).

The alveolar pattern can be the most commonly missed, particularly using radiographs, yet it is the most prevalent and clinically significant pattern in cats, and includes atelectasis (O'brien, 2016). Atelectasis is characterised as an alveolar or interstitial pattern on radiographs and CT. A recent paper has also described a different form of atelectasis in cats and a dog termed rounded atelectasis, which shows predominantly homogeneously contrast enhancing sub pleural masses that were histologically confirmed as atelectasis, in cats with concurrent pleural disease (Fukuda et al., 2023).

Other causes of an alveolar or unstructured interstitial pattern include pneumonia, haemorrhage, infiltrative neoplasia or oedema which cause an increased lung density with the same or greater lung volume. Enlarged pulmonary arteries or veins can create an increased pulmonary density, called a vascular pattern, for example in heartworm disease. Structured interstitial patterns can be caused by neoplasia. The most common primary pulmonary neoplasm is adenocarcinoma, and less commonly squamous cell carcinoma and bronchoalveolar carcinoma, granulomas, cysts, abscesses or haematomas.

Bronchial patterns can be seen with chronic bronchitis and feline asthma. Cats develop a cohort of diseases that differ to dogs including allergic diseases and often the same diseases can present differently in CT or radiographic imaging in cats compared to dogs (Day, 2016). For example, feline bronchial disease can present with normal radiographic findings, hyperinflation from air trapping or diffuse bronchial pattern (O'brien, 2016). Feline cardiogenic pulmonary oedema also does not have a defined pattern or distribution but can have an unstructured interstitial pattern with or without a concurrent alveolar pattern (Larson, 2020).

A reduction in lung density occurs more rarely, such as hyperinflation which is seen with air trapping which can cause a greater lung volume, with a concurrent reduced lung density, for example in allergic small airway disease, emphysema and obstructive bronchial masses (Mai et al., 2008). Hyperinflation can also be seen in perfusion deficits wherein, reduced pulmonary perfusion decreases lung opacity and promotes hyperventilation (e.g. right to left shunts, pulmonic stenosis, right heart failure, pulmonary thromboembolism and hypovolaemia) and in central nervous stimulation (e.g. stress, hyperthyroid cats or aggressive animals, metabolic acidosis, shock and brainstem pathology) (Mai et al., 2008). Hypovolaemia can also cause a reduced lung density with a similar lung volume (Larson and Berry, 2023).

Masseau and Reinero (2019) argue that using the pattern based approach to characterise the distribution and anatomic localisation is imperative to interpreting lung CT studies, and the historic terms of bronchial, interstitial, alveolar pattern should not be used with consideration given to the following lung pattern descriptions: 1. increased attenuation (ground glass opacity, consolidation, attenuation greater than soft tissue) 2. decrease attenuation (air trapping, cystic lung disease, emphysema, hypoperfusion), nodular patterns (within the air spaces, interstitial, attenuation greater than soft tissue) 4. linear

patterns (reticular, sub pleural interstitial thickening, peribronchialvascular interstitial thickening, parenchymal band, honeycomb pattern) 5. mixed patterns (mosaic, tree-in-bud, crazy paving, halo and reverse halo signs) with the anatomic localisation being 1. pleural 2. sub pleural 3. peri-bronchovascular 4. parenchymal 5. random.

Despite these limitations, CT is considered the gold standard for quantification of changes in lung density and volume therefore providing an excellent tool for non-invasive measurements of lung mechanics (Lamb and Jones, 2016; Simon et al., 2005; Foo et al., 2018). This research aims to evaluate the effect of position on lung attenuation in healthy cats.

2.4 Contrast media in feline hepatobiliary and lung imaging

Contrast enhanced computed tomography (CECT) is increasingly used in veterinary medicine. It uses positive or negative contrast media to create a visual subjective and/or objective (HU) difference to the surrounding tissues to allow improved conspicuity of organ anatomy and vasculature and/or provide functional information.

In contrast CT, positive contrast media tissues that contain or excrete contrast have a higher attenuation (HU) or density than adjacent tissues because more x-rays are attenuated by the contrast media containing structures (Lusic and Grinstaff, 2012). Positive contrast is particularly useful for abdominal imaging. The pulmonary parenchyma is reported to be best evaluated without IV iodinated contrast and typically utilises the inherent negative contrast of gas in the lungs (Masseau and Reinero, 2019). Commonly the contrast media most utilised in lung imaging is non-ionic iodinated contrast e.g. iohexol and contrast enhanced ultrasonography microbubbles in non-cardiac thoracic disorders that have been shown to assist in identifying lesion edges, establishing regions of ischaemia and necrosis in lesions so that they can be avoided during sampling and the distribution of pulmonary vessels (Linta et al., 2017). There is currently no standardised protocol for thoracic CT including post contrast imaging. Contrast may be useful as atelectatic lung tissue is reported to enhance after contrast administration, while neoplastic tissue remains hypoattenuating (Henninger, 2003).

Positive contrast media is typically administered intravenously and a dynamic phase is obtained, including an arterial, portal and venous phase to assess for vascular and parenchymal changes, with the potential for additional delayed sequences depending on the clinical concerns (Greco et al., 2023; Pollard and Puchalski, 2011). The arterial phase is acquired either immediately, or a few seconds after IV contrast injection and the venous phase occurs after contrast medium has passed from the arterial vessels into the venous circulation via the capillary beds of the organs (Masseau and Reinero, 2019).

Non-ionic iodinated IV contrast media, such as iohexol is commonly used in CT studies and is excreted renally via glomerular filtration, and an increase in the conspicuity of the vasculature, organ parenchyma and urinary tract occurs. Despite the renal excretion of Iohexol contrast media, hepatic parenchymal contrast enhancement also occurs, yet the excretion characteristics are inadequate for visualisation of the biliary system.

Other positive contrast media include, hepatobiliary contrast that is absorbed by hepatocytes and is excreted through the bile via enterohepatic circulation into the intestines and excreted via faeces. Hepatobiliary contrast media increases the conspicuity of the liver, gallbladder and bile ducts and allows for both functional and morphologic examination of the hepatobiliary tract. Hepatobiliary contrast media includes iodinated, manganese and gadolinium-based media.

This thesis utilised two different types of contrast, firstly a positive gadolinium based hepatobiliary contrast medium that has both functional and morphologic features in the hepatic CT study. Secondly, gas, a natural but negative contrast in the lung CT study. In both studies, we assessed the changes in density by objectively measuring the attenuation (HU) of the hepatobiliary system and lung respectively over time, to develop new applications in CT imaging of the hepatobiliary tract and lung in healthy cats and to evaluate their potential use in future investigations of feline pulmonary and hepatobiliary diseases. There are few reports in the literature of hepatobiliary imaging in cats using CT and to the author's knowledge there are no reports of Gd-EOB-DTPA use in cats and no studies investigating Gd-EOB-DTPA in cats with CT imaging prior to this thesis (Tanaka et al., 2017; Noguchi et al., 2023). The study in this thesis hypothesised that Gd-EOB-DTPA would be a safe hepatobiliary contrast media to improve conspicuity of the hepatobiliary tract using CT in healthy cats, due to its higher atomic number than traditional iodinated contrast media, and because of its moderately high biliary excretion rate, potentially faster hepatobiliary excretion compared to other hepatobiliary contrast media, and proven effectiveness in people and canines. We also selected Gd-EOB-DTPA due to the ready availability in Australia at the time of the study and the possible variation in excretion characteristics, particularly as older cats may have renal disease and can therefore potentially excrete preferentially into the hepatobiliary tract.

Specific features of positive hepatobiliary contrast media and positive pulmonary contrast media are outlined below.

2.4.1 Hepatobiliary contrast media:

2.4.1.1 Iodinated contrast media, use and side effects

Oral, percutaneous and IV administration of iodinated hepatobiliary contrast media have been reported in dogs and cats with variable efficacy and adverse effects (Chau et al., 2017; Carlisle, 1977). Unfortunately, the oral hepatobiliary contrast media relied on a significant delay in imaging, up to 12 - 14 h post contrast administration, in which time a diagnosis and potential medical or surgical management could have commenced (Carlisle, 1977). Percutaneous cholangiographic iodinated or sonographic contrast media, have shown effective demonstration of biliary anatomy, and patency of the CBD at the MDP yet they also have risks including leakage of contrast media into the abdomen (Kim et al., 2019; Ji et al., 2015).

Currently the only iodinated hepatobiliary contrast media in Australia is meglumine iotroxate, which was temporarily unavailable at the time of study planning and execution.

i. Iodipamide meglumine (Cholografin(TM))

A biliary specific iodinated positive contrast media used IV for cholangiography and cholecystography and is rapidly excreted by the liver wherein, 90% is excreted via enterohepatic excretion and 10% via renal excretion (Bracco Diagnostics, 2017). It is reported for use in IV doses in human adults is 20 mL and 0.3 - 0.6 mL/kg in children and infants (Bracco Diagnostics, 2017). Canine IV doses have been reported at 0.6 ml/kg and 0.9 ml/kg to provide good opacification of the biliary tract using radiography (Miller, 2014). In people, contrast is reported to appear within the bile in 10-15 mins after IV injection and allows visualisation of the hepatic and bile ducts. Bile ducts should be visible 25 minutes after injection with maximum filling by 2.0 - 2.5 hours (h) (Bracco Diagnostics, 2017). CT studies assessing Iodipamide meglumine at 1 ml/kg in dogs noted that the optimal time to image the bile ducts, gallbladder and cystic ducts was 60 mins (Miller, 2014).

Contraindications for Iodipamide meglumine use in people include dehydration, hypersensitivity to iodipamide salts or with severe liver or renal impairment (Bracco Diagnostics, 2017). Reported side effects include mild transient symptoms following rapid injection, hypersensitivity and respiratory difficulties and rarely anaphylaxis (Bracco Diagnostics, 2017). Canine studies have not reported significant side effects (Miller, 2014). Early studies investigating cholangiography in cats reported Iopidamine meglumine at 0.05 ml - 1.00 ml/kg over two minutes with contrast detected in the gall bladder 40 mins later and at 2.0 - 2.5 h post injection excellent images of the gallbladder was seen in all animals (Carlisle, 1977). Vomiting and defecation were consistent adverse effects after injection, in conjunction with swallowing, licking of lips and restlessness as well as diarrhoea and depression that lasted up to 24 h and appeared more significant with increasing dose (Carlisle, 1977). Renal injury has been reported in the cat following rapid IV and intra-arterial injections in the cat (Carlisle, 1977).

ii. Meglumine iotroxate (Biliscopin(TM))

A biliary specific positive contrast media administered IV for cholangiography and cholecystography and is excreted through the bile (Bayer Group, 2018). In humans IV doses of 100 ml (105 mg meglumine iotroxate per ml) are normally used via slow IV injection and is visualised in the bile ducts in humans 30 - 60 mins after administration via an infusion over 30 - 60 mins (Bayer Group, 2018). A study in cats showed it is safe to use Meglumine iotroxate in normal cats at an IV dose of 72 and 144 mg I/kg at 1 ml/min and resulted in opacification of the gallbladder and bile duct 20 mins after administration (Fujita and Orima, 1994). Meglumine iotroxate has also been reported in cats to detect obstructive biliary disease (Tanaka et al., 2018) and in a cat at doses of 100 mg I/kg IV over 30 mins with gallbladder agenesis, with imaging performed at 45 mins and 60 mins after the start of contrast medium injection without anaesthesia (Noguchi et al., 2023). Doses up to 3 ml/kg have been reported in dogs, administered as an infusion over 10 mins (Uno et al., 2009). Interestingly, studies comparing Meglumine iotroxate (Biliscopin) to Iodipamide meglumine (Cholegrafin) in dogs showed faster biliary excretion of Meglumine iotroxate (15 - 30 mins) (Taenzer and Volkhardt, 1979; Miller, 2014). A study of 10 dogs

with gallbladder mucocoeles using a dose of 100 mg I/kg IV over 30 min showed good visualisation of the biliary tract in all dogs, except in one dog with hyperbilirubinaemia and impaired hepatic function (Hayakawa et al., 2018).

Meglumine iotroxate has protein binding characteristics which increases the risk of adverse reactions, which in humans includes anaphylaxis, urticaria and respiratory distress (Tanaka et al., 2018; Pasanen et al., 1992; Persson et al., 2006). Contraindications in people include dehydration, severe cardiovascular compromise, iodine hypersensitivities, thyrotoxicosis, severe liver or renal impairment, monoclonal IgM gammopathy (Bayer Group, 2018). It has been reported to have the same contrast effect in cats as humans, that responded to antihistamine administration and mild elevation in ALT or AST 24 h after administration of contrast, and licking and vomiting occurred in 10/12 cats (Fujita and Orima, 1994).

iii. *Iosulamide meglumine (cholografin meglumine)*

This media is no longer available in the USA and is not available in Australia. Studies had shown advantages in animal tests with an IV toxicity lower than that of Iodipamide meglumine in the mouse and rat. It was also shown to have good cholangiocholecystographic visualisation in cats and monkeys with a similar time and degree of opacification (Rosenberg, 1980). A study in dogs showed that higher doses of Iosulamide meglumine did not result in improved opacification of the biliary tree and was unlikely to have an advantage over other contrast media in dogs (Berk et al., 1981).

2.4.1.2 Manganese contrast media, use and side effects

Manganese based contrast media have also been reported in humans, and animals (rats, monkeys, dogs, guinea pigs and rabbits). **T**o the author's knowledge there is no reported use in cats (Amersham Health, 2003). Manganese based hepatobiliary contrast medium is no longer commercially available in Australia.

i. *Mangafodipir trisodium (Mn-DPDP) (Teslascan(TM))*

Mangafodipir trisodium is a positive contrast specifically taken up by hepatocytes (45 - 55% biliary excretion), resulting in an increase in signal intensity of normal hepatic parenchyma (Amersham Health, 2003; Seale et al., 2009). Therefore, normal liver parenchyma gives a high lesion-to-liver contrast improving detection, characterisation and evaluation of liver lesions. In delayed phases, mangafodipir trisodium is excreted into the biliary system. It is administered in humans at a dose of 0.5 µmol/kg via slow IV infusion (1 - 2 mins) with delayed phase imaging from 10 mins to several hours (Seale et al., 2009). Limitations include the inability for dynamic imaging (Seale et al., 2009). Reports in dogs used doses of 10, 30 and 100 µmol MnDpDp/kg (Toft, K.G. et l, 1997). In human studies, gadoextic acid was tolerated better than Mangafodipir trisodium (Hamm et al., 1995).

Side effects include mild flushing, nausea, dizziness, raised blood pressure and heart rate (Seale et al., 2009). This medium was withdrawn from the marked in the USA in 2003 and

European Union (EU) in 2010 due to potential neurological risks in patients with liver dysfunction. There is no known use of Mangafodipir trisodium in cats.

2.4.1.3 Gadolinium contrast media, use and side effects

Gadolinium-based contrast media include both extracellular space media and hepatocyte specific media that are normally utilised in MRI, although studies have also shown their sporadic use in CT in dogs (up to 0.7 mmol Gd/kg), rabbits and humans (up to 0.5 mmol Gd/kg) (Chau et al., 2017; Schmitz et al., 1997a, b).

Gd-EOB-DTPA and other oral and IV contrast media have been used with CT in dogs and humans to improve visualisation of the liver and biliary tract (Schmitz et al., 1997a; Gold et al., 1979; Caoili et al., 1999; Chau et al., 2017). CT cholangiography is also reported to potentially provide more accuracy than MRC with contrast (Heller and Lee, 2005) and MDCT cholangiography with its higher spatial resolution can provide significantly better visualisation of second order biliary branching than conventional MRC (Yeh et al., 2009).

Use of Gd-EOB-DTPA as a contrast medium has resulted in improvements in tumour detection and the ability to distinguish between benign and malignant lesions of hepatocellular or non-hepatocellular origin in the delayed phase, independent of the vascularity of a lesion during early dynamic phase imaging because of its hepatocyte specificity (Burke et al., 2013; Van Beers et al., 2012). For example, lesions with altered hepatocyte function (e.g. hepatic adenoma, nodular hyperplasia, and hepatocellular carcinoma) have variable contrast enhancement, compared with results for normal hepatic parenchyma (Van Beers et al., 2012; Yonetomi et al., 2012; Constant et al., 2016; Chau et al., 2017). Similarly, metastatic lesions that lack hepatocytes, have no contrast enhancement (Van Beers et al., 2012). Gd-EOB-DTPA enhanced MRI can potentially provide quantitative assessment of liver perfusion and hepatocyte function in diffuse liver disease (Van Beers et al., 2012; Chau et al., 2017). The excretion properties of Gd-EOB-DTPA have also been used in the functional assessment of biliary anatomy with MRI, including bile duct injury, obstruction or stricture; sphincter of Oddi dysfunction; differentiation of biliary from extrabiliary lesions (including bilomas); identification of biliary-enteric anastomoses; and diagnosis of cholecystitis in people (Lee et al., 2009). Gd-EOB-DTPA is reported to have reduced contrast induced side effects and greater hepatobiliary excretion in humans compared to other hepatobiliary contrast media (Heller and Lee, 2005). Other reported means of improving biliary visualisation could include investigating a low dose morphine administration, as morphine constricts the sphincter of Oddi, and leading to distension of the biliary ducts which may improve conspicuity of contrast within the biliary structures (Heller and Lee, 2005).

Despite gadolinium-based contrast media being more expensive than iodinated contrast media, the potential benefits include a more rapid excretion of contrast into the biliary tract compared to iodinated contrast media and therefore, potentially a faster study time and diagnosis. They can also be used in patients with known or high-risk to iodinated contrast reactions (Pollard and Puchalski, 2011). Gadolinium-based contrast media are normally utilised in MRI at lower doses, as they have a paramagnetic effect with a brighter signal in

T1 weighted images, increasing the signal from tissues with increased blood flow. Despite the more frequent use in MRI, studies have demonstrated that gadolinium-based hepatobiliary contrast media using CT showed that the CBD was a sharply delineated hyperattenuating tubular structure in dogs (Schmitz et al., 1997a). Chau et al. (2017) demonstrated that Gd-EOB-DTPA enhancement of the biliary tract using CT in dogs was achieved 65 mins after IV infection of contrast media.

Studies in animals of gadolinium-based contrast media have shown that rats were reported to be the best biliary excretors, then dogs (32 - 43%), then rabbits and lastly monkeys (3 - 12%) which have a similar excretion rate to humans (Hamm et al., 1995; Lorusso et al., 1999). Results in animal experiments proved that there was complete elimination of the hepatobiliary contrast media in cases of severe impairment of hepatobiliary or renal excretory function, so that one pathway compensates for the absence of the other pathway (Hamm et al., 1995).

Gadolinium-based hepatobiliary contrast media are good candidates to be utilised in CT imaging, given the benefits of CT compared to MRI among other imaging modalities. The major criteria to determine contrast enhancement using CT is the efficiency of absorption of x-rays by contrast medium and the concentration of the contrast medium in the organ of interest. Gadolinium has a 40% higher rate of attenuation of x-rays than iodine at 120 KV as it has a higher atomic number 64 and a higher k absorption edge value 50.2 KeV compared to iodine, whose atomic number is 53 and k absorption edge value is 33.2 KeV (Schmitz et al., 1997a; Lusic and Grinstaff, 2013). This means that gadolinium containing structures will have more image contrast due to the differential photoelectric absorption of x-rays compared to iodine, and should increase the visibility of gadolinium containing structures using CT. Higher doses of gadolinium media are required in CT imaging compared to MRI because they have a lower molar concentration per dose compared to iodinated contrast media (Lusic and Grinstaff, 2013; Pollard and Puchalski, 2011). Reports in dogs have shown that the visualisation of liver, blood vessels, gallbladder and bile ducts was improved with increasing doses of Gd-EOB-DTPA (up to 0.7 mmol Gd/Kg) in the dog (Schmitz et al., 1997a**)**.

Despite the increased cost of gadolinium compared to other contrast media, this may be beneficial as fewer imaging modalities may be required, with a faster diagnosis of confirmed hepatobiliary disease, particularly given the global assessment of CT and cross-sectional assessment of anatomy and functional information compared to other modalities, which may outweigh the cost. It can be also be utilised in the small subset of patients with iodine related allergies.

i. *Gadobenate Dimeglumine (gadolinium benzyloxypropionictetraacetate - Gd-BOPTA) (Multihance(TM))*

Gd-BOPTA is reported to undergo 3 - 5% biliary excretion and 95% renal excretion. The recommended dose for liver imaging in humans is 0.05 mmol/kg IV bolus injection (2 mL/ sec) (Seale et al., 2009; Regional Health Limited, 2005). There are reports in dogs at IV doses of 0.2 mmol/kg with no reported reactions (Louvet and Douconseille, 2015). It has

also be reported in rats, rabbit, dog and monkey (Lorusso et al., 1999). The timing of imaging post contrast include a dynamic phase at 10 seconds (s), 45 s, 90 s and a delayed phase at 40 mins - 120 mins (Seale et al., 2009). Gadobenate dimeglumine first appears in bile in humans at 20 mins (peak biliary approx 1 h) and in dogs at 14.8 mins (Louvet and Douconseille, 2015). At 23 - 25 mins images were similar to those at 60 mins (Louvet and Douconseille, 2015). The hepatocellular phase is reported between 45 mins to 60 mins (peak) to 2 - 3 h due to the smaller percentage of biliary excretion (Cher et al., 2010).

Reported side effects in humans include mild nausea, flushing, injection site pain, taste perversion, nausea. It may be preferred in patients with high bilirubin due to the preferential renal excretion. Gadobenate dimeglumine has been reported in cats (off label) and is routinely used in MRI studies in veterinary medicine. Gadobenate dimeglumine is available in Australia.

ii. *Gadoxetic acid (Gadolinium ethoxybenzyl-diethylenetriaminepentaacetic acid - Gd-EOB-DTPA) (Eovist(TM)/Primovist(TM))*

Gd-EOB-DTPA is reported to undergo 43.1% - 53.2% biliary excretion and 41.6% - 51.2% renal excretion with uptake by the same transporter as bilirubin transport, so that biliary obstruction or reduced hepatobiliary function can be suspected in patients with reduced or no visualisation of the biliary tree 20 - 30 mins after administration (Lee et al., 2009; Bayer New Zealand Limited, 2012). The recommended dose in humans is 0.025 mmol/kg bolus IV injection (2 mL/sec) using MRI (Seale et al., 2009; Bayer New Zealand Limited, 2012). Gd-EOB-DTPA provides a shorter acquisition time compared to Gadobenate dimeglumine. In people, the timing of imaging post contrast is a dynamic phase at 10 s, 45 s, 90 s and a delayed phase at 10 mins – 2 h (Seale et al., 2009; Bayer New Zealand Limited, 2012). It first appears in human bile at 10 mins (peak biliary 10 mins). The hepatocellular phase peak is at 20 mins with a persistent enhancement up to 2 h. Gd-EOB-DTPA shows a weaker enhancement in arterial and venous phase. Gd-EOB-DTPA has been reported for use in dogs using MRI and CT at doses of 0.3, 0.5, 0.7 mol Gd/Kg and in humans using CT at doses of up to 0.5 mmol Gd/Kg with no increase in adverse effects (Chau et al., 2017; Schmitz et al., 1997a; Schmitz et al., 1997b; Marks et al., 2013; Yonetomi et al., 2012; Lux et al., 2024; Dohr et al., 2007).

Side effects in humans include mild nausea, flushing, headache, injection site pain, taste perversion similar to Gadobenate dimeglumine. Gd-EOB-DTPA is contraindicated in patients with renal impairment as there is an increased risk of developing Nephrogenic Systemic Fibrosis (Bayer New Zealand Limited, 2012). Gd-EOB-DTPA is available in Australia.

Disadvantages of Gd-EOB-DTPA include a lower injection volume which may lead to errors in dynamic imaging and increased cost compared to iodinated media (Lusic and Grinstaff, 2013). It is also reported to have minimal interstitial late phase enhancement due to early clearing from the interstitial space and is not as optimal for inflammation or evaluating organs other than liver. In cases with high bilirubin or biliary tract obstruction,

contrast may not be visualised in the hepatobiliary system and may be preferentially renal excreted (Lee et al., 2009).

2.4.2 Pulmonary contrast media:

There are several types of positive contrast media including iodinated (most common), barium (obsolete) and manganese (research) used in lung imaging. Negative contrast or inherent gas in the lungs is also utilised in pulmonary imaging as it is more radiolucent than the surrounding soft tissue of the pulmonary parenchyma including the interstitium and pulmonary vessels that have a soft tissue radio-opacity (Rudolf et al, 2008).

2.4.2.1 Iodinated contrast media, use and side effects

i. *Iohexol (Omnipaque(TM))*

Iohexol is a non-ionic (low osmolar) iodinated contrast (GE Healthcare Australia Pty Ltd, 2021). It is typically used IV at typically 700 mgI/kg to assess thoracic cardiovasculature (angiocardiography), pleural, mediastinal and thoracic wall lesions as well as some pulmonary lesions.

Allergic reactions and contrast induced nephropathy are well known adverse reactions associated with iodinated contrast media. Recently a new phenomenon has been reported in humans wherein there is a transient decrease in the tracheal diameter (by 2.5%) and lung volume (by 4.4 %) in the arterial phase occurs (Yasaka et al., 2024). This phenomenon has not been documented in cats and it is unknown whether this may affect lung attenuation due to a reduction in lung volume.

2.4.2.2. Manganese contrast media

ii. *Manganese chloride*

Manganese chloride is a solution instillation using a 4.7 T magnet has been experimentally evaluated in the rat lung (Gobbo et al., 2012). No clinical application has been noted in feline imaging.

Section 3 - Feline hepatobiliary anatomy and a review of hepatobiliary disease and lung anatomy.

3.1 Feline hepatobiliary anatomy and hepatobiliary disease

3.1.1 Feline hepatic and biliary anatomy:

It is essential to understand the anatomy of the feline hepatobiliary system when undertaking hepatobiliary imaging studies. The feline liver is the largest accessory gland associated with the digestive system and the largest internal organ. It is composed of the right lateral, right medial and caudal lobe (caudate and papillary processes), the left lateral, left medial and quadrate lobes, with the hepatic parenchyma containing arteries, veins (portal and hepatic) and a network of bile ducts that comprise the intra-hepatic portion of the biliary system (Rojo Rios et al., 2023).

The liver consists of a functional and metabolic venous drainage system. The portal veins are functional veins and transport products of the digestive system through the portal vein to the liver whereby nutrients and toxins are processed by the hepatocytes (Rojo Rios et al., 2023). The metabolic system comprises the principal hepatic veins that drain into the caudal vena cava (Rojo Rios et al., 2023). The hepatic artery provides oxygenated blood to the liver (Rojo Rios et al., 2023).

Bile is composed of bile pigments, bile salts, cholesterol, lecithin, phospholipids and inorganic salts and is formed in the hepatocytes and actively secreted into the bile canaliculi to the interlobular ducts and then the intra and extra hepatic ducts, that then drain into the gallbladder. The gallbladder is a teardrop shaped organ that stores and concentrates bile and is located in the cranioventral abdomen between the right middle and quadrate liver lobes and has a short cystic duct that connects it with the long and sinuous common bile duct (CBD) (Neer, 1992; Center, 2009; Ettinger and Feldman, 2010). The gallbladder has a volume of approximately 1 ml/kg body weight (Ettinger and Feldman, 2010; Neer, 1992). Duplex gallbladders or accessory gallbladders are reported in one in eight cats and duplex cystic ducts have been observed in some cats (Woods, 2012; Otte et al., 2017).

There are varying descriptions of the feline vascular and biliary anatomy in the literature (Rojo Rios et al., 2023; Jaffey, 2022). Rojo Rios et al. (2023) found that bile from the right hepatic (lateral and medial) and caudate (caudate and papillary process) liver lobes enter the right intra hepatic duct, bile from the papillary process goes into the right and left intra hepatic ducts and bile from the left hepatic lobe (lateral and medial) and quadrate liver lobe, and a branch from the caudate lobe (caudate process) enters the left intra hepatic duct. The intra hepatic ducts then emerge from the liver as the extra hepatic ducts. The right extra hepatic duct flows into the cystic duct. The left extra hepatic duct and the cystic duct form the CBD. The CBD joins the ascending duodenum at the major duodenal papilla

(MDP). Rojo Rios et al. (2023) state that other studies have noted variations in these systems including a more recent paper by Rahmani et al. (2023a) showing the left and right extra hepatic ducts join the cystic duct together to form the CBD. It is likely that anatomic variations of the biliary anatomy exist within the species.

Bile formation is important as it facilitates excretion of endogenous and exogenous waste products and allows for the efficient digestion and absorption of lipids in the intestinal lumen (Jaffey, 2022). Gallbladder contraction is initiated by cholecystokinin and bile is released into the CBD via the MDP and through the sphincter of Oddi, a muscular valve that controls the flow of bile and pancreatic secretions into the duodenum (Jaffey, 2022a). Disruptions to this passage can result biliary disease.

80% of cats have a biliary ductal anatomy wherein the CBD fuses with the major pancreatic duct, in an ampulla before draining into the duodenum forming the MDP, approximately three centimetres caudal to the pylorus (Jaffey, 2022a; Center, 2009; Marolf et al., 2012; Marolf, 2016). This anatomical difference in cats, in part predisposes them to inflammatory hepatobiliary tract disease, because of the frequent concurrence of pancreatic and biliary disease and because infection or inflammation can more easily spread to the adjacent structures due to their close proximity, including the intestinal tract, pancreas and biliary system (Mayhew, 2002; Marolf, 2017; Gaschen, 2009; Brain et al., 2005). Only 20% of cats have an accessory pancreatic duct that enters the duodenum through the minor duodenal papilla, two centimetres distal to the MDP (Center, 2009; Mayhew, 2002).

3.1.2 Feline hepatobiliary disease with an emphasis on biliary disease:

Feline hepatobiliary anatomy causes differences in the aetiology of hepatobiliary disease in cats compared to other species. It is important to understand the breadth of hepatobiliary diseases affecting cats, as this can improve a timely diagnosis. In particular, since cats with hepatobiliary disease often present with non-specific clinical signs including vomiting, diarrhoea, anorexia, lethargy, abdominal enlargement and pain, icterus and rarely haematemesis (Neer, 1992; Zoran, 2012). Clinical signs can be mild, may wax and wane for weeks or can rarely present peracutely. Cats with severe hepatic pathology may have only a mild to moderate increase in the serum liver enzyme activity (Newell, 1996; Leveille et al., 1996; Neer, 1992). Therefore, the specific cause of feline hepatic disease remains a diagnostic challenge in veterinary medicine, as clinical signs and physical examination findings are similar for most hepatobiliary disorders (Newell, 1996; Leveille et al., 1996; Neer, 1992; Gaillot et al., 2007).

Biliary disease is more common in cats than disease of the hepatic parenchyma and is likely in part due to the cat's biliary ductal anatomy wherein the CBD joins with the pancreatic duct prior to entry onto the duodenal papilla (Spillmann et al., 2014; Marolf et al..2012; Otte et al., 2017). The hepatic parenchyma is usually affected secondarily to systemic disease, while the biliary system is the primary target for infectious agents (e.g. bacteria and flukes) and non-infectious conditions e.g. neoplasia and cysts (Otte et al., 2017). Histologic sampling is recommended to distinguish between multiple diffuse liver

diseases and the best predictors of hepatic malignancies in cats are concurrent abnormalities in the spleen and abdominal lymph nodes (Marolf et al., 2012). The world small animal veterinary association (WSAVA) liver standardisation group categorised feline and canine hepatic disease into four main groups (Van den Ingh et al., 2006): non-neoplastic parenchymal diseases, neoplastic diseases, biliary disease and vascular disorders.

3.1.2.1 Non-neoplastic parenchymal diseases include lipidosis, steroid induced hepatopathy, amyloidosis, cirrhosis, inflammation (hepatitis), necrosis (e.g. toxic hepatopathy, ischaemia, immune mediated), abscessation, granulomas, and metabolic storage disease (Van den Ingh et al., 2006; Gaschen, 2009; Boland and Beatty, 2017; Rojo Rios et al., 2023).

Cats have a unique set of liver diseases that occur more commonly compared with typical diseases in dogs, including hepatic lipidosis, feline cholangiohepatitis complex and infectious hepatopathies (such as feline infectious peritonitis, flukes, histoplasmosis and toxoplasmosis), as well as toxic hepatopathies (Zoran, 2012; Rojo Rios, 2023).

3.1.2.2 Neoplastic diseases include hepatocellular (nodular hyperplasia, adenoma, hepatocellular carcinoma), cholangiocellular (biliary adenoma, biliary carcinoma, and mixed), neuroendocrine (hepatic carcinoids), primary vascular and mesenchymal (haemangiosarcoma, fibrosarcoma, leiomyosarcoma, myelolipoma), haematopoeitic (lymphoma and histocytic sarcoma, mastocytosis) and metastatic neoplasia (Van den Ingh et al., 2006; Gaschen, 2009; Zoran, 2012).

3.1.2.3 Biliary disease has been classed into four main morphologic categories:

i. Biliary cystic disease and biliary atresia

Biliary cystic disease can be congenital or acquired. Congenital biliary cystic diseases often affect cats especially Persians and solitary biliary cysts and choledocal cysts (segmental dilation of the CBD) have been reported uncommonly and are classified depending on shape, extent and location (Cullen, 2009; Spillmann et al., 2014; Grand et al., 2010; Best et al., 2010; Spain et al., 2017). Biliary atresia is a rare congenital abnormality and has been reported in a 6 month old cat (Hampson et al., 1987; Van den Ingh et al., 2006). Gallbladder agenesis has been described in two cats (Noguchi et al., 2023; Balakrishnan et al., 2006).

Primary tumours of the gallbladder and biliary tree are rare (Ettinger and Feldman, 2010). Biliary cystadenomas in cats are uncommon benign liver tumours that are distinct from polycystic disease of the kidney and liver (Nyland et al., 1999; Adler and Wilson, 1995). They comprise greater than 50% of all feline hepatobiliary tumours affecting older cats (male predisposition) (Ettinger and Feldman, 2010). The origin in humans and animals is not determined, however congenital and developmental origins are suspected (Adler and Wilson, 1995). They commonly arise from the intra hepatic bile ducts and less frequently from the extra hepatic bile ducts and are often an incidental finding by palpation, ultrasonography, radiography or computed tomography (Nyland et al., 1999; Adler and

Wilson, 1995; Ettinger and Feldman, 2010). They can be focal, multifocal and involve single or multiple hepatic lobes and are slow growing with malignant transformation reported that is characterised by the presence of calcification or large solid tumour component (Adler and Wilson, 1995; Ettinger and Feldman, 2010).

Ultrasonographic findings of biliary cystadenomas are variable, however they must include a cystic component within the mass as well as an histopathologic diagnosis (Nyland et al., 1999; Adler and Wilson, 1995). Differential diagnoses include other cystic liver lesions such as hepatic or biliary cysts, haematomas or abscess, parasitic cysts, tortuous biliary structures or other liver tumours such as cystadenocarcinoma, cholangiocarcinoma, haemangiosarcoma or feline polycystic disease of the liver or kidney (Nyland et al., 1999). Certain metastatic masses such as pancreatic or ovarian adenocarcinoma can also produce cystic masses within the liver (Nyland et al., 1999).

ii. Cholestasis

Cholestasis is impaired bile flow associated with dysfunction of the biliary tree and is characterised by either intra hepatic or extra hepatic causes. Intra hepatic cholestasis is associated with a wide spectrum of hepatic diseases including developing secondary to bile duct destruction and fibrosis as part of the cholangitis syndrome and is normally diagnosed by histopathology (Van den Ingh et al., 2006; Woods, 2012). Some cholestatic drugs e.g. methimazole, cyclosporin, rifampicin and cloxacillin and endotoxins have been associated with reduced bile flow (Otte et al., 2017). Extra hepatic cholestasis due to biliary obstruction (EHBO) is uncommon in cats and can be caused by any pathologic process that obstructs the flow of bile from the liver and gallbladder into the duodenum, causing stasis of bile and dilatation of the bile ducts proximal to the obstruction (Leveille et al., 1996; Van den Ingh et al., 2006). Causes of EHBO in the cat include extra luminal compression, intra luminal obstruction (choleliths, mucinous cystic hyperplasia) or mural thickening (neoplasia or inflammatory processes) (Leveille et al., 1996; Gaillot et al., 2007; Buote et al., 2006; Van den Ingh et al., 2006). The most common causes of EHBO in the cat include cholelithiasis (including microlithiasis and sludge), cholangitis, cholecystitis, and impaired contractility of the gallbladder, as well as less commonly pancreatitis, biliary neoplasia, biliary mucocoele, parasitic infection, diaphragmatic hernia and foreign body obstruction (Mayhew, 2002; Woods, 2012; Leveille et al., 1996; Linton et al., 2015; Otte et al., 2017). Tumours of the pancreas and duodenum or tumours and abscess of the hilus of the liver and portal lymph nodes may also cause compression of the bile ducts (Leveille et al. 1996; Gaschen, 2009).

Multiple studies have shown that cats with cholangitis (39% - 65%) have pancreatitis concurrently (Marolf et al., 2012). In these cats, reflux of the pancreatic secretions into the feline biliary tree can predispose them to cholestasis and ascending infection (Brain et al., 2005). As cats have high numbers of bacteria in their proximal small intestine, the reflux of duodenal contents into the pancreatic and biliary systems is more pathogenic compared to other species by causing secondary bacterial colonisation (Brain et al., 2005). Inflammatory bowel disease can compound these issues, as abnormalities in intestinal

motility can cause further reflux of intestinal contents into the CBD (Brain et al., 2005). In acute feline pancreatitis, a temporary reversible obstruction of the CBD can occur from external compression (Mayhew, 2002; Brain et al., 2005). Since the CBD passes adjacent to the pancreatic parenchyma before fusing with the pancreatic duct and entering the duodenum, pancreatic swelling, oedema or fibrosis can cause obstruction of the CBD (Mayhew, 2002). The association of these co-morbidities pancreatitis, inflammatory bowel disease and cholangitis syndrome is termed ‘triaditis’ (Day, 2016). Microlithiasis or sludged bile can also transiently obstruct the distal CBD causing intermittent bile duct occlusion and idiopathic pancreatitis in the cat (Center, 2009). The shorter distance between the entrance of the MPD and the CBD into the duodenum in cats, compared to the dog can result in smaller lesions causing obstruction of both the pancreatic duct and CBD (Neer, 1992).

Cholelithiasis and choledocolithiasis (stones in the CBD) account for less than one percent of cats with liver disease, with most cases being diagnosed at necropsy (Neer, 1992). Feline choleliths contain cholesterol, bilirubin derivatives and calcium salts and can be mineralised or non-mineralised (Ettinger and Feldman, 2010; Gaschen, 2009). Cholelithiasis can be asymptomatic or the cause or result of EHBO, and can be in the gallbladder lumen or bile ducts where they can potentially cause an obstruction (Mayhew, 2002; Center, 2009; Gaschen, 2009). Experimental ligation of the CBD results in bile sludging and cholelith formation in the canine gallbladder within three days of ligation (Mayhew, 2002). In cats, although bile sludging occurs, prolonged experimental ligation (up to 42 days) of the CBD failed to induce cholelith formation (Mayhew, 2002). Choledocholiths can also be primary, such as those developing directly in the CBD or secondary, forming in the gallbladder and then passing into the CBD (Ettinger and Feldman, 2010).

The site, severity and chronicity of the obstruction, as well as the compliance of the biliary tree and the elasticity of the liver are potential factors contributing to the variation in dilation of the different segments of the biliary tree (Gaillot et al., 2007). The CBD should be less than 4mm diameter in normal cats in non-obstructive biliary disease (Leveille et al., 1996). A CBD greater than 5mm is suggestive of post hepatic obstruction with the degree of CBD dilation influenced by the duration of biliary obstruction (Leveille et al., 1996). A shorter duration of clinical signs is associated in cats with choleliths, compared to EHBO from inflammation or tumours (Gaillot et al., 2007).

Factors that determine the preferential dilation of extra hepatic or intra hepatic ducts have not yet been elucidated (Gaillot et al., 2007) and extra hepatic and intra hepatic ducts are not usually visible ultrasonographically in normal cats (Leveille et al., 1996). Ninety percent of cats with biliary tract obstruction had ultrasonographically visible dilated intra hepatic and/or extra hepatic ducts (Gaillot et al., 2007). Intra hepatic duct dilation is reported to take 5 - 7 days following an obstruction (Ettinger and Feldman, 2010). This is a similar finding in dogs and humans where intra hepatic dilation has been considered an early sign of biliary obstruction and may be evident ultrasonographically within 24 - 48 h of complete obstruction (Neer, 1992; Gaillot et al., 2007). Dilation of the intra-hepatic and/or extra-

hepatic ducts can be suggestive, but not definitive of EHBO as it has also been associated with non-obstructive hepatobiliary disease (Gaillot et al., 2007). Relief of the obstruction also does not lead to an immediate reduction in diameter of the dilated ducts (Gaschen, 2009). After prolonged distension of the CBD in dogs, loss of elasticity of the duct can result in permanent distension, although gallbladder enlargement usually resolves (Mayhew, 2002). Gallbladder dilation is also an unreliable sign of EHBO as it was seen variably in 38% (Buote et al., 2006), 43% (Gaillot et al., 2007), or 62% (Mayhew et al., 2002) of cats with EHBO. Icteric cats may also require serial imaging as definitive signs of EHBO can become evident over time, although other diagnostic modalities such as CT and scintigraphy may be helpful in assessing patients with suspected EHBO despite the requirement for anaesthesia (Buote et al., 2006).

Radiographs can detect about 50% of choleliths, yet other radiographic signs of EBDO are non-specific and as such currently ultrasonography has been reported as the best and most cost-effective method for evaluating the biliary system in cats and dogs with reports up to 85% accuracy for diagnosis of EHBO in cats (Buote et al., 2006). Ultrasonography is also useful in examining other organs such as the liver, pancreas and intestine (Buote et al., 2006). Other studies have shown variable ultrasonographic detection rates of obstructive cholelithiasis ranging from 20% (Mayhew et al., 2002) to 88% (Eich and Ludwig, 2002), which is likely due to technical difficulties imaging the distal portion of the CBD with bowel gas preventing accurate assessment (Gaillot et al., 2007).

Biliary carcinomas can cause cholestasis and are the most common feline hepatobiliary tumour and second most common in dogs (Ettinger and Feldman, 2010). Cats tend to have both intra hepatic and extra hepatic biliary duct tumours, in contrast to dogs which commonly arise from the intra hepatic ducts and rarely in the gallbladder (Ettinger and Feldman, 2010). Often tumours are advanced at the time of diagnosis with metastasis common, as they are diagnosed as a result of biliary obstruction (Ettinger and Feldman, 2010). Ductal carcinomas are reported to have irregular wall thickening (Gaillot et al., 2007). Ultrasonographic features have been reported to be unhelpful in differentiating tumour from inflammatory disease in 82% of masses as the size, shape, echogenicity and location of the masses were similar (Gaillot et al., 2007).

Differentiating the cause of cholestasis is important because surgical intervention of an EHBO may be necessary and mortality has been found to be associated with the underlying cause, with tumours having the highest mortality rate and choleliths the lowest (Gaillot et al., 2007; Leveille et al., 1996).

iii. Cholangitis

Feline inflammatory hepatobiliary disorders are usually centred on the biliary tract with secondary involvement of the hepatic parenchyma (Brain et al., 2005). Cholangitis targets the bile ducts with variable bile duct proliferation and fibrosis (Marolf et al., 2013). In 2003 the WSAVA's liver disease and pathology standardisation research group reclassified cholangitis/cholangiohepatitis complex in cats into three groups: neutrophilic (acute or chronic) cholangitis, lymphocytic cholangitis and chronic cholangitis (Marolf et al., 2013;

Cullen, 2009; Brain et al., 2005; Boland and Beatty, 2017). Cats with cholangitis or cholecystitis may not be icteric (Brain et al., 2005). Inflammatory disease has also been reported to be the most common or second most common hepatic disorder in cats after idiopathic hepatic lipidosis (Marolf et al., 2012; Ettinger and Feldman, 2010; Boland and Beatty, 2017). Hirose et al. (2014) diagnosed inflammatory liver disease in 50% of abnormal biopsies submitted to Japan and 25.7% of cases in the United States had inflammatory disease and 49.7% had hepatic lipidosis (Gagne et al., 1996).

A gallbladder wall thickness greater than one millimetre (mm) using ultrasonography has been shown to accurately predict gallbladder disease in cats (Hittmair et al., 2001). Intra and extra hepatic dilation of the biliary tree and pancreatitis may also be present in cats with cholangitis (Marolf et al., 2012; Ettinger and Feldman, 2010). Ultrasonography was also shown to be 87% sensitive and 90% specific in the diagnosis of cholangitis (Newell et al., 1998). As in humans, gallbladder debris/sludge in cats may be correlated with the clinical history of fasting or indicate either intra or extra hepatic cholestasis or intrinsic gallbladder disease and thickening of the bile duct wall may be seen (Marolf et al., 2012; Gaschen, 2009).

As well as ascending infection, obstructive abnormalities of the biliary system such as congenital anomalies, cholelithiasis or neoplasia also predispose cats to cholecystitis and acute neutrophilic cholangitis (Brain et al., 2005). Bacterial colonisation of the gallbladder may develop due to either biliary reflux of intestinal bacteria, haematogenous or lymphatic dissemination (Brain et al., 2005). A normal biliary-enterobacterial cycle allows rapid elimination of bacteria from bile (Brain et al., 2005). In feline cholelithiasis, a concurrent hepatobiliary infection with enteric bacteria is a common finding (Brain et al., 2005; Mayhew, 2002). Cats presenting with neutrophilic cholangitis were normally young to middle aged cats, however it has been diagnosed in patients up to 12 years old and commonly has an acute onset of pyrexia, lethargy and anorexia of five days duration or less (Brain et al., 2005). Bile duct dilation and gallbladder wall changes may not occur in cats with neutrophilic cholecystitis (Gaschen, 2009).

Cytologic and microbial evaluation should be completed by ultrasonography guided cholecystocentesis in cases of suspected acute neutrophilic cholangitis or cholecystitis, however there are risks of gallbladder rupture associated with this procedure (Center, 2009; Brain et al., 2005). Surgical exploration may be preferable when there is ultrasonographic evidence of severe cholecystitis, concurrent infiltrative enteropathy or acute severe pancreatitis (Brain et al., 2005).

Lymphocytic cholangiohepatitis is also common in cats and cannot be differentiated from neutrophilic cholangitis sonographically except that cats with lymphocytic cholangitis are more likely to develop free abdominal fluid (Brain et al., 2005; Marolf et al., 2013).

Chronic cholangitis can occur from long term inflammation of the bile ducts including bacterial infection and immune mediate conditions and is also associated with liver fluke. Some species of fluke readily infect the biliary tree and liver of cats (Platynosomum concinnum and Amphimerus pseudofelineus) with no known breed or sex predilection

(Ettinger and Feldman, 2010). Metochis conjunctus a human liver fluke and Eurytrema procyonis, a feline pancreatic fluke can also be found in the biliary tree of cats. Outdoor predatory cats are at increased risk in endemic areas of SE USA, Carribean or Hawaii and China, Japan, SE Asia and Northern Europe (Ettinger and Feldman, 2010). Bacterial cholangitis, ductal fibrosis and extra hepatic biliary obstruction are known sequelae to parasitic cholangitis (Ettinger and Feldman, 2010). Abdominal radiographs are unremarkable other than possible hepatomegaly, yet ultrasonography can reveal ductal dilation and biliary obstruction secondary to its obstruction from fibrosis (Neer, 1996).

iv. Disease of the gallbladder such as mucocoeles, cholecystitis and infarction (Van den Ingh et al., 2006; Gaschen, 2009; Cullen, 2009).

Gallbladder mucocoele is rare in the cat with only three reported cases (Woods, 2012) and may be because cats have fewer mucous glands in their gallbladder compared to dogs (Center, 2009). Ultrasonography is considered the gold standard for diagnosis of canine biliary mucocoeles (Woods, 2012). The traditional ultrasonographic striated hyperechoic ‘kiwi fruit’ appearance in dogs is not reported in cats and they seem to have the appearance of the ‘early’ canine biliary mucocoele (Woods, 2012). Woods (2012) reported that the biliary mucocoele in their patient was not detected ultrasonographically, possibly because of immobile hypoechoic mucous which is better visualised ultrasonographically when surrounded by echogenic bile which was not present in their case.

Cholecystitis is more common in cats than dogs and is generally associated with bacterial infections (Gaschen, 2009). Cholecystitis is used to describe inflammatory conditions of the gallbladder, as well as gallbladder related symptoms without choleliths and encompasses a variety of acute and chronic disease with and without bacterial or parasitic infections (Ettinger and Feldman, 2010). Predisposing factors in cats include bile stasis, gallbladder mucocoele, ascending bacterial or parasitic diseases, biliary neoplasia, infarction and haematogenous spread of bacteria or blunt trauma (Center, 2009; Ettinger and Feldman, 2010). Necrotising cholecystitis can occur with or without gallbladder rupture and bile peritonitis and requires prompt surgical intervention as it has increased risk of complications and higher mortality rate (Ettinger and Feldman, 2010; Center, 2009). Emphysematous cholecystitis is a rare manifestation of acute cholecystitis complicated by gas producing organisms such as Escherichia coli and Clostridium perfringens and is frequently associated with perforation and death in humans (Neer, 1992; Ettinger and Feldman, 2010). Gas accumulation in the lumen, wall or pericholecystic tissues is extremely rare in the cat and rare in the dog (Neer, 1992). In humans, it occurs most commonly in the elderly with predisposing causes include cystic artery infarction and cholelithiasis with human diabetics comprising up to 40% of patients (Ettinger and Feldman, 2010). Radiographically, emphysematous cholecystitis is seen as a spherical ovoid to gas opacity superimposed over the hepatic silhouette (Gaschen, 2009). On ultrasonography irregular or pinpoint sized hyperechoic structures that produce ring down artefacts in the gallbladder or liver parenchyma should consider cholecystitis, cholangitis, choledochitis or abscess formation as differentials (Gaschen, 2009). Depending on the amount of reverberation artefact from the gas and the gallbladder wall, echogenic

sediment and fluid may or may not be seen (Ettinger and Feldman, 2010). CT is ideal to visualise gas in the gallbladder lumen, wall and biliary ducts (Ettinger and Feldman, 2010). Cholecystocentesis is contraindicated in emphysematous cholecystitis as sepsis secondary to anaerobic bacterial infection is likely (Brain et al., 2005).

Neoplastic disease of the gallbladder wall can cause focal thickening and is less common than benign cystic hyperplasia of the mucous glands which appear as broad-based or pedunculated hyperechoic structures (Gaschen, 2009).

Gallbladder torsion and porcelain gallbladders are extremely rare in dogs (Neer, 1992). Radiographically a porcelain gallbladder is partially to completely mineralised radio-opacity and ultrasonographically, there is a highly echogenic gallbladder with curvilinear appearance that casts a distinct acoustic shadow. In humans, there is an increased risk for biliary neoplasia and cholecystectomy is the treatment of choice (Ettinger and Feldman, 2010). Gallbladder infarction with necrotising cholecystitis has also been documented in 12 dogs (Ettinger and Feldman, 2010). Neither of these disorders have been reported in the feline veterinary literature.

Biliary tract rupture and secondary bile peritonitis can occur from pathologic rupture secondary to calculi, cholecystitis and blunt and/or sharp abdominal trauma such as automobile injuries and are rare in the cat. Bile leakage can also occur after bile duct damage during surgery or after post-operative surgical complications such as dislodging of clips or wound dehiscence of an anastamosis with bile normally collecting close to the source, although it may occasionally have a more remote location (Heoffel et al., 2006). A retrospective study of dogs showed that there was a strong correlation between the cause of biliary tract rupture and the site of the rupture (Neer, 1992). For example, ductal rupture was associated with blunt abdominal trauma whereas gallbladder rupture was associated with cholelithiasis and/or cholecystitis (Neer, 1992). Biliary rupture has been described in a cat with gallbladder agenesis with concurrent choledolithiasis (Noguchi et al., 2023).

Sonographic signs of rupture include loss of the gallbladder wall continuity, hyperechoic surrounding mesentery and free peritoneal fluid and is 85% sensitive (Gaschen, 2009). MRCP without contrast is useful in the diagnosis of bile leaks, however it doesn’t provide functional information and only shows indirect evidence of bile leakage such as ascites, peri-hepatic fluid collections and soft tissue oedema (Heoffel et al., 2006). Mangafodipir trisodium and Gd-EOB-DTPA, IV hepatobiliary contrast media have shown anatomic localisation of the biliary tract and detection of bile collections and bile extravasation from injured bile ducts in humans (Heoffel et al., 2006; Lee et al., 2009).

3.1.2.4 Vascular disorders that include congestion, portosystemic shunts, portal vein thrombosis or compression, portal hypertension, portal vein hypoplasia, arteriovenous fistula (Gaschen, 2009).

3.2 Feline lung anatomy

Knowledge of the anatomy of the feline lung is important when evaluating imaging for pathologic or non-pathologic changes and to prioritise differential diagnoses. The function of the respiratory system is similar to humans and is divided into two parts, the conducting system to provide oxygen to support tissue metabolism and the exchange system to remove carbon dioxide (McDonough and Southard, 2017). The conducting system consists of the oral and nasal cavities, pharynx, larynx, trachea, bronchi and proximal bronchioles and no gas exchange occurs in this system (McDonough and Southard, 2017). Cat lung lobe anatomy and lung parenchyma differs to humans and as such, different terminology is used in cats compared to people. (Greco et al., 2023; Masseau and Reinero, 2019). Cats lack a secondary pulmonary lobule which likely changes the appearance of pulmonary pathology in cats and as such, pulmonary pathology and imaging findings cannot be directly extrapolated from data in people (Masseau and Reinero, 2019). Cats have a left side of the lung that has a left cranial lung lobe divided into cranial and caudal parts by an intralobar fissure and a left caudal lung lobe; and the right side of the lung is divided into four sections: a right cranial, middle, caudal and accessory lobe (Masseau and Reinero, 2019). The trachea bifurcates into the left and right principal bronchus. The right cranial bronchus, right middle bronchus, right accessory bronchus and the right caudal lobar bronchi exit from the right principal bronchus and the left cranial lobar bronchus and left caudal bronchus exit from the left principal bronchus (Caccamo et al., 2007). From the lobar bronchi, the segmental and sub segmental bronchi branch into proximal bronchioles (Caccamo et al., 2007). Distal to the proximal bronchioles is the gas exchange system, which includes the respiratory bronchioles, alveoli, alveolar capillaries and the thin respiratory membrane that separates the alveolar spaces from the capillary lumens (McDonough and Southard, 2017).

The lung is predominantly composed of air, with less percentage of lung tissue which consists of alveoli, interstitial tissue, bronchial walls and blood. The lungs have dual blood supply, with oxygenated blood travelling to the lungs via the bronchial circulation (via the broncho-oesophageal artery and the right apical bronchial artery) and deoxygenated blood travelling via the pulmonary circulation (pulmonary artery) (Gulati and Balasubramanya, 2024). Oxygenated blood is transported away from the lungs via the pulmonary veins into the left atrium and the bronchial veins drain into the azygous vein.

The feline thorax is narrowed ventrodorsally and more elongated compared to the dog (Larson and Berry, 2023). It is unknown whether this variation may change the characteristics of lung density and atelectasis in cats compared to dogs and people.

Section 4 - Research Publications:

4.1 Chapter 1 - Developing a novel protocol for hepatic computed tomography and cholangiography by use of gadoxetic acid in healthy cats

Cats with hepatobiliary disease commonly present with non-specific clinical signs, making a timely diagnosis difficult. Imaging plays an important role in the diagnosis of the cause of hepatobiliary disease to accurately prognosticate and guide therapeutic options to improve the patient's outcome. There is currently no gold standard imaging technique to investigate hepatobiliary disease in cats. Iodine based contrast media have been used more commonly in the past to investigate the cause of hepatobiliary disease, however gadolinium contrast is currently being investigated. Newer gadolinium-based hepatobiliary contrast media with higher hepatobiliary excretion rates and fewer reported side effects have shown promising results in humans and dogs with CT. CT is also increasingly utilised in veterinary medicine due to its advantages, such as being fast and repeatable, with increased availability and good sensitivity of visualisation of cross-sectional anatomy. Based on previous research data that showed Gd-EOB-DTPA at 0.3 mmol/kg IV in dogs showed adequate biliary contrast enhancement in sedated dogs using CT (Chau et al., 2017), we investigated the feasibility of Gd-EOB-DTPA using CT in cats for hepatic imaging and cholangiography. Further potential benefits of this study are that CT can be used in patients with metallic implants and gadolinium-based contrast media can be used in patents with iodine sensitivities.

We hypothesised that there would be similar enhancement in the hepatobiliary tract in healthy cats using Gd-EOB-DTPA compared to previous studies in dogs and humans. Further, the aim of this study was to investigate the utility and safety of Gd-EOB-DTPA, a positive gadolinium-based contrast media in healthy cats at three doses, to determine the optimal timing for hepatobiliary image acquisition and evaluate the contrast-enhanced hepatobiliary anatomy. Gd-EOB-DTPA has not been reported in cats prior to this study and was the only hepatobiliary contrast media available in Australia at the time of the study.

CT cholangiography and hepatic imaging was performed experimentally in five healthy research cats 0, 5, 25, 45, 65, and 85 minutes after IV administration of a functional and morphologic contrast media, Gd-EOB-DTPA at low (0.0125 mmol/kg), medium (0.1 mmol/kg), and high (0.3 mmol/kg) doses. Hepatobiliary enhancement for each dose was objectively assessed over time using attenuation (HU) of predetermined regions of interest (ROIs) including the liver, gallbladder, cystic duct, bile duct and hepatic ducts and by use of a subjective semiquantitative visual assessment score using two board certified veterinary radiologists and a third year radiology resident to separately assess the anonymised and randomised CT images of each cat at 65 minutes after injection of each of the three doses of contrast agent, using a scoring system to grade visualisation on a scale of 0 to 3 (0 = absent, 1 = poor contrast enhancement with ill defined borders, 2 =

moderate contrast enhancement with incomplete delineation of borders and 3 = excellent contrast enhancement along the length of the duct with well defined borders throughout the entire length of the duct). The ability to visually detect contrast media in the duodenum (yes or no) was also scored and whether there was motion artefact (yes or no).

Statistical analysis was performed with a $P<0.05$ (Genstat, version 17) for the liver, gallbladder, cystic duct and bile duct by use of restricted maximum likelihood model to assess the timing and effect of the dose of contrast agent on enhancement. The objectively determined enhancement values (HU) were square root transformed to ensure normality of the data. Fixed effects included age, body weight, timing, anatomic structure, and dose of contrast media. Visual assessment scores were analysed by use of ordinal logistical regression. Fixed effects included the dose of contrast media and the investigator. Both of the fixed effects and the interaction between the fixed effects were evaluated.

In our study, we demonstrated that Gd-EOB-DTPA was safe to use in healthy cats at a dose of up to 0.3 mmol/kg with a normal post contrast physical examination and no significant changes in complete blood count, serum biochemistry and urinalysis 48 hours after contrast administration and with normal vitals performed every 8 h for 3 - 5 days after injection and two weeks after each contrast dose at the research facility. No contrast related adverse side effects were documented at 0.0125 mmol/kg, 0.1 mmol/kg and 0.3 mmol/kg doses. Further, using CT we demonstrated that each increase in dose of contrast medium resulted in a significant increase in HU across the hepatobiliary system ($P<0.001$). The timing of hepatobiliary enhancement was different in the cat, with the liver parenchyma having a significantly higher HU at 45 mins, with homogenous enhancement at all doses of contrast medium. The contrast-enhanced cystic and bile duct HU were significantly higher and maximal at 65 mins with the contrast-enhanced gallbladder HU not plateauing by 85 mins. Using the visual assessment scoring system, at a high dose of contrast medium, 12 of 60 (20%) biliary tract scores indicated no enhancement (score of 0), 34 (57%) indicated poor enhancement (score of 1), and 14 (23%) indicated moderate enhancement (score of 2). This study demonstrated that no cat had excellent enhancement of the biliary tract (score of 3) at any dose of Gd-EOB-DTPA. Contrast was not observed in the duodenum in any cat at any dose of contrast medium.

Despite the small size of the normal hepatobiliary tract in healthy cats, CT provided an excellent imaging modality for identifying and evaluating the cross-sectional anatomy with objective measurements (HU) and semiquantitative subjective assessment of all regions of the contrast enhanced hepatobiliary tract in anaesthetised healthy cats in sternal recumbency. Anaesthesia also allowed for excellent image quality with no motion artefact observed in any of the scans.

The limitations of this study include the small number of cats in each phase. Also, a single investigator performing the objective contrast measurements of the hepatobiliary system may have introduced bias. As the feline biliary tract is small and tortuous, measurements were difficult to obtain in some cats and may have included additional sampling error or

volume averaging. The study ended at 85 minutes and the plateau and any decline in enhancement for the gallbladder were not identified, therefore we cannot be certain that maximum enhancement was identified. Additional anaesthesia time did not appear warranted given the data from human and canine studies.

Despite the lack of excellent visual contrast enhanced opacification to improve conspicuity of the biliary tract in healthy cats within the time frame used in the study, the objective results of the increased density of the liver with Gd-EOB-DTPA may be useful in future imaging using CT to assess liver function or in assessment of the liver parenchyma in cats with hepatic pathology. This study may also guide future investigations into the use of Gd-EOB-DTPA enhanced hepatic CT imaging and/or hepatic MRI imaging and potentially MR cholangiography in cats where typically lower doses of Gd-EOB-DTPA are required.

Publication 1

Authors: Pilton, J. L., Chau, J., Foo, T. S., Hall, E. J., Martinez-Taboada, F., Podadera, J. M., & Makara, M. A.

Title: Hepatic computed tomography and cholangiography by use of gadoxetic acid in healthy cats.

Year or Publication: 2019

Journal: American journal of veterinary research 80(4), 385–395.

Hepatic computed tomography and cholangiography by use of gadoxetic acid in healthy cats

Joanna L. Pilton BVSc
Jennifer Chau BVSc
Timothy S. Foo BVMS
Evelyn J. Hall BScAgr, PhD
Fernando Martinez-Taboada LV
Juan M. Podadera Dr Med Vet
Mariano A. Makara Dr Med Vet

Received June 4, 2018.
Accepted September 4, 2018.

From the Units of Diagnostic Imaging (Pilton, Chau, Foo, Podadera, Makara) and Anaesthesia (Martinez-Taboada), School of Veterinary Science, Faculty of Science, and School of Life and Environmental Sciences (Hall), Faculty of Science, University of Sydney, Sydney, NSW 2006, Australia.

Address correspondence to Dr. Pilton (joanna.pilton@sydney.edu.au).

OBJECTIVE
To evaluate 3 doses of gadoxetic acid (Gd-EOB-DPTA) for hepatic CT and cholangiography in cats and to determine optimal timing for hepatobiliary image acquisition and evaluation of the contrast-enhanced hepatobiliary anatomy.

ANIMALS
6 healthy cats.

PROCEDURES
Cats were anesthetized; sequential CT scans were performed 0, 5, 25, 45, 65, and 85 minutes after IV administration of Gd-EOB-DTPA at low (0.0125 mmol/kg), medium (0.1 mmol/kg), and high (0.3 mmol/kg) doses. Hepatobiliary enhancement for each dose was objectively assessed over time and by use of a subjective semiquantitative visual assessment score.

RESULTS
No contrast-related adverse effects were detected. Each increase in dose of contrast medium resulted in a significant increase in HU across the hepatobiliary system. The liver had a significantly higher number of HU at 45 minutes, with homogenous enhancement at all doses of contrast medium. Contrast-enhanced cystic and bile duct HU were significantly higher and maximal at 65 minutes. Contrast-enhanced gallbladder HU did not plateau by 85 minutes. At a high dose of contrast medium, 12 of 60 (20%) biliary tract scores indicated no enhancement, 34 (57%) indicated poor enhancement, and 14 (23%) indicated moderate enhancement. No cat had excellent enhancement of the biliary tract at any dose.

CONCLUSIONS AND CLINICAL RELEVANCE
Gd-EOB-DTPA–enhanced hepatic CT and cholangiography in cats were safely performed and provided good hepatic enhancement but poor to moderate enhancement of the biliary tract. This technique may be useful for assessing the liver parenchyma in cats, but its value for assessing the biliary tract is questionable. (*Am J Vet Res* 2019;80:385–395)

Hepatobiliary disease is common in cats because of their unique anatomy in which the bile duct and pancreatic duct frequently open concomitantly onto the major duodenal papilla.[1–4] Inflammatory hepatobiliary disease (cholangitis or cholangiohepatitis) is commonly centered on the biliary tract with possible secondary involvement of the hepatic parenchyma.[5,6] It can be evident as neutrophilic, lymphocytic, or chronic cholangitis (associated with liver flukes), with neutrophilic cholangitis often occurring with concurrent pathological conditions such as pancreatitis and inflammatory bowel disease.[7,8] Other pathological conditions of the intrahepatic hepatobiliary system include hepatic lipidosis, primary or metastatic neoplasia, and hepatic cirrhosis.[2,9] Additionally, extrahepatic hepatobiliary pathological conditions including gallbladder mucocele; congenital malformations such as choledochal cysts; disorders of the sphincter of Oddi; and extrahepatic biliary obstruction caused by stricture, malformations, parasites, choledocholiths or sludge, foreign bodies, pancreatitis, abscesses, or nonhepatobiliary neoplasia have also been described.[2,10–16] Regardless of the underlying cause of hepatobiliary disease, cats often have nonspecific clinical signs and biochemical changes that do not reflect the prognosis or functional reserve of the hepatobiliary system.[16–18]

A number of imaging modalities including ultrasonography, radiography, cholecystography, cholangiography, CT, ERCP, MRI, MRCP, and nuclear scintigraphy have been used to evaluate the hepatobiliary system in cats.[2,16–30] These techniques provide information on gross morphological or functional abnormalities of the liver and biliary tract, although findings are generally not disease specific. Other limitations of these techniques include poor sensitivity,

ABBREVIATIONS

ERCP	Endoscopic retrograde cholangiopancreatography
Gd-EOB-DTPA	Gadoxetic acid
MRCP	Magnetic resonance cholangiopancreatography
ROI	Region of interest

reliance on good patient compliance or operator skill (or both), poor visibility of anatomic structures owing to interference from bowel gas, high costs, limited availability, invasiveness, the need for patients to be anesthetized, and a lack of inherent contrast resolution.[1,19,24,26,29] In addition, there are various adverse effects after IV administration of iodinated cholangiographic contrast agents in cats.[21]

The criterion-referenced standard for evaluation of the biliary tract in human medicine is endoscopic retrograde cholangiography, which allows for delineation of the biliary tract with high spatial resolution.[31] The advantage of endoscopic retrograde cholangiography and ERCP is the option for concurrent treatment and collection of biopsy specimens, if required.[26,31–33] Disadvantages include the risk of acute pancreatitis, cholangitis, perforation, and hemorrhage attributable to its invasiveness.[1,26] Although these complications were not reported in a study[26] that involved the use of ERCP in cats, the risks of ERCP appear to outweigh the advantages in cats owing to the fact that their small size makes this technique diagnostically challenging, particularly because choledocholiths and neoplasia seem to be less common in cats than in humans. In other studies,[1,33] it was reported that MRCP was as accurate as ERCP for visual evaluation of the biliary anatomy of humans without being invasive or relying on ionizing radiation or operator skill. Additionally, MRCP enables concurrent assessment of the liver and pancreas as well as the biliary and pancreatic ducts proximal to an obstruction, particularly when combined with standard T1- and T2-weighted sequences.[1,34] When concurrent diagnostic and interventional procedures are not expected, MRCP is the preferred method. In addition, MRCP can be used with hepatocyte-specific contrast agents (eg, Gd-EOB-DTPA). This hepatocyte-specific contrast agent has improved the ability of investigators to visually examine and characterize focal liver lesions and provide both morphological and functional information on the biliary tract of humans,[33–38] dogs,[39–43] rats,[36] and rabbits.[42] Gadoxetic acid enters hepatocytes via an organic ion transport system and is excreted into the biliary system via ATP-dependent glutathione S-transferase.[35] Given the hepatocyte specificity of Gd-EOB-DTPA, use of this contrast agent has resulted in improvements in tumor detection and the ability to distinguish between benign and malignant lesions of hepatocellular or nonhepatocellular origin in the delayed phase, independent of the vascularity of a lesion during early dynamic phase imaging.[36,37] For example, lesions with altered hepatocyte function (eg, hepatic adenoma, nodular hyperplasia, and hepatocellular carcinoma) have variable contrast enhancement, compared with results for normal hepatic parenchyma.[37,39–41] Similarly, metastatic lesions that lack hepatocytes have no contrast enhancement.[37] Additionally, Gd-EOB-DTPA–enhanced MRI can potentially provide quantitative assessment of liver perfusion and hepatocyte function in diffuse liver disease.[37,41] The excretion properties of Gd-EOB-DTPA have also been used in the functional assessment of biliary anatomy with MRI, including bile duct injury, obstruction or stricture; sphincter of Oddi dysfunction; differentiation of biliary from extrabiliary lesions (including bilomas); identification of biliary-enteric anastomoses; and diagnosis of cholecystitis in people.[35]

Because of their paramagnetic properties, gadolinium-based contrast agents typically have been used in combination with MRI. The MRI procedures require only a 5% to 20% molar dose of a metal, compared with the dose needed for CT, to provide diagnostically useful tissue contrast.[42] However, biliary MRI requires a high-field magnet (1.5 T) that is not routinely used at veterinary clinics because of the high cost and limited availability. An alternative imaging modality is CT, which is now widespread at veterinary clinics and has a faster image acquisition time, fewer artifacts, and improved image resolution and reconstruction techniques and may be performed in sedated animals (rather than anesthetized animals).[27,33,41,44,45] Computed tomography frequently is used in human medicine to diagnose pathological biliary conditions.[45] The high atomic number of gadolinium also makes it a good contrast medium for CT.[42] Previous CT evaluations of the abdomen of dogs[41] and humans[38] after administration of gadolinium-based contrast agents revealed adequate visual examination of the liver and biliary tract.

To the author's knowledge, there has been no reported use of Gd-EOB-DTPA in cats. Therefore, the objectives of the study reported here were to determine a dose of Gd-EOB-DTPA that could be safely administered to healthy cats, identify any adverse effects, determine the optimal CT scan time for Gd-EOB-DTPA in the liver and biliary tract, and determine whether Gd-EOB-DTPA could improve visual assessment of the hepatobiliary anatomy via CT in healthy cats. We hypothesized that Gd-EOB-DTPA would be a contrast agent that could be safely used with CT to improve conspicuity of the hepatobiliary system in healthy cats.

Materials and Methods

Animals

Five healthy cats were recruited from a privately owned research facility.[a] All procedures were performed at the veterinary teaching hospital at the University of Sydney. Cats were included in the study when no abnormalities were detected during physical examination, there were no hepatic or renal abnormalities on biochemical analysis and urinalysis, and there were no major changes for a CBC. Ultrasonographic examination[b] of the hepatobiliary system was performed on each cat prior to initial noncontrast CT to rule out preexisting diseases. Cats were excluded from the study when hepatobiliary ultra-

sonography or the initial noncontrast CT revealed abnormalities. The study was approved by the Animal Ethics Committee of the University of Sydney.

Experimental procedures

Three phases of contrast-enhanced CT examinations were conducted for each cat; there was a washout period of at least 1 week between phases. Each phase involved IV administration of a dose of Gd-EOB-DTPA.[c] The first phase involved a low dose of contrast agent (0.0125 mmol/kg); that dose was based on half the recommended clinical dose for humans.[46] The second phase involved a medium dose of contrast agent (0.1 mmol/kg), and the third phase involved a high dose of contrast agent (0.3 mmol/kg).

Before each CT scan was performed, the cats were anesthetized and positioned in sternal recumbency. Alfaxalone[d] (0.2 mg/kg, IM) and butorphanol tartrate[e] (0.2 mg/kg, IM) were administered as preanesthetic medications. Alfaxalone (1 to 2 mg/kg) was administered IV for anesthetic induction to enable tracheal intubation, and anesthesia was maintained with isofluorane[f] in oxygen. During the procedure, a crystalloid solution[g] was administered (5 mL/h, IV), and physiologic variables (heart rate, respiratory rate, noninvasively measured blood pressure, end-tidal carbon dioxide concentration, and oxygen saturation) of cats were monitored continuously.

Apnea was induced by hyperventilation prior to each scan to avoid motion artifact. Each CT scan was conducted in accordance with the same CT protocol. A 16-slice multidetector CT scanner[h] was used. An air calibration was performed every other day, and a quality control scan was performed monthly with an ROI phantom. A helical precontrast scan (0 minutes) and 5 postcontrast scans (5, 25, 45, 65, and 85 minutes after administration of contrast agent) were acquired. Contrast agent was delivered via rapid manual injection, which was followed immediately by rapid administration of a bolus of saline (0.9% NaCl) solution[i] (3 mL, IV). At 90 minutes after injection of the contrast agent, cats were repositioned in dorsal recumbency to assess the distribution of contrast agent within the gallbladder and to subjectively visually assess the bile duct after the change in body position. No objective measurements were obtained while cats were positioned in dorsal recumbency, and these data were not included in the statistical analysis.

The abdomen CT protocol for both sternal and dorsal recumbency involved use of a detector row arrangement of 16 data channels with a detector width of 0.75 mm (16 X 0.75 mm), tube current of 90 mA, and tube potential of 120 kV (peak). The display field of view was determined for each cat; it included the diaphragm cranially and pubis caudally. Images were reconstructed with a slice thickness of 1.5 mm with a soft tissue kernel.

A CBC, biochemical analysis, and urinalysis were performed for each cat 48 hours after each dose of contrast agent. Vital parameters were monitored every 8 hours for 3 to 5 days after injection of the contrast agent. Two weeks after each phase of the study, the cats were examined at the research facility to assess general health.

Image analysis

Objective analysis—One investigator (JLP) objectively measured the number of HU of the hepatobiliary system for various anatomic structures, including the liver, gallbladder, cystic duct, and bile duct. The cystic duct is dorsally directed and was defined as the region from the neck of the gallbladder to the insertion of the hepatic ducts in the region of the porta hepatis.[3] The hepatic ducts were defined as the ducts that drained each lobe of the liver.[3] The hepatic ducts may join to form a common hepatic duct before entering the cystic duct.[3] The bile duct was defined as the portion of the duct distal to the union of the cystic duct and hepatic ducts to its opening onto the major duodenal papilla.[3] The HU of the hepatic ducts were not measured because of the inconsistent ability to visually evaluate the structures.

Standardized ROIs or points of interest were drawn on transverse CT images of each structure on a DICOM workstation and reviewed by use of software.[j] Data for ROIs or points of interest were exported to a spreadsheet,[k] and time-attenuation curves were generated for each part of the biliary tract and liver. When the liver was evaluated, a similar anatomic location was obtained for each ROI (0.5 cm^2), and care was used to not include vessels in the ROIs. For the gallbladder, each ROI (0.5 cm^2) was measured at the dorsal aspect of the gallbladder (neck of the gallbladder) where contrast was visible. In the cystic duct and bile duct, a single point of interest was used to measure enhancement at a location where structures were clearly visible.

Visual analysis—Two board-certified veterinary radiologists (MAM and JMP) and a veterinarian in the third year of a radiology residency program (TSF) separately assessed the CT images of each cat obtained at 65 minutes after injection of each of the 3 doses of contrast agent. Investigators were not aware of the dose administered to each cat, and images were anonymous and randomized. Investigators used a visual assessment scoring system to determine a score for the gallbladder, cystic duct, bile duct, and hepatic ducts (where they were visible from the porta hepatis to the insertion onto the bile duct) and comment on the ability to visually detect contrast agent in the duodenum (yes or no) and whether there was motion artifact (yes or no). Visual detection of contrast agent within these structures was graded on a scale of 0 to 3 (0 = absent, 1 = poor contrast enhancement with ill-defined borders, 2 = moderate contrast enhancement with incomplete delineation of borders, and 3 = excellent contrast enhancement along the length of the duct with well-defined borders throughout the entire length of the duct). This visual assessment

scoring system has been used for evaluation of the biliary system.[41]

Statistical analysis

Statistical analysis was performed with a commercially available software program.[1] For all analyses, significance was set at values of $P \leq 0.05$. Data for the liver, gallbladder, cystic duct, and bile duct were analyzed by use of a restricted maximum likelihood model to assess the timing and effect of the dose of contrast agent on enhancement. The objectively determined enhancement values (number of HU) were square root transformed to ensure normality of the data. Fixed effects included age, body weight, timing, anatomic structure, and dose of contrast agent.

Visual assessment scores of the investigators for each biliary structure (gallbladder, cystic duct, bile duct, and hepatic ducts) were analyzed by use of ordinal logistic regression. Fixed effects included the dose of contrast agent and investigator. Both of the fixed effects and the interaction between the fixed effects were evaluated.

Results

Animals

None of the cats was excluded on the basis of results of the ultrasonographic examination or initial noncontrast CT examination. One cat was excluded during the first phase of the study because it developed pneumomediastinum immediately after intubation and prior to administration of the contrast agent. The pneumomediastinum resolved without any complications. Another cat was recruited to replace this cat for the second and third phases of the study.

One cat developed diarrhea during hospitalization after the first phase; however, this was suspected to be transient or related to the diet because the diarrhea resolved immediately after the cat's diet was changed to a commercially available prescription gastrointestinal diet. This cat was fed the same commercially available prescription gastrointestinal diet during the subsequent phases of the study and had no further episodes of diarrhea.

Evaluation of safety

Gadoxetic acid was safely used in the 4 healthy cats during the first phase (0.0125 mmol/kg, IV) and the 5 healthy cats during the second (0.1 mmol/kg, IV) and third (0.3 mmol/kg, IV) phases. There were no immediate contrast-related reactions and no hematologic, biochemical, or urinary abnormalities at 48 hours after administration of the contrast agent for all of the cats at each dose of contrast agent. There were no physical examination abnormalities at any time after the administration of contrast agent to all cats at each dose.

Objective measurements

Age ($P = 0.21$) and body weight ($P = 0.92$) of cats did not significantly influence objective measurements of the biliary tract. There was a significant ($P < 0.001$) effect of dose of contrast agent on enhancement of all hepatobiliary structures because each increase in dose of contrast agent resulted in a significant increase in the mean number of HU **(Figure 1)**.

For each anatomic structure (liver, gallbladder, cystic duct, and bile duct) and each time point of contrast enhancement, the liver had homogenous contrast enhancement at all doses and had a significantly higher number of HU at 45 minutes, compared with the number of HU at 0, 5, and 25 minutes; however, there was no significant change in the number of HU in the liver after 45 minutes **(Table 1)**. Furthermore, the liver had a significantly higher number of HU than all other anatomic structures (gallbladder, cystic duct, and bile duct) at each time point (0, 5, 25, 45, 65, and 85 minutes; Figure 1). Mean ± SD maximum liver enhancement was 70 ± 6 HU at 0.0125 mmol/kg, 72 ± 15 HU at 0.1 mmol/kg, and 82 ± 17 HU at 0.3 mmol/kg. Mean difference between liver attenuation at time 0 and maximum liver attenuation was 2 ± 3 HU at 0.0125 mmol/kg, 15 ± 2 HU at 0.1 mmol/kg, and 19 ± 5 HU at 0.3 mmol/kg. Number of HU for the gallbladder differed significantly at each time point and did not reach maximum enhancement by 85 minutes after injection of contrast agent. In comparison, the number of HU in the cystic duct and bile duct was significantly higher at 65 minutes than at 0, 5, 25, and 45 minutes **(Figure 2)**. Maximum number of HU in both the cystic duct and bile duct was detected at 65 minutes, and there was no significant difference between the number of HU at 65 minutes and the number of HU at 85 minutes.

In all cats, the contrast agent distributed nonhomogenously in the gallbladder and was concentrated in the nondependent portion of the gallbladder when the position was changed from sternal to dorsal recumbency, similar to results for dogs[41] and people[42] **(Figure 3)**. The ability to visually assess the bile duct while cats were positioned in dorsal recumbency, as determined subjectively by an investigator, was not affected by the change in body position.

Visual assessment scoring of the biliary tract

Visual assessment scoring was conducted 65 minutes after injection of the contrast agent because there was not a significant difference in enhancement of the liver and biliary tract after that time. A total of 48 scores was obtained for the low dose of contrast agent (4 anatomic structures for each of 3 investigators for each of 4 cats), and 60 scores were obtained for the medium and high doses of contrast dose agent (4 anatomic structures for each of 3 investigators for each of 5 cats). There was no significant difference among scores of the 3 investigators for any anatomic structure (gallbladder, $P = 0.27$; cystic duct, $P = 0.47$; bile duct, $P = 0.20$; and hepatic ducts, $P = 0.59$). Motion artifact was not recorded by any investigator during any phase of the study. Contrast agent was not observed in the duodenum in any cat at any dose of the contrast medium.

Total visual assessment scores for all anatomic structures in the biliary tract at 65 minutes were evaluated **(Figure 4)**. For the low dose of contrast agent, 36 of 48 (75%) biliary tract scores indicated absent contrast enhancement, 12 (25%) scores indicated poor contrast enhancement with ill-defined borders, and 0 (0%) scores indicated moderate or excellent contrast enhancement. For the medium dose of contrast agent, 15 of 60 (25%) biliary tract scores indicated absent contrast enhancement, 32 (53%) indicated poor contrast enhancement, and 13 (22%) indicated moderate contrast enhancement with incomplete delineation of the borders. For the high dose of contrast agent, 12 of 60 (20%) biliary tract scores indicated absent contrast enhancement, 34 (57%) indicated poor contrast enhancement, and 14 (23%) indicated moderate contrast enhancement. None of the cats had excellent enhancement in any of the biliary structures at any dose of contrast agent.

Accordingly, there was a consistently significant effect of the dose of contrast agent for each

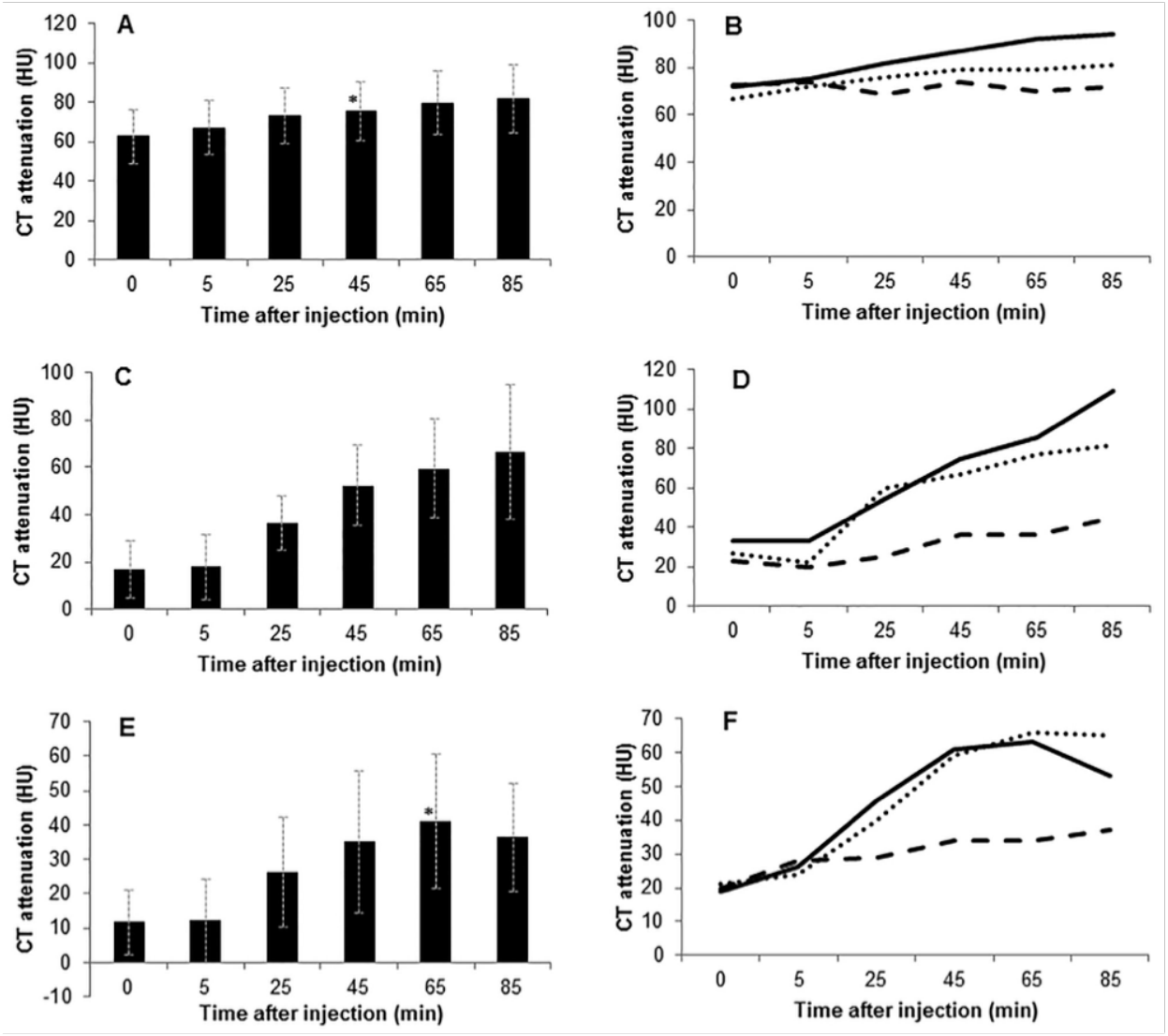

Figure 1—Mean ± SD (A, C, and E) and maximum (B, D, and F) values for CT attenuation of the liver (A and B), gallbladder (C and D), and bile duct (E and F) at the time of IV injection of contrast medium (time 0) and 5, 25, 45, 65, and 85 minutes after injection. For panels A, C, and E, results represent data after injection of the high dose of Gd-EOB-DTPA (0.3 mmol/kg; n = 14), whereas for panels B, D, and F, results represent data after injection of the low (0.0125 mmol/kg; dashed line [4]), medium (0.1 mmol/kg; dotted line [5]), or high (0.3 mmol/kg; solid line [5]) dose of Gd-EOB-DTPA. The mean CT attenuation of the hepatobiliary system has a similar pattern of increasing contrast enhancement over time, although the liver (A) has a significantly ($P \leq 0.05$) higher number of HU at each time point, compared with values for the gallbladder (C) and bile duct (E). Contrast enhancement reached a value (asterisk) that differed significantly ($P \leq 0.05$) from the value at time 0 (in the liver at 45 minutes after injection and in the bile duct at 65 minutes after injection); however, contrast enhancement did not reach a maximum value in the gallbladder by 85 minutes after injection of contrast agent. For panels B, D, and F, the mean maximum CT attenuation similarly was increased over time with increases in enhancement and increasing doses of contrast agent. Notice that the scale on the *y*-axis differs among panels.

Table 1—Mean CT enhancement (number of HU) of anatomic structures of the hepatobiliary system before (time 0) and at various times after IV injection of Gd-EOB-DTPA at a low (0.0125 mmol/kg; n = 4), medium (0.1 mmol/kg; 5), and high (0.3 mmol/kg; 5) dose.

		Time after injection (min)					
Hepatobiliary structure	**Dose**	**0**	**5**	**25**	**45**	**65**	**85**
Liver	Low	68.5	68.0	65.0	67.8	66.5	66.0
	Medium	56.6	63.0	66.0	69.2	70.8	70.2
	High	62.8	67.2	73.0	75.8	79.6	81.8
Gallbladder	Low	19.8	16.2	22.8	31.5	32.5	38.0
	Medium	16.8	14.2	29.4	42.0	49.0	55.2
	High	16.8	18.0	36.4	52.4	59.6	66.6
Cystic duct	Low	18.8	20.0	31.8	30.5	34.3	36.8
	Medium	19.0	17.4	33.2	48.8	49.6	49.4
	High	17.0	20.0	34.0	49.4	56.0	53.4
Bile duct	Low	16.5	21.3	23.8	28.3	28.8	31.8
	Medium	13.8	18.0	18.4	34.2	39.8	38.2
	High	11.8	12.2	26.4	35.2	41.0	36.4

A 0.5-cm^2 ROI was measured in the liver; care was used so that vessels were not included in the ROI. A 0.5-cm^2 ROI was measured at the neck of the gallbladder. A single point of interest was obtained for the cystic duct and bile duct where the structures were clearly visible. The cystic duct is dorsally directed and was defined as the region from the neck of the gallbladder to the insertion of the hepatic ducts in the region of the porta hepatis. The bile duct was defined as the portion of the duct distal to the union of the cystic duct and hepatic ducts and extending to its opening onto the major duodenal papilla.

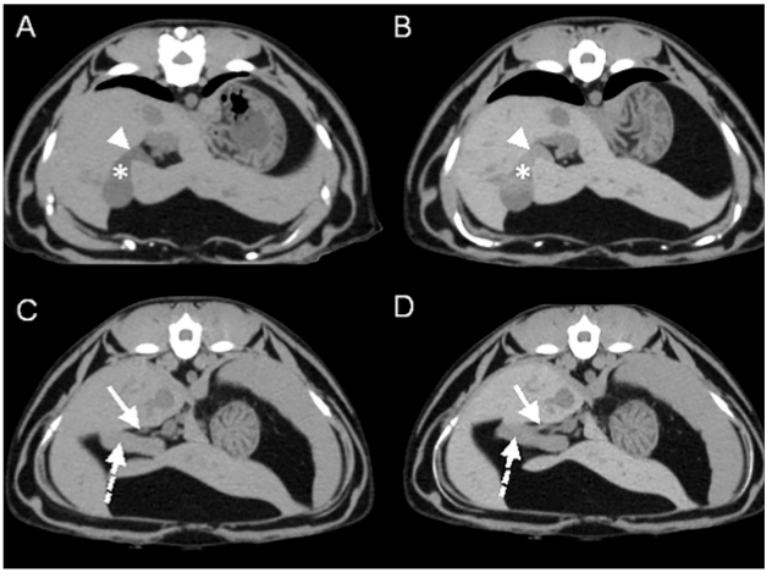

Figure 2—Transverse plane CT images obtained by use of a soft tissue kernel of the cystic duct (A and B) and bile duct (C and D) in a cat before (A and C) and 65 minutes after (B and D) IV administration of a high dose of Gd-EOB-DTPA (0.3 mmol/kg). In panels A and B, the neck of the gallbladder (asterisk) and the cystic duct (arrowhead) are indicated. In panels C and D, notice the bile duct (arrow with solid line) immediately proximal to the point at which it enters the duodenum (arrow with dashed line).

anatomic structure (gallbladder, cystic duct, bile duct, and hepatic ducts; **Figure 5**). In the gallbladder, visual assessment scores were 9.5 times as likely to be higher for the medium dose ($P = 0.007$) and 14.2 times as likely to be higher for the high dose ($P = 0.002$), compared with the visual assessment score for the low dose. Visual assessment scores for the cystic duct were 10.1 and 20.0 times as likely to be higher for the medium ($P = 0.014$) and high ($P = 0.002$) dose, respectively, compared with the visual assessment score for the low dose. Visual assessment scores for the bile duct were 10.4 and 5.8 times as likely to be higher for the medium ($P = 0.005$) and high ($P = 0.029$) dose, respectively, compared with the visual assessment score for the low dose. Visual assessment scores for the hepatic duct were 14.3 and 21.3 times as likely to be higher for the medium ($P = 0.005$) and high ($P = 0.002$) dose, respectively, compared with the visual assessment score for the low dose. However, there was not a significant difference in visual assessment scores between the medium and high dose for any of the anatomic structures (gallbladder, OR = 1.5; cystic duct, OR = 2.0; bile duct, OR = 0.6; and hepatic ducts, OR = 1.5).

The best visual assessment scores were for 1 cat at the high dose of contrast agent. That cat had 8 of 12 scores that indicated moderate enhancement and 4 of 12 scores that indicated poor enhancement of all biliary structures (gallbladder, cystic duct, bile duct, and hepatic ducts). For the same dose of contrast agent, another cat had 4 of 12 scores that indicated poor enhancement and 8 of 12 scores that indicated absent enhancement.

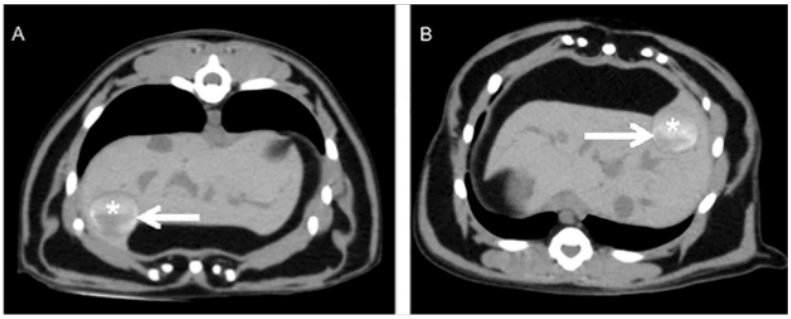

Figure 3—Transverse plane CT images obtained by use of a soft tissue kernel of the liver and gallbladder after CT cholangiography performed with a high dose of Gd-EOB-DTPA (0.3 mmol/kg, IV) for a cat positioned in sternal (A) and dorsal (B) recumbency. Notice that the contrast agent redistributes nonhomogenously to the nondependent portion of the gallbladder (asterisk), delineating the contrast agent from bile in the dependent portion of the gallbladder (arrow).

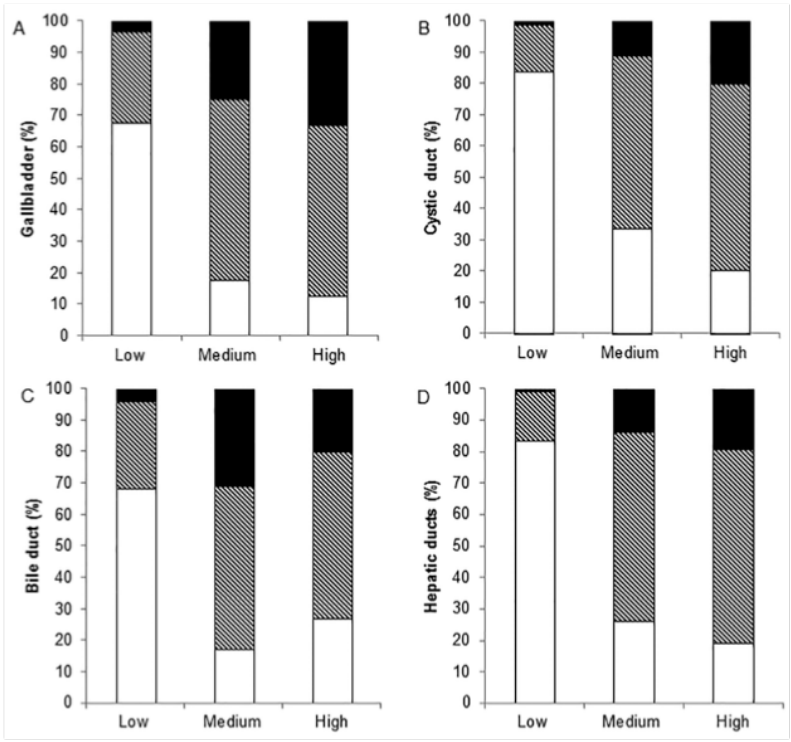

Figure 4—Combined subjective visual assessment scores of 3 investigators for the gallbladder (A), cystic duct (B), bile duct (C), and hepatic ducts (D) at 65 minutes after IV injection of a low (0.0125 mmol/kg; n = 4), medium (0.1 mmol/kg; 5), and high (0.3 mmol/kg; 5) dose of Gd-EOB-DTPA to cats. Visual assessment scores were graded on a scale of 0 to 3 (0 = absent [white bars], 1 = poor contrast enhancement with ill-defined borders [diagonal-striped bars], 2 = moderate contrast enhancement with incomplete delineation of borders [black bars], and 3 = excellent contrast enhancement along the length of the duct with well-defined borders throughout the entire length of the duct [gray bars]). The low dose had a higher percentage of scores that indicated absent contrast for all anatomic structures than did the medium and high doses. The medium and high doses provided improved visual assessment scores, with a high percentage of scores indicative of poor to moderate contrast enhancement in the biliary tract and a low percentage of scores indicative of absent contrast enhancement. Notice that none of the biliary structures had excellent contrast enhancement.

Discussion

The study reported here provided evidence that Gd-EOB-DTPA can be safely administered IV as a contrast agent in healthy cats and that use of Gd-EOB-DTPA resulted in some degree of enhancement of the hepatobiliary system. No acute major adverse effects were identified after IV injection of Gd-EOB-DTPA in cats of the present study. Adverse effects are rare in humans (0.1% to 1%) and include nausea, vasodilation, headache, taste perversion, rash, vomiting, increases in blood pressure, respiratory disorders, feeling hot, and injection site pain.[46] In dogs, a transient prolonged corrected QT interval has been reported at doses of Gd-EOB-DTPA of 0.1 mmol/kg.[46] Although nephrogenic systemic fibrosis has not been reported for Gd-EOB-DTPA, cautious use is recommended in human patients with a reduced glomerular filtration rate because nephrogenic systemic fibrosis reportedly can develop within days to weeks following administration of other gadolinium agents.[37,46,47] The cats in the present study did not have any adverse effects. This may have been attributable to the fact that there was a small study population, cats were anesthetized at the time of injection, or the study ended too soon to enable us to evaluate cats for nephrogenic systemic fibrosis. There were no abnormalities for the physical examinations performed after each phase of the study or for a medical history obtained via verbal communication with research facility personnel 2 weeks after phases 1 and 3 of the study.

All doses of Gd-EOB-DTPA resulted in overall poor visual assessment of the biliary tract in healthy cats by use of CT, which raised questions about the clinical value of this technique for use in cats. In agreement with results of other studies, there were large individual differences in visual assessment scores and objective enhancement characteristics of the biliary structures among cats within the same dose group, which was suspected to have been attributable to individual differences in the number and type of hepatocytes and biliary transport proteins among cats.[41] The difference in results between the study reported here and studies of humans[38] and dogs[41,42] may be related to the manner in which different species accumulate and excrete compounds via the hepatobiliary system. In humans, approximately 50% of Gd-EOB-DTPA is reportedly excreted via the hepatobiliary system,[37,48] whereas

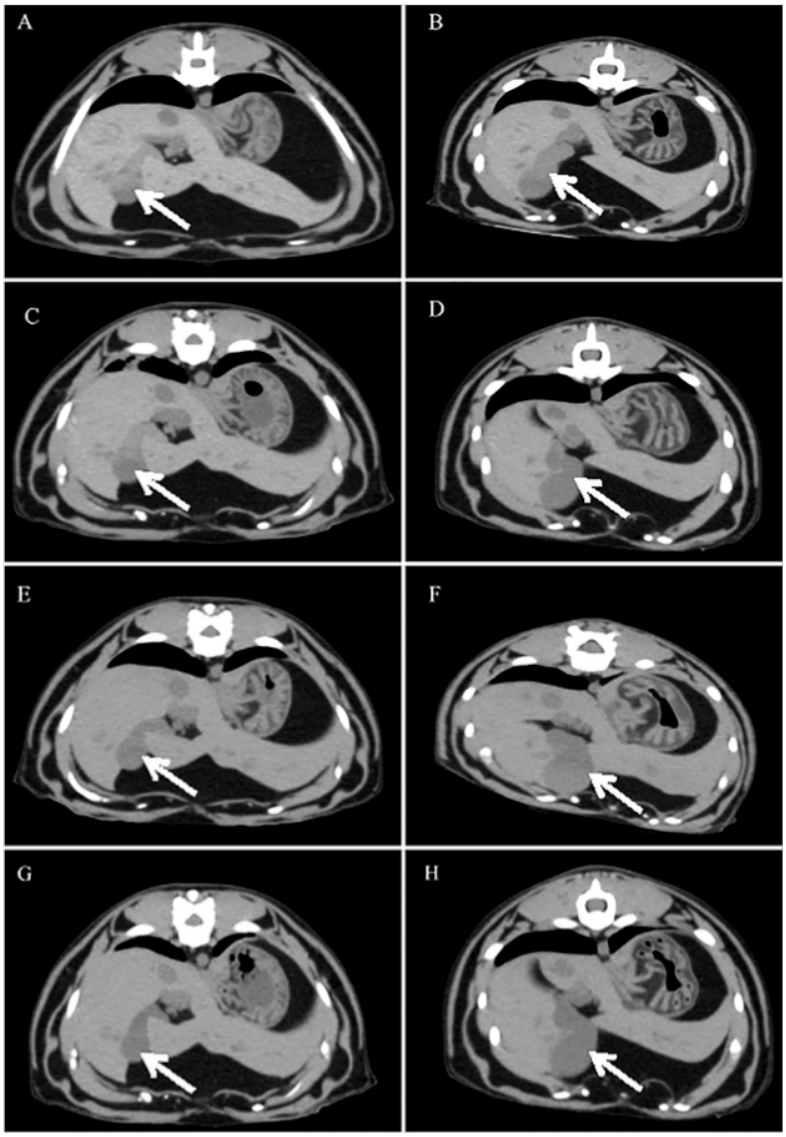

Figure 5—Transverse plane CT images obtained by use of a soft tissue kernel of the gallbladder (arrow) of 2 cats (cat 1 = A, C, E, and G; cat 2 = B, D, F, and H) at 65 minutes after IV injection of a high (0.3 mmol/kg; A and B), medium (0.1 mmol/kg; C and D), and low (0.0125 mmol/kg; E and F) dose of Gd-EOB-DTPA and before administration of contrast agent (G and H). Although there was a similar pattern of an increase in subjective enhancement of the gallbladder with an increase in dose of contrast agent for both cats, there were differences in the number of HU and visual assessment scores between cats for the same dose of contrast agent. There was similar contrast enhancement within the gallbladder of cats 1 and 2 for the high dose (A and B); however, for the medium and low doses, cat 1 (C and E, respectively) had greater contrast enhancement within the gallbladder than did cat 2 (D and F, respectively).

excretion via the same system in rats[48] is 63% to 80% and in monkeys[48] is 32% to 34%. Variability in the excretion rates of contrast agents among species has also been confirmed in other evaluations of nonhepatocyte-specific contrast agents (eg, gadobenate dimeglumine), which are agents that have the highest biliary excretion rate when administered to rats, followed by dogs, rabbits, and monkeys.[49] Although the authors are not aware of any pharmacokinetic evaluations of Gd-EOB-DTPA in cats, it is likely that the biliary excretion rates of cats differ from those reported for other species. A study[50] of biliary excretion of nongadolinium compounds with a molecular weight similar to that of Gd-EOB-DTPA (726 Da) suggested that cats had intermediate biliary excretion of compounds with a high molecular weight (355 to 495 Da), whereas rats and dogs had good biliary excretion and rabbits and monkeys had poor biliary excretion. Thus, it would be expected that cats would excrete Gd-EOB-DTPA at least as well as humans and possibly less well than dogs. Although pharmacokinetic evaluation and a comparison between hepatic and renal enhancement were beyond the scope of the study reported here, they would be beneficial to provide a better understanding of the hepatobiliary and renal excretion properties of Gd-EOB-DTPA in cats.

Dose of Gd-EOB-DTPA had a significant effect on hepatobiliary enhancement. Higher doses were used for the second and third phases of the present study, compared with the dose used for enhanced MRI in humans[46] or dogs.[39,40,51] This was based on the fact that the dose required for CT is higher than the dose required for MRI.[38,42] A low dose was chosen for the first phase of the present study to minimize the risk of adverse effects because use of Gd-EOB-DTPA in cats had not been reported. A significant effect of the dose of contrast agent for each biliary structure was detected between the medium and high doses, compared with results for the low dose; however, there were no significant differences detected between the medium and high doses. This was most likely attributable to the smaller increase in dose (factor of 3) between the medium and high doses, compared with a larger increase (factor of ≥ 10) between the low dose and medium or high dose. Despite this, increases in the dose of contrast agent resulted in higher mean enhancement values (independent of age and body weight) for all anatomic structures in the hepatobiliary system. This is similar to the dose-dependent enhancement seen for dogs in other studies.[41,42] Although the relationship between dose and enhancement in the present study is similar to that detected in studies of dogs[41,42] and humans,[38,43,47] the overall biliary enhancement in the study reported here was lower in cats when considering a similar dose of contrast agent.

Despite the fact there were suboptimal biliary tract visual assessment scores, optimal objective CT contrast enhancement of the cystic and bile ducts was detected at 65 minutes at all doses. This timing is similar to results in a study[41] of dogs in which the time of contrast agent enhancement was also not dose dependent. Therefore, future clinical investigations of biliary pathological conditions of cats by use of Gd-EOB-DTPA could be conducted between 65 and 85 minutes after injection of contrast agent because there was not a significant difference in the number of HU between these times. In the present study, contrast enhancement of the gallbladder differed significantly at each time point and did not reach a plateau by the time of the last scan (85 minutes after injection of contrast agent). Therefore, maximal enhancement of the gallbladder was not determined in the study reported here. In human medicine, Gd-EOB-DTPA–enhanced MRI evaluations revealed intense enhancement of the bile duct from 10 minutes after injection of contrast agent, with scanning and assessment of the biliary tract recommended at 20 to 30 minutes after injection.[35,37,52] However, improved image quality of the bile ducts was detected after a scan delay of 50 to 60 minutes for patients without hepatobiliary dysfunction.[52] It is unclear whether further increasing a delay for image acquisition of cats would result in increased enhancement of the gallbladder.

Clear homogenous contrast enhancement of the liver was detected in the present study. This finding has potential use for the characterization of diffuse or focal hepatic disease in cats by use of CT in clinical studies. The time of contrast enhancement of the liver was similar in all cats, with no significant change in liver enhancement after 45 minutes for all doses of contrast agent. Similar to results of CT and MRI evaluations of dogs with hepatic lesions,[39,40,43] cats with diffuse or focal hepatic pathological conditions may have a reduction in, delay of, or lack of contrast enhancement in affected regions of the liver, compared with values for normal hepatic parenchyma. On the basis of results for the study reported here, these changes may be best visually assessed between 45 and 85 minutes after injection of contrast agent. Despite a continued increase in the number of HU after 45 minutes, it is unclear whether a longer interval after injection of the contrast agent would have improved conspicuity of hepatic lesions given that there was not a significant difference in liver enhancement after 45 minutes. The enhancement curve for the liver of the cats in the present study differed from that described for dogs.[42] In that study,[42] time of maximum enhancement in dogs was dose dependent. It was argued that saturation may have delayed peak enhancement.[42] The reason that the highest dose in the present study did not result in delayed hepatic enhancement is unclear. A possible explanation would be that we may have terminated the study before maximum enhancement was reached. Alternatively, it is possible that the doses in the present study were below the saturation value that results in delayed biliary excretion in dogs.[42] Future studies are needed to investigate higher doses of contrast agents and longer periods of image acquisition.

For all anatomic structures (gallbladder, cystic duct, and hepatic ducts), except for the bile duct, the odds of having a higher visual assessment score were increased when considering the high dose to the low dose and comparing that with the medium dose to the low dose. Interestingly, the OR for the bile duct was higher when comparing the medium dose to the low dose (OR, 10.4) than when comparing the high dose to the low dose (OR = 5.8). The reason for this relationship is unclear, but it may have been attributable to the small size and sinuous shape of the bile duct. In the case of the cystic duct, a possible explanation for the low visual assessment scores may have been related to border effacement with the adjacent hepatic parenchyma. Another reason may have been their tortuosity. In most of the cats, the hepatic ducts were visible only along part of their length (typically just proximal to their entry into the bile duct). This finding is similar to that for a study[41] of dogs in which the hepatic ducts were also found to be the least reliably visible structure with Gd-EOB-DTPA–enhanced CT.

Limitations of the present study included the small number of cats in each phase, particularly because 1 cat was excluded from the first phase of the study. However, because significant differences were detected with the small study population, the use of an additional cat in the first phase was considered unnecessary. A single investigator performed the objective contrast measurements of the hepatobiliary system, which may have introduced bias. Furthermore, because the feline biliary tract is small and tortuous, in particular the bile duct, measurements were difficult to obtain for some cats and may have included additional sampling error or volume averaging. Thinner slices may have reduced this limitation. The study ended at 85 minutes, and the plateau and any decline in enhancement for the gallbladder were not identified. Therefore, we cannot be certain that maximum enhancement was identified. However, additional time for image acquisition and anesthesia did not appear to be warranted, given the data from studies of humans and dogs. Higher doses were not tested in the study reported here because of ethical considerations and cost limitations for implementing additional phases.

In the study reported here, Gd-EOB-DTPA–enhanced hepatic CT and cholangiography provided clear homogenous hepatic enhancement but poor to moderate enhancement of the biliary tract. These results suggested that this technique may be useful for image analysis of the liver parenchyma; however, its value for evaluation of the biliary tract of cats is questionable. No major adverse effects were detected in the healthy cats of the present study. A positive relationship in contrast enhancement was reported

with increases in the dose of contrast agent. Optimal time for imaging of the liver was 45 minutes, whereas optimal time for imaging of the biliary tract was 65 minutes after injection of contrast agent. This information may guide future investigations on the use of Gd-EOB-DTPA–enhanced MRI cholangiography of cats.

Acknowledgments

This manuscript represents a portion of a thesis submitted by Dr. Pilton to the School of Veterinary Science, Faculty of Science at the University of Sydney as partial fulfillment of the requirements for a Master in Veterinary Clinical Studies degree.

The authors declare that there were no conflicts of interest.

Presented in abstract form at the 2017 Australia and New Zealand College of Veterinary Scientists Science Week, Gold Coast, QLD, Australia, July 2017.

Footnotes

a. Eurofins SCEC Agroscience Services Pty Ltd, Lane Cove West, NSW, Australia
b. Siemens Acuson S2000, Siemens AG, Erlangen, Germany.
c Primovist, Bayer Australia Ltd, Pymble, NSW, Australia.
d. Alfaxan, Jurox Pty Ltd, Rutherford, NSW, Australia.
e. Butorgesic, Troy Laboratories Pty Ltd, Smithfield, NSW, Australia.
f. Isoflo, Abbott Australasia Pty Ltd, Botany, NSW, Australia.
g. Hartmann solution, Baxter Healthcare Pty Ltd, Toongabbie, NSW, Australia.
h. Phillips, 16-slice Brilliance CT, version 2.3, Phillips Medical Systems Netherlands, Eindohoven, Netherlands.
i. Pfizer Australia Pty Ltd, West Ryde, NSW, Australia.
j. Osirix, version 4.1.2, 32-bit, Pixmeo SARL, Bernex, Switzerland.
k. Microsoft Excel, version 2010, Microsoft Corp, Redmond, Wash.
l. Genstat, version 17, VSNi, Hemel Hempstead, England.

References

1. Marolf AJ, Stewart JA, Dunphy TR, et al. Hepatic and pancreaticobiliary MRI and MR cholangiopancreatography with and without secretin stimulation in normal cats. *Vet Radiol Ultrasound* 2011;52:415–421.
2. Center SA. Diseases of the gallbladder and biliary tree. *Vet Clin North Am Small Anim Pract* 2009;39:543–598.
3. Smallwood JE. Digestive system. In: Hudson L, Hamilton W, eds. *Atlas of feline anatomy for veterinarians*. Philadelphia: WB Saunders Co, 1993;166–167.
4. Neer TM. A review of disorders of the gallbladder and extrahepatic biliary tract in the dog and cat. *J Vet Intern Med* 1992;6:186–192.
5. Brain PH, Barrs VR, Martin P, et al. Feline cholecystitis and acute neutrophilic cholangitis: clinical findings, bacterial isolates and response to treatment in six cases. *J Feline Med Surg* 2006;8:91–103.
6. Boland L, Beatty J. Feline cholangitis. *Vet Clin North Am Small Anim Pract* 2017;47:703–724.
7. Weiss DJ, Gagne JM, Armstrong PJ. Relationship between inflammatory hepatic disease and inflammatory bowel disease, pancreatitis, and nephritis in cats. *J Am Vet Med Assoc* 1996;209:1114–1116.
8. Cullen JM. Summary of the World Small Animal Veterinary Association Standardization Committee Guide to Classification of Liver Disease in Dogs and Cats. *Vet Clin North Am Small Anim Pract* 2009;39:395–418.
9. Selmic LE. Hepatobiliary neoplasia. *Vet Clin North Am Small Anim Pract* 2017;47:725–735.
10. Bennett SL, Milne M, Slocombe RF, et al. Gallbladder mucocoele and concurrent hepatic lipidosis in a cat. *Aust Vet J* 2007;85:397–400.
11. Woods KS, Brisson BA, Defarges AM, et al. Congenital duplex gallbladder and biliary mucocele associated with partial hepatic cholestasis and cholelithiasis in a cat. *Can Vet J* 2012;53:269–273.
12. Furneaux RW. A series of six cases of sphincter of Oddi pathology in the cat (2008–2009). *J Feline Med Surg* 2010;12:794–801.
13. Della Santa D, Schweighauser A, Forterre F, et al. Imaging diagnosis—extrahepatic biliary tract obstruction secondary to a duodenal foreign body in a cat. *Vet Radiol Ultrasound* 2007;48:448–450.
14. Brioschi V, Rousset N, Ladlow JF. Imaging diagnosis—extrahepatic biliary tract obstruction secondary to a biliary foreign body in a cat. *Vet Radiol Ultrasound* 2014;55:628–631.
15. Linton M, Buffa E, Simon A, et al. Extrahepatic biliary duct obstruction as a result of involuntary transcavitary implantation of hair in a cat. *JFMS Open Rep* 2015;1:2055116915610359.
16. Léveille R, Biller DS, Shiroma JT. Sonographic evaluation of the common bile duct in cats. *J Vet Intern Med* 1996;10:296–299.
17. Sherding RG. Feline jaundice. *J Feline Med Surg* 2000;2:165–169.
18. Newell SM, Selcer BA, Roberts RE, et al. Hepatobiliary scintigraphy in the evaluation of feline liver disease. *J Vet Intern Med* 1996;10:308–315.
19. Newell SM, Graham JP, Roberts GD, et al. Quantitative hepatobiliary scintigraphy in normal cats and in cats with experimental cholangiohepatitis. *Vet Radiol Ultrasound* 2001;42:70–76.
20. Head LL, Daniel GB. Correlation between hepatobiliary scintigraphy and surgery or postmortem examination findings in dogs and cats with extrahepatic biliary obstruction, partial obstruction, or patency of the biliary system: 18 cases (1995–2004). *J Am Vet Med Assoc* 2005;227:1618–1624.
21. Carlisle C. A comparison of technics for cholecystography in the cat. *Vet Radiol* 1977;18:173–176.
22. Larson MM. Ultrasound imaging of the hepatobiliary system and pancreas. *Vet Clin North Am Small Anim Pract* 2016;46:453–480, v–vi..
23. Marolf AJ, Leach L, Gibbons DS, et al. Ultrasonographic findings of feline cholangitis. *J Am Anim Hosp Assoc* 2012;48:36–42.
24. Gaillot HA, Penninck DG, Webster CRL, et al. Ultrasonographic features of extrahepatic biliary obstruction in 30 cats. *Vet Radiol Ultrasound* 2007;48:439–447.
25. Policelli Smith R, Gookin JL, Smolski W, et al. Association between gallbladder ultrasound findings and bacterial culture of bile in 70 cats and 202 dogs. *J Vet Intern Med* 2017;31:1451–1458.
26. Spillmann T, Willard MD, Ruhnke I, et al. Feasibility of endoscopic retrograde cholangiopancreatography in healthy cats. *Vet Radiol Ultrasound* 2014;55:85–91.
27. Marolf AJ. Computed tomography and MRI of the hepatobiliary system and pancreas. *Vet Clin North Am Small Anim Pract* 2016;46:481–497 (vi.).
28. Rosenberg FJ, Ackerman JH, Nickel AR. Iosulamide: a new intravenous cholangiocholecystographic medium. *Invest Radiol* 1980;15:S142–S147.
29. Marolf AJ, Kraft SL, Dunphy TR, et al. Magnetic resonance (MR) imaging and MR cholangiopancreatography findings in cats with cholangitis and pancreatitis. *J Feline Med Surg* 2013;15:285–294.
30. Marolf AJ. Diagnostic imaging of the hepatobiliary system: an update. *Vet Clin North Am Small Anim Pract* 2017;47:555–568.
31. Schindera ST, Nelson RC, Paulson EK, et al. Assessment of the optimal temporal window for intravenous CT cholangiography. *Eur Radiol* 2007;17:2531–2537.
32. Spillmann T, Schnell-Kretschmer H, Dick M, et al. Endoscopic retrograde cholangio-pancreatography in dogs with chronic gastrointestinal problems. *Vet Radiol Ultrasound* 2005;46:293–299.
33. O'Connor OJ, O'Neill S, Maher MM. Imaging of biliary tract disease. *AJR Am J Roentgen* 2011;197:W551–W558.
34. Maccioni F, Martinelli M, Al Ansari N, et al. Magnetic reso-

nance cholangiography: past, present and future: a review. *Eur Rev Med Pharmacol Sci* 2010;14:721–725.
35. Lee NK, Kim S, Lee JW, et al. Biliary MR imaging with Gd-EOB-DTPA and its clinical applications. *Radiographics* 2009;29:1707–1724.
36. Burke C, Alexander Grant L, Goh V, et al. The role of hepatocyte-specific contrast agents in hepatobiliary magnetic resonance imaging. *Semin Ultrasound CT MR* 2013;34:44–53.
37. Van Beers BE, Pastor CM, Hussain HK. Primovist, Eovist: what to expect? *J Hepatol* 2012;57:421–429.
38. Schmitz SA, Häberle J, Balzer T, et al. Detection of focal liver lesions: CT of the hepatobiliary system with gadoxetic acid disodium, or Gd-EOB-DTPA. *Radiology* 1997;202:399–405.
39. Yonetomi D, Kadosawa T, Miyoshi K, et al. Contrast agent Gd-EOB-DTPA (EOB.Primovist®) for low-field magnetic resonance imaging of canine focal liver lesions. *Vet Radiol Ultrasound* 2012;53:371–380.
40. Constant C, Hecht S, Craig LE, et al. Gadoxetate disodium (Gd-EOB-DTPA) contrast enhanced magnetic resonance imaging characteristics of hepatocellular carcinoma in dogs. *Vet Radiol Ultrasound* 2016;57:594–600.
41. Chau J, Podadera J, Young A, et al. Use of gadoxetic acid for computed tomographic cholangiography in healthy dogs. *Am J Vet Res* 2017;78:828–839.
42. Schmitz SA, Wagner S, Schuhmann-Giampieri G, et al. A prototype liver-specific contrast medium for CT: preclinical evaluation of gadoxetic acid disodium, or Gd-EOB-DTPA. *Radiology* 1997;202:407–412.
43. Schmitz SA, Wagner S, Schuhmann-Giampieri G, et al. Gd-EOB-DTPA and Yb-EOB-DTPA: two prototypic contrast media for CT detection of liver lesions in dogs. *Radiology* 1997;205:361–366.
44. Shanaman MM, Hartman SK, O'Brien RT. Feasibility for using dual-phase contrast-enhanced multi-detector helical computed tomography to evaluate awake and sedated dogs with acute abdominal signs. *Vet Radiol Ultrasound* 2012;53:605–612.
45. Patel NB, Oto A, Thomas S. Multidetector CT of emergent biliary pathologic conditions. *Radiographics* 2013;33:1867–1888.
46. Eovist (gadoxetate disodium) prescribing information, 2010. Wayne, NJ: Bayer HealthCare Pharmaceuticals Inc. Available at: www.accessdata.fda.gov/drugsatfda_docs/label/2010/022090s004lbl.pdf. Accessed Jun 5, 2017.
47. Mendichovszky IA, Marks SD, Simcock CM, et al. Gadolinium and nephrogenic systemic fibrosis: time to tighten practice. *Pediatr Radiol* 2008;38:489–496.
48. Hamm B, Staks T, Mühler A, et al. Phase I clinical evaluation of Gd-EOB-DTPA as a hepatobiliary MR contrast agent: safety, pharmacokinetics, and MR imaging. *Radiology* 1995;195:785–792.
49. Louvet A, Duconseille A-C. Feasibility for detecting liver metastases in dogs using gadobenate dimeglumine-enhanced magnetic resonance imaging. *Vet Radiol Ultrasound* 2015;56:286–295.
50. Abou-El-Makarem MM, Millburn P, Smith RL, et al. Biliary excretion in foreign compounds. Species difference in biliary excretion. *Biochem J* 1967;105:1289–1293.
51. Marks AL, Hecht S, Stokes JE, et al. Effects of gadoxetate disodium (EOVIST®) contrast on magnetic resonance imaging characteristics of the liver in clinically healthy dogs. *Vet Radiol Ultrasound* 2014;55:286–291.
52. Choi IY, Yeom SK, Cha SH, et al. Diagnosis of biliary stone disease: T1-weighted magnetic resonance cholangiography with Gd-EOB-DTPA versus T2-weighted magnetic resonance cholangiography. *Clin Imaging* 2014;38:164–169.

4.2 Chapter 2 - Developing novel applications in thoracic imaging by assessing the effect of body position and time on quantitative computed tomographic measurements of lung volume and attenuation in healthy anaesthetised cats.

CT is the gold standard imaging modality to quantify changes in lung density and volume in humans. There is a lack of veterinary information, particularly in cats, regarding pulmonary volume and attenuation changes in relation to changes in body position over time. The changes in lung volume and attenuation (HU) in relation to changes in body position can potentially affect the assessment of pathologic changes within the lung. Normally, the difference in attenuation measured using HU between gas and soft tissue allows contrast and increased conspicuity between adjacent structures. A reduced volume and increased lung attenuation, which is typical in the dependent lung during anaesthesia or recumbency, will reduce the contrast between gas and soft tissue in the lung, therefore potentially masking pulmonary pathology, as well as result in possible border effacement with pathological tissue.

Cats often undergo thoracic imaging in conjunction with abdominal imaging due to non-specific clinical signs and for evaluation of potential thoracic pathology, given the increased sensitivity of thoracic CT compared to radiographs and to effectively utilise the time, increased risk and expense of anaesthesia. Following this, our aim in this second study was to use CT in healthy anaesthetised cats to quantify lung volume and attenuation (HU) changes in relation to different body positions over time. Again, we utilised CT as the preferred imaging modality because of its ability to allow evaluation of cross-sectional anatomy and the improved accessibility to the modality with fast, reproducible scanning and semi-automated segmentation techniques. This information would be useful to better understand positioning for all anaesthetised cat CT studies, to understand which recumbency would minimise lung atelectasis, as well as being particularly useful for future evaluation of pulmonary pathology using thoracic CT. We hypothesised that atelectasis would occur in the dependent lung and would progress over time under anaesthesia.

In this second study, a separate group of eight healthy research cats were anaesthetized and positioned in sternal recumbency for 20 min and then in left, right and left lateral recumbency respectively (40 mins / position). Expiratory helical CT scan of the thorax was performed over set time points (0 and 20 mins in sternal recumbency and at 0, 5, 10, 20, 30 and 40 minutes in lateral recumbency) in each recumbency. Each scan was acquired in expiratory pause and all cats were spontaneously breathing. A single observer (third year radiology resident) performed all measurements and segmentation of the lungs to separate the left and right lung fields (excluding the trachea to the level of the mainstem bronchi and major blood vessels) with an attenuation range of - 1280 to + 100 HU for each helical CT acquisition. The lung volume was calculated for the segmented left or right lung using a compute-volume tool and the segmented lung ROIs were exported into a multi-image analysis graphic user interface tool for calculating of lung attenuation (HU). CT measurements of lung volume and attenuation were determined and the extent of lung

areas that were classified as hyperaerated (-1000 to -901 HU), normoaerated (-900 to -501 HU), poorly aerated (-500 to -101 HU) or non-aerated (-100 to +100 HU) and were documented.

Mean lung volume and attenuation values of the dependent lungs were compared to those of the non dependent lungs across all lateral positions. The volume and attenuation value of the left lung and the right lung were compared across all positions as well as the dependent lung. Data was analysed with a restricted maximum likelihood procedure. Fixed effects considered for inclusion were position, time, and dependent or non dependent status for analysis with volume and attenuation (HU) as the outcomes and were position, time, dependent and nondependent status, attenuation and right or left lung for lug attenuation analysis. Percentages were logarithmically transformed before analysis to maintain the assumption for normality. Cat was included as a random effect in each model. A value of $P< 0.05$ was considered significant for all analyses. Posthoc analysis involving least significant differences were conducted to determine the significance of pairwise differences.

We found that cats in lateral recumbency, have a significantly greater lung attenuation and reduced volume on CT in the dependent lung than the non-dependent lung ($P = 0.014$). Within the dependent lung, there was a significantly higher percentage of poorly aerated lung tissue (– 500 to – 101 HU) compared to the non-dependent lung (mean attenuation -641.7 HU) These changes occurred immediately after positioning in lateral recumbency and remained static with no further significant time related change ($P = 0.978$ for mean lung attenuation and $P = 0.998$ for mean volume). The percentage of true atelectasis (– 100 to + 100 HU) in the lungs, as defined objectively by HU compared to visual assessment, of the healthy cats in the present study was minimal. It was also documented that cats had less poorly aerated lung, and the lowest lung attenuation in sternal recumbency compared to the dependent lung in lateral recumbency. This is similar to previous studies in dogs in which sternal recumbency resulted in the highest functional residual capacity (Rozanski et al., 2010) and the least quantifiable atelectasis (Lee et al., 2017). Finally, when cats were placed in the contralateral recumbency, the non-dependent lung lobe rapidly recovered with a significant decrease in attenuation and increase in volume without hyperinflation. Anaesthesia also allowed optimal image quality in this study, without motion artefact affecting the study quality and image assessment.

Limitations of the study include the small number of cats, lack of evaluation of intra- or interobserver repeatability for lung segmentation, effect of positioning sequence and a deep plane of anaesthesia. Morphologic pulmonary disease was ruled out using an initial diagnostic CT scan, although functional pulmonary studies were not performed. As such, the presence of functional pulmonary disease that may influence pulmonary aeration cannot be completely excluded.

From this research, we propose that cats are placed in sternal recumbency for morphologic imaging studies, to reduce changes in lung density and volume that may potentially mask pulmonary pathology due to the reduction in gas contrast with poorly

aerated or non-aerated lung. Further research could be carried out in cats with pulmonary pathology to determine whether the recumbency related lung changes, such as poorly aerated lung will affect visualisation of pulmonary pathology. Conversely, in some functional respiratory diseases, such as feline asthma and air trapping, emphysema, or COPD, there is an increase in lung volume and reduced attenuation due to air trapping. It is possible that in these cases, the lung retains its volume without a change in density during recumbency. Further research is required in this field. This study may provide potential applications for future research by providing a baseline for diagnosis and quantification of feline lung pathology, in particular in research associated with functional pulmonary diseases that may in turn prove useful for the diagnosis, prognosis, and treatment monitoring of feline lung diseases.

Publication 2

Authors: Foo, T.S., Pilton, J.L., Hall, E.J., Martinez-Taboada, F., Makara, M.

Title: Effect of body position and time on quantitative computed tomographic measurements of lung volume and attenuation in healthy anesthetized cats.

Year of Publication: 2018

Journal: American journal of veterinary research 79(8), 874-883.

Effect of body position and time on quantitative computed tomographic measurements of lung volume and attenuation in healthy anesthetized cats

Timothy S. Foo BVMS
Joanna L. Pilton BVSc
Evelyn J. Hall BScAgr, PhD
Fernando Martinez-Taboada DVM
Mariano Makara Dr Med Vet

Received August 8, 2018.
Accepted September 28, 2017.

From the Units of Diagnostic Imaging (Foo, Pilton, Makara) and Anaesthesia (Martinez-Taboada), Faculty of Science, School of Veterinary Science, and the School of Life and Environmental Sciences (Hall), University of Sydney, Sydney, NSW 2006, Australia.

Address correspondence to Dr. Makara (mariano.makara@sydney.edu.au).

OBJECTIVE
To quantify the effect of time and recumbency on CT measurements of lung volume and attenuation in healthy cats under general anesthesia.

ANIMALS
8 healthy research cats.

PROCEDURES
Anesthetized cats were positioned in sternal recumbency for 20 minutes and then in left, right, and left lateral recumbency (40 minutes/position). Expiratory helical CT scan of the thorax was performed at 0 and 20 minutes in sternal recumbency and at 0, 5, 10, 20, 30, and 40 minutes in each lateral recumbent position. For each lung, CT measurements of lung volume and attenuation and the extent of lung areas that were hyperaerated (–1,000 to –901 Hounsfield units [HU]), normoaerated (–900 to –501 HU), poorly aerated (–500 to –101 HU), or nonaerated (–100 to +100 HU [indicative of atelectasis]) were determined with a semiautomatic threshold-based technique. A restricted maximum likelihood analysis was performed.

RESULTS
In lateral recumbency, the dependent lung had significantly greater attenuation and a lower volume than the nondependent lung. Within the dependent lung, there was a significantly higher percentage of poorly aerated lung tissue, compared with that in the nondependent lung. These changes were detected immediately after positioning the cats in lateral recumbency and remained static with no further significant time-related change.

CONCLUSIONS AND CLINICAL RELEVANCE
Results indicated that once anesthetized healthy cats were positioned in lateral recumbency, the dependent lung lobes underwent a rapid reduction in lung volume and increase in lung attenuation that did not progress over time, predominantly attributable to an increase in poorly aerated lung tissue. (*Am J Vet Res* 2018;79:874–883)

From results of a study in humans,[1] it is known that the physical density of the lung is determined by 3 components: lung tissue, blood, and gas. The relative proportions of these 3 components are closely associated with changes in lung volume, whereby a reduction in lung volume leads to an increase in the overall physical density of the lung.[1–4] Pronounced changes in lung density and volume occur commonly during anesthesia or recumbency, situations where there is a significant and rapid increase in lung density and a significant reduction in lung volume within the dependent lung regions.[2–15] The most common and well-described result of these lung changes is the development of pulmonary atelectasis, with atelectasis being defined in CT images as pixel attenuation values of –100 to +100 HU.[2–6,9] In CT examinations, pulmonary atelectasis was the most prevalent pulmonary abnormality for 144 of 352 (41%) cats without respiratory tract signs.[16] Because veterinary patients are commonly anesthetized and positioned in LR, SR, or DR for procedures such as thoracic radiography and CT, these lung changes have clinically important implications. Pulmonary atelectasis can complicate the interpretation of diagnostic imaging in 2 ways. Pulmonary atelectasis is potentially an incidental finding, but can mimic pathological lesions leading to misdiagnosis of pulmonary abnormalities.[17,18] Also, pulmonary atelectasis may mask evidence of intrathoracic disease and complicate interpretation of thoracic radiographic and CT findings.[16,17] Although the lung changes related to recumbency may challenge the diagnosis of lung disease, they could also provide

ABBREVIATIONS

COPD	Chronic obstructive pulmonary disease
DR	Dorsal recumbency
HU	Hounsfield units
LLR	Left lateral recumbency
LLR1	First period of left lateral recumbency
LLR2	Second period of left lateral recumbency
LR	Lateral recumbency
RLR	Period of right lateral recumbency
ROI	Region of interest
SR	Sternal recumbency

useful functional information. By application of the concept of gravitational differences in lung attenuation, lateral decubitus CT has been successfully used as an alternative method to obtain expiratory scans in humans who are unable to follow breath-holding instructions. By accentuating the differences in lung attenuation between diseased lung tissue and atelectasis, this technique has allowed detection of air-trapping in human patients for whom CT scans obtained in a supine position were inconclusive.[19–21]

Computed tomography is considered the gold standard for quantification of changes in lung density and volume. On the basis of differences in attenuation (expressed in HU), it is possible to distinguish areas of lung tissue that are hyperaerated (–1,000 to –901 HU), normoaerated (–900 to –501 HU), poorly aerated (–500 to –101 HU), or nonaerated (–100 to +100 HU [indicative of atelectasis]).[6,14] In the past decade, the application of this quantitative CT analysis of lung volume and attenuation in veterinary medicine has continued to expand, thereby improving our understanding of changes in pulmonary attenuation.[15,19] However, there is a lack of information in veterinary medicine regarding quantification of lung volume and attenuation in relation to different body positions and changes in those variables over time, particularly for cats. The purpose of the study reported here was to use CT to quantify lung volume and attenuation changes over time and to estimate the prevalence of atelectasis (attenuation, –100 to +100 HU) in anesthetized healthy cats in different body positions. Our hypotheses were that there would be a significant increase in lung attenuation with development of atelectasis within the dependent lung during LR, compared with findings during SR, and that this change would increase in severity over time.

Materials and Methods

Animals

Eight healthy adult domestic shorthair cats belonging to an experimental animal provider[a] were selected and transported to the University of Sydney for the duration of the prospective experimental study. The cats were allowed a period of acclimation prior to commencement of the study and also a period of monitored recovery after completion of the study before being returned to the source. The study was approved by the Animal Ethics Committee of the University of Sydney.

Cats were considered healthy on the basis of no history of respiratory tract disease and results of a physical examination (cardiac and pulmonary auscultation, abdominal palpation, and measurements of rectal temperature, heart rate, respiratory rate, and pulse rate) that were within reference ranges. For each cat, no abnormalities were detected during thoracic CT without contrast agent administration. In addition, a CBC, serum biochemical analyses, and assessment of serum total thyroxine concentration to detect major abnormalities that would preclude any cat from undergoing general anesthesia were performed. Minor serum biochemical abnormalities (including mildly high activities of creatine kinase and alanine aminotransferase and concentrations of total protein, sodium, and potassium) were not considered important. Among the 8 cats, there were 5 neutered males, 1 sexually intact male, and 2 spayed females. The cats' median age was 4 years (range, 1 to 6 years) and median weight was 4.15 kg (range, 3.4 to 5.8 kg). All cats were considered to be in good body condition (5 to 7 as determined on a 9-point scale).

Study design

Each cat was anesthetized and positioned in SR for 20 minutes and then positioned in LR for three 40-minute periods (ie, LLR1, RLR, and then LLR2). Helical CT examination of the thorax was performed at 0 and 20 minutes when cats were in SR and at 0, 5, 10, 20, 30, and 40 minutes when cats were in each LR position. The 0-minute time point was defined as the time that cats were first placed in each position. Each scan was acquired in expiratory pause, and all cats were spontaneously breathing. Following the CT examination, the cats were allowed to recover from anesthesia routinely. The CT images were then sent to the hospital picture archiving system for analysis at a later time.

Anesthesia

Food but not water was withheld from each cat for 12 hours before anesthesia. Thirty minutes prior to the CT examination, each cat was sedated with alfaxalone[b] (2 mg/kg), acepromazine maleate[c] (0.02 mg/kg), butorphanol tartrate[d] (0.2 mg/kg), and medetomidine (10 μg/kg)[e] administered IM. Fifteen minutes later, a 22-gauge catheter was aseptically placed into a cephalic vein, and alfaxalone[b] was administered IV to effect. Prior to endotracheal intubation, 0.1 mL of lidocaine hydrochloride[f] diluted to 1% was administered topically to the larynx of each cat to prevent laryngeal spasm and facilitate intubation. Following endotracheal intubation, anesthesia was maintained with isoflurane[g] (1.0% to 1.5%) in oxygen through a Bain nonrebreathing circuit (flow rate, 1 L/min). Throughout anesthesia, Hartman solution[h] was administered IV at a rate of 5 mL/kg/h. During the experimental procedure, heart rate, respiratory rate, arterial blood pressure, peripheral hemoglobin oxygen saturation as measured by pulse oximetry, rectal temperature, and end-tidal CO_2 concentration were monitored.

CT examination

All CT scans (regardless of the cats' position) were acquired with the same 16-slice multidetector CT scanner.[i] Transverse CT images of the thorax of each cat were acquired with the same settings as follows: 120 kVp; 150 mAs; collimation, 16 X 1.5 mm; gantry rotation speed, 0.5 seconds; field of view, 180

mm; matrix, 512 X 512 pixels; slice thickness, 2 mm (with 1-mm increments); and collimator pitch, 1.438. A high-resolution algorithm and lung reconstruction filter were used. Acquisition times varied between 3.045 and 3.494 seconds. Timing of each scan was coordinated by visualization of a mainstream capnography (no time delay) trace with the scan obtained during the expiratory pause. The CT scan was repeated immediately if there was notable motion artifact that resulted in a poor-quality scan.

CT lung segmentation

A single observer (TSF) performed all measurements and segmentation with an image analysis workstation[j,k] and software.[l] For each helical CT acquisition, the lungs were segmented from the rest of the thorax as an ROI and further separated into the right and left lung fields. This was achieved in 4 stages. First, the lungs were segmented from the surrounding structures with a 3-D growing ROI tool by setting a threshold attenuation range of –1,280 to –200 HU **(Figure 1)**. Second, the trachea was then manually removed from the ROI down to the level of the mainstem bronchi. Third, the segmented lungs were then separated manually into the left lung and right lung fields. The accessory lung lobe was included in the right lung field. Fourth, within each lung field, regions between –199 and +100 HU were manually included into the ROI by use of the brush tool taking care to exclude major blood vessels to the level of the primary bronchi. The end result was separate ROIs of the left and right lung fields (excluding the trachea to the level of the mainstem bronchi and major blood vessels) with an attenuation range of –1,280 to +100 HU for each helical CT acquisition.

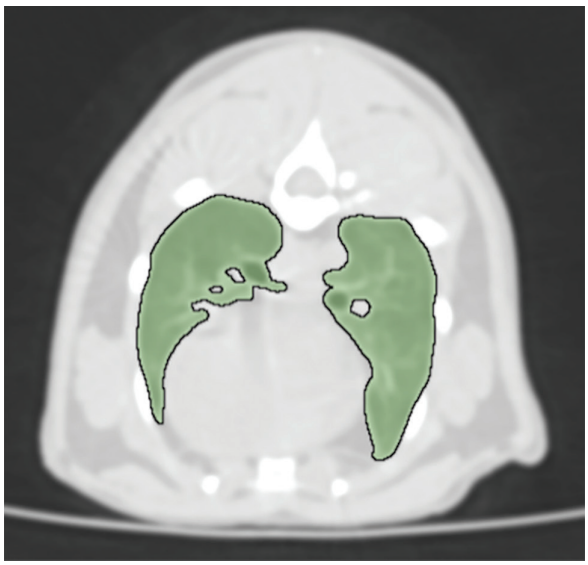

Figure 1—Illustration of the semiautomatic segmentation of both lung fields as an ROI (green) as determined for 1 of 8 cats used in a study to quantify the effect of time and recumbency on CT measurements of lung volume and attenuation in healthy anesthetized cats. In a representative CT image, the lungs are segmented from the surrounding structures with a 3-D growing ROI tool by setting a threshold attenuation range of –1,280 to –200 HU. The trachea was then manually removed from the ROI to the level of the mainstem bronchi. The segmented lungs were then separated manually into the left lung and right lung fields; the accessory lung lobe was included in the right lung field. Regions of –199 to +100 HU within each lung field were manually included into the ROI by use of the brush tool (excluding major blood vessels to the level of the primary bronchi). Thus, separate ROIs for the left and right lung fields (excluding the trachea to the level of the mainstem bronchi and major blood vessels) with an attenuation range of –1,280 to +100 HU for each helical CT acquisition were obtained. Lung volume (expressed as cm^3) was determined by use of an image analysis workstation and software; segmented lung ROIs were analyzed to determine lung attenuation (HU). In the present study, a classification scheme[12] was used for lung attenuation analysis as follows: hyperaerated (–1,000 to –901 HU), normoaerated (–900 to –501 HU), poorly aerated (–500 to –101 HU), and nonaerated (–100 to +100 HU) lung tissue.

Quantitative CT analysis

Lung volume was calculated for the segmented right or left lung by use of the image analysis workstation and software. A compute-volume tool was used to calculate the lung volume (expressed as cm^3). The segmented lung ROIs were exported into a multi-image analysis graphic user interface tool[m] for calculation of lung attenuation. By means of a generate-histogram tool, lung attenuation (expressed as HU) histograms of the segmented lung ROIs were generated. The raw data from each histogram were then exported into a spreadsheet[n] for statistical analysis. The following classification scheme[12] was used for lung attenuation analysis: hyperaerated (–1,000 to –901 HU), normoaerated (–900 to –501 HU), poorly aerated (–500 to –101 HU), and nonaerated (–100 to +100 HU) lung tissue.

Statistical analysis

Mean lung volume and attenuation value of the dependent lungs were compared with those of the nondependent lungs across all lateral positions. The volume and attenuation value of the left lung were each compared across all positions. Similarly, the volume and attenuation value of the right lung were each compared across all positions. The lung volume and attenuation value of the dependent lung was also compared across all lateral positions. Data were analyzed with a restricted maximum likelihood procedure.[o] Fixed effects considered for inclusion were position, time, and dependent or nondependent status for analyses with volume (cm^3) and attenuation (HU) as the outcomes and were position, time, dependent or nondependent status, attenuation, and right or left lung for lung attenuation analysis. Percentages were logarithmically (log_e) transformed before analysis to maintain the assumption of normality. Cat was included as a random effect in each model. A value of $P < 0.05$ was considered significant for all analyses. Posthoc analyses involving least significant differences were conducted to determine the significance of pairwise differences.

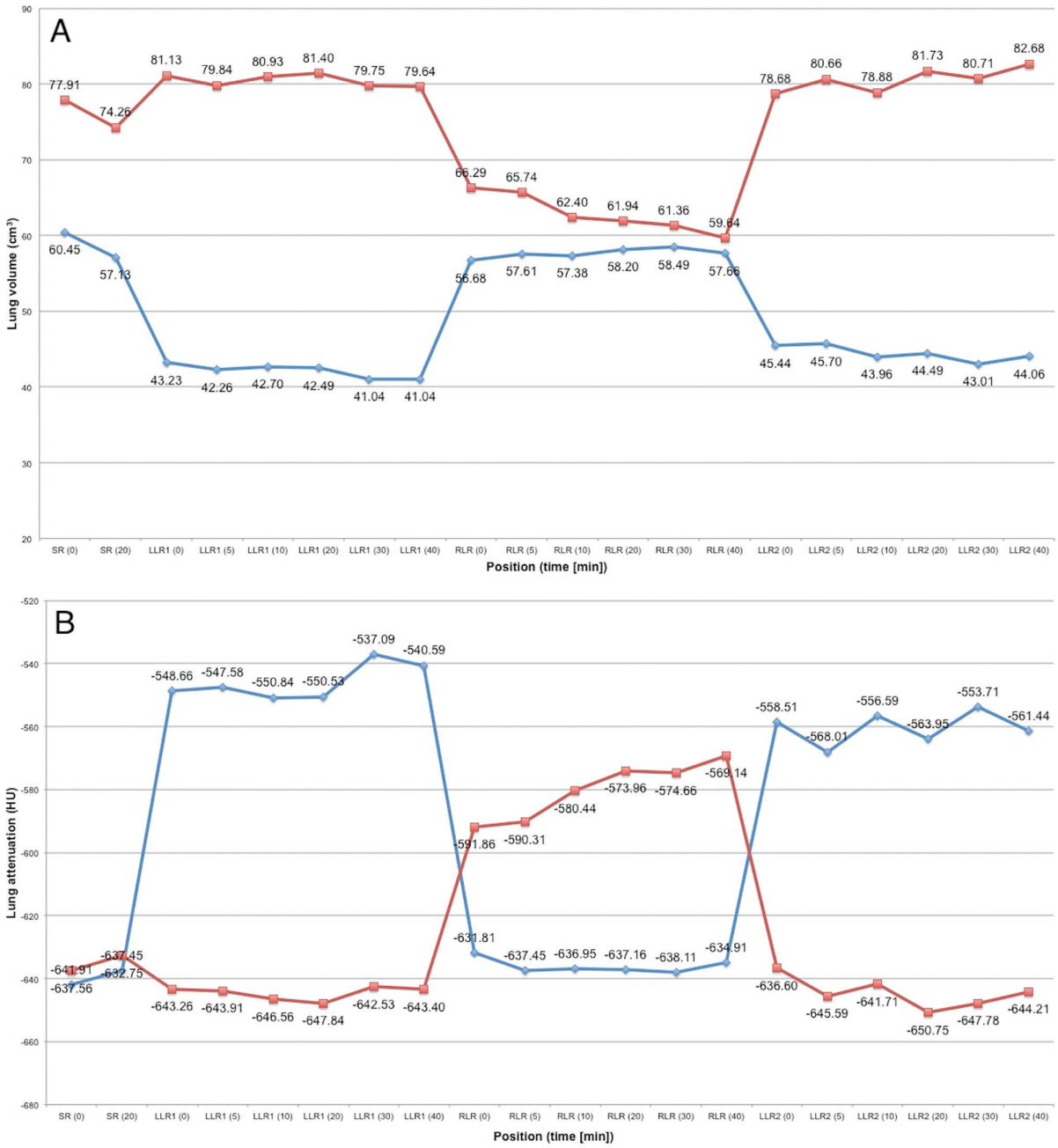

Figure 2—Mean lung volume (A) and attenuation (B) of the right (red line) and left (blue line) lungs of 8 healthy anesthetized cats that were positioned in SR for 20 minutes and then underwent LLR1, RLR, and LLR2 (40 min/position) during which expiratory helical CT scans of the thorax were performed (at 0 and 20 minutes when cats were in SR and at 0, 5, 10, 20, 30, and 40 minutes in each LR position). At the time that each cat's position was modified, there is a significant and rapid decrease in volume and increase in attenuation for dependent lungs with no further significant change over time (up to 40 minutes). ***See*** Figure 1 for remainder of key.

Results

The cats' condition remained stable throughout the duration of the study as determined on the basis of heart rate, respiratory rate, arterial blood pressure, hemoglobin oxygen saturation, rectal temperature, and end-tidal CO_2 concentration. These variables remained within reference limits, and no complications were recorded.

Overall attenuation and volume analysis

There was a significant (P = 0.014) difference in overall attenuation and volume between the dependent and nondependent lungs when all data for the dependent lung were compared with those for the nondependent lung for all lateral positions (ie, during LLR1, RLR, and LLR2). There was a significantly

higher mean attenuation (–565.5 HU [SD, 41.3 HU]) and lower mean volume (49.8 cm^3 [SD, 12.2 cm^3]) for the dependent lung, compared with the mean attenuation (–641.7 HU [SD, 31.4 HU]) and mean volume (72.9 cm^3 [SD, 14.6 cm^3]) for the nondependent lung in each position. There were no significant differences in mean lung attenuation or mean volume (P = 0.978 and 0.998 respectively) among scans performed at 0, 5, 10, 20, 30, and 40 minutes in each position. These findings indicated that the maximal changes in attenuation and volume within the dependent and nondependent lungs occurred rapidly, and those variables did not significantly progress over time **(Figure 2)**. Given that there were no significant differences in mean attenuation or mean volume over time when cats were in SR or during LLR1, RLR, or LLR2, further comparisons were performed with means calculated for each period of recumbency from data obtained at all time points during that period.

Comparison of the left lung variables when cats were in SR and during LLR1, RLR, and LLR2 revealed that the left lung had a significant increase in attenuation during LLR1 (–545.9 HU) and LLR2 (–560.4 HU), compared with the value during SR (–639.7 HU). There was also a significant decrease in volume of the left lung during LLR1 (42.1 cm^3) and LLR2 (44.4 cm^3), compared with the value during SR (58.8 cm^3). During RLR, the left lung had a significant decrease in attenuation (–636.1 HU) and increase in volume (57.7 cm^3), compared with data obtained during LLR1 and LLR2. There was no significant decrease in attenuation or increase in volume of the left lung during RLR, compared with findings when cats were in SR, indicating recovery but no significant hyperinflation of the nondependent left lung. During LLR1 and LLR2, there were no significant differences in attenuation or volume of the left lung.

Comparison of the right lung variables when cats were in SR and during LLR1, RLR, and LLR2 revealed that the right lung had a significant increase in attenuation during RLR (–590.4 HU), compared with the value during SR (–635.2 HU). There was also a significant decrease in the volume of the right lung during RLR (62.9 cm^3), compared with the value during SR (76.1 cm^3). During LLR1 and LLR2, the right lung had a significant decrease in attenuation (LLR1, –644.6 HU; LLR2, –644.4 HU) and increase in volume (LLR1, 80.5 cm^3; LLR2, 80.6 cm^3), compared with data obtained during RLR. There was no significant decrease in attenuation of the right lung during LLR1 and LLR2, compared with findings when cats were in SR. However, there was a small but significant increase in the volume of the right lung during LLR1 and LLR2, compared with the lung volume during SR, indicating recovery and also a degree of hyperinflation of the nondependent right lung. During LLR1 and LLR2, there were no significant differences in attenuation or volume of the right lung.

Data obtained for the dependent lung during LLR1, RLR, and LLR2 indicated that the right lung had a significantly lower attenuation during RLR (–590.4 HU), compared with findings for the left lung during LLR1 (–545.9 HU) and LLR2 (–560.4 HU). Thus, it appeared that the dependent right lung (during RLR) underwent a less pronounced decrease in attenuation, compared with the dependent left lung (during LLR1 or LLR2). The dependent right lung also had a significantly higher volume (62.9 cm^3), compared with values for the dependent left lung during LLR1 and LLR2; however, this difference was likely attributable to the overall higher volume of the right lung.

Table 1—Mean percentage of hyperaerated, poorly aerated, normoaerated, and nonaerated tissue of the right and left lungs of 8 healthy anesthetized cats that were positioned in SR for 20 minutes and then underwent LLR1, RLR, and LLR2 (40 min/position).

Position	Aeration classification	Right lung (%)	Left lung (%)
SR	Hyperaerated	0.24[a]	0.26[b]
	Poorly aerated	16.64	16.44[a,c]
	Nonaerated	1.19	1.18[a]
	Normoaerated	81.45	81.86
LLR1	Hyperaerated	0.33	0.26[d]
	Poorly aerated	15.89[d]	30.36[d]
	Nonaerated	1.18	1.78
	Normoaerated	82.19	65.17
RLR	Hyperaerated	0.35	0.42
	Poorly aerated	25	17.01[e]
	Nonaerated	1.5	1.38
	Normoaerated	72.6	80.56
LLR2	Hyperaerated	0.43	0.3
	Poorly aerated	16.02	27.52
	Nonaerated	1.23	1.82
	Normoaerated	81.94	68.51

Expiratory helical CT scans of the thorax were performed at 0 and 20 minutes when cats were in SR and at 0, 5, 10, 20, 30, and 40 minutes in each LR position. For the CT images, the lungs were segmented from the surrounding structures with a 3-D growing ROI tool by setting a threshold attenuation range of –1,280 to –200 HU. The trachea was then manually removed from the ROI to the level of the mainstem bronchi. The segmented lungs were then separated manually into the left lung and right lung fields. The accessory lung lobe was included in the right lung field. Regions of –199 to +100 HU within each lung field were manually included into the ROI by use of the brush tool (excluding major blood vessels to the level of the primary bronchi). Thus, separate ROIs for the left and right lung fields (excluding the trachea to the level of the mainstem bronchi and major blood vessels) with an attenuation range of –1,280 to +100 HU for each helical CT acquisition were obtained. By use of an image analysis workstation and software, segmented lung ROIs were analyzed to determine lung attenuation (HU). All attenuation classification analyses were performed with means calculated for each period of recumbency from data obtained at all time points during that period. A classification scheme[12] was used for lung attenuation analysis as follows: hyperaerated (–1,000 to –901 HU), normoaerated (–900 to –501 HU), poorly aerated (–500 to –101 HU), and nonaerated (–100 to +100 HU) lung tissue.

[a]For a given lung field, the value obtained when the cats were in SR differed significantly from the value obtained during LLR2. [b]For a given lung field, the value obtained when the cats were in SR differed significantly from the value obtained during RLR. [c]For a given lung field, the value obtained when the cats were in SR differed significantly from the value obtained during LLR1. [d]For a given lung field, the value obtained during LLR1 differed significantly from the value obtained during RLR. [e]For a given lung field, the value obtained during RLR differed significantly from the value obtained during LLR2.

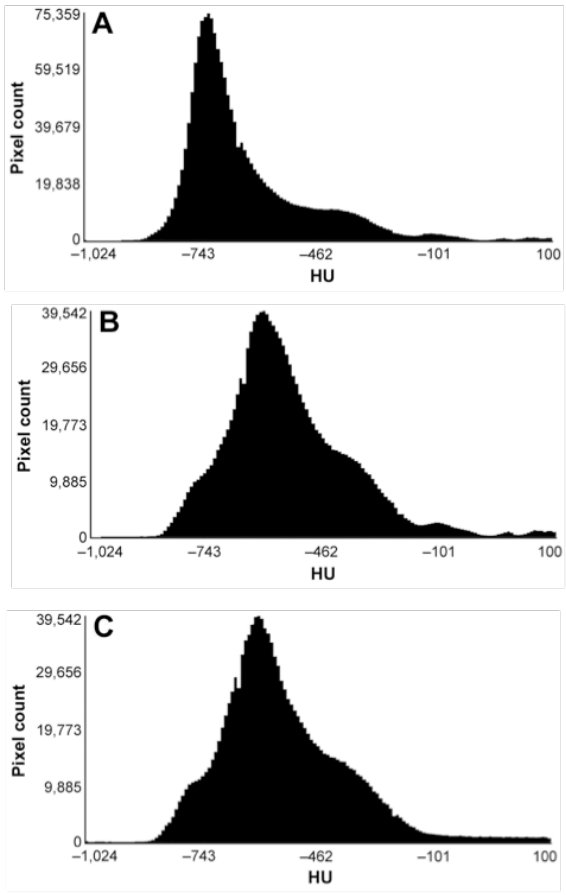

Figure 3—Representative histograms to illustrate the distribution of HU values for the left lung of 1 of the 8 study cats in Figure 2 during SR (A), immediately after the start of LLR1 (B), and at 40 minutes of the LLR1 (C). Notice the significant shift of the curve toward the right (increase in HU) as soon as the cat is transitioned into LLR. At the 40-minute point of LLR1, there is no further significant change in HU. Notice that the degree of true atelectasis (attenuation of lung tissue, –100 to +100 HU) is not notable at any time point. ***See*** Figures 1 and 2 for remainder of key.

Sternal recumbency resulted in the lowest overall lung attenuation value (–636.4 HU), compared with overall values during all other periods of recumbency (LLR1, –595.3 HU; RLR, –608.1 HU; and LLR2, –602.4 HU). The volume of the right (76.1 cm^3) and left (58.8 cm^3) lungs in SR differed significantly; however, there was no significant difference in attenuation (left lung, –639.7 HU; right lung, –635.2 HU). This difference in volume between the left and right lungs was again attributed to the naturally larger volume of the right lung.

Lung attenuation classification

Similar to comparisons of lung attenuation and volume, all attenuation classification analyses were performed with means calculated for each period of recumbency from data obtained at all time points during that period. During LLR1, the percentage of poorly aerated lung tissue (30.36%) was significantly increased, compared with that when cats were in SR (16.44% **[Table 1]**). This was visualized as a shift of the HU curve toward the right **(Figure 3)**. During LLR2, the percentages of poorly aerated (27.52%) and nonaerated areas of the left lung (1.82%) were significantly increased, compared with the findings when cats were in SR (16.44% and 1.18%, respectively). During RLR, the left lung had a significantly higher percentage of hyperaerated tissue (0.42%), compared with that when cats were in SR (0.26%) or during LLR1 (0.26%), and a significantly lower percentage of poorly aerated tissue (17.01%), compared with that during LLR1 (30.36%) or LLR2 (27.52%). Other comparisons of left lung attenuation in relation to periods of recumbency yielded no significant differences.

During RLR, the percentage of poorly aerated lung tissue in the right lung was significantly greater than that during LLR1 (15.89% [Table 1]). During LLR2, the percentage of hyperaerated lung tissue of the right lung (0.43%) was significantly greater than that identified when the cats were in SR (0.24%). Other comparisons of right lung attenuation in relation to periods of recumbency yielded no significant differences.

Discussion

Compared with findings when cats were in SR, the dependent lung lobes during LR underwent a rapid and significant reduction in overall lung volume and an increase in attenuation, changes that were compatible with a reduction in pulmonary aeration. The changes in dependent lung lobe volume and attenuation occurred immediately after positioning the cats in LR and then remained static with no further significant change in either variable throughout each of the three 40-minute periods of LR. It was previously assumed that prolonged LR results in a greater degree of recumbency-associated atelectasis.[17,22] This was not proven in the present study, given that a reduction in pulmonary aeration within the dependent lung occurred immediately following repositioning and did not worsen over time. A recent study[14] in dogs revealed a similar rapid reduction in aeration of the dependent lung, wherein a reduction in aeration of the dependent lung lobes was detected within 3 to 8 minutes after positioning in LR and was associated with little progression over time. From the results of the present study, it is unclear whether prolonged LR (> 40 minutes) would lead to a further reduction in pulmonary aeration and increase in the degree of atelectasis. Given the lack of progressive change in those variables in the study cats over time during LLR1, RLR, or LLR2, we think it is unlikely that the degree of pulmonary aeration would decrease further with LR of > 40 minutes' duration. Moreover, placement of research cats in LR for periods > 40 minutes may be neither necessary nor ethically justifiable.

The present study was designed to maximize the potential formation of atelectasis (nonaerated lung) in the study cats. This was achieved by use of inhalation anesthesia[23] with 100% inspired oxygen concentration[15] and acquisition of helical CT scans during the expiratory pause. Despite these factors, analysis of the lung attenuation classification revealed that the overall percentage of atelectasis formation during SR or LR in the present study was small (up to 1.82%). The most significant change in the dependent lung in LR was an increase in the percentage of poorly aerated lung tissue. Although there was a significant increase in nonaerated lung tissue within the dependent left lung lobe during LLR1, compared with the percentage when cats were in SR, this difference was small (1.82% vs 1.18%). Differences in the percentage of nonaerated lung tissue among other positions were not significant. These findings suggested that the rapid increase in lung attenuation observed in the dependent lungs during LR is primarily a result of an increase in the percentage of poorly aerated lung tissue, rather than a significant increase in the percentage of nonaerated lung tissue. Results of the present study are consistent with those of a recent investigation[14] that used a cross-sectional quantitative evaluation method in dogs, which determined that atelectasis formation (–100 to +100 HU) did not occur in healthy anesthetized dogs maintained in LR. This finding was in contrast to results of previous studies that revealed a high prevalence of atelectasis in anesthetized cats placed in DR[15] or SR.[16] A reason for this discrepancy may be that atelectasis was measured subjectively in the previous studies[15,16] in contrast to the present study wherein atelectasis was objectively measured and defined as lung attenuation between –100 to +100 HU.[4,12] It is possible that subjective assessment of lung attenuation may have resulted in areas of poorly aerated lung tissue (≤ –101 HU) being interpreted as atelectasis. In another study[15] of anesthetized cats, atelectasis was measured objectively, and results indicated that the degree of atelectasis formation was higher than that determined in the cats of the present study. Two important methodological differences may explain this discrepancy. First, the cats in that study[15] underwent CT following routine ovariohysterectomy resulting in a significantly longer time before the scans were performed (mean interval, 62.2 minutes), compared with procedures in the present study. It is possible that the increased duration of anesthesia may have contributed to the higher degree of atelectasis in the cats that underwent surgery. However, given the lack of progression of the lung changes over time in the present study, we think that it is unlikely that the prolonged period of anesthesia contributed significantly to the difference in atelectasis formation. Second, the cats in that study[15] were placed in DR for the duration of the procedure, unlike the protocol used in the present study in which cats were positioned in SR, LLR, and RLR. Although the effect of DR was not assessed in the present study, it is known that lung attenuation increases during DR, compared with the effects of placement in other recumbent positions.[24,25]

A recumbency-associated increase in lung attenuation or radiographic opacity can complicate the interpretation of CT or radiographic assessments of veterinary patients. It has always been assumed that this was a result of border effacement of areas of lung disease with atelectatic lung tissue.[17] On the basis of the results of the present study, increased lung attenuation or radiographic opacity in diagnostic imaging studies may largely be attributable to an increase in the percentage of poorly aerated lung tissue, and not necessarily a result of increases in the degree of true atelectasis or percentage of nonaerated lung tissue. However, it is unclear whether the increase in lung attenuation found in the present study could still interfere with the identification of lung disease. Future studies to investigate lesion detection in association with the dependent-nondependent status of lungs may provide useful information in this regard.

Compared with the data obtained when the cats of the present study were in SR, the significant reduction in pulmonary aeration of the dependent right lung during RLR was less pronounced than the significant reduction in pulmonary aeration of the dependent left lung during LLR1 or LLR2. This finding supported that of a previous study,[14] in which there was no decrease in aeration of the right lung lobes in dogs placed in RLR but patchy areas of abnormally increased attenuation were infrequently detected in the left cranial lung lobe in dogs placed in LLR. Another recent study[24] revealed that ground-glass opacities were detected more frequently and were more severe in CT images from dogs in LLR, compared with findings for other positions. The reasons for this are still unclear and at this stage speculative. The presence of a cardiac notch may reduce compression of the right middle lung lobe by the heart, leading to a smaller reduction in pulmonary aeration. The phrenicopericardial ligament may also act as an anchor to the apex, thereby limiting displacement of the heart and subsequent lung compression in RLR, compared with changes associated with LLR.

In the present study, the lowest overall lung attenuation was detected when cats were in SR. This was consistent with results of previous studies involving dogs, in which positioning in SR resulted in the highest functional residual capacity[26] and least amount of quantifiable atelectasis,[24] compared with findings for dogs positioned in LR. Among the cats of the present study, mild compensatory hyperinflation of the nondependent right lung was noted during LLR1 and LLR2 as evidenced by a significant increase in volume of the nondependent right lung, compared with right lung volume when cats were in SR. A similar effect was not observed in the left lung during RLR. A reason for lack of compensatory hyperinflation in the left lung may be the study design, wherein the cats were transitioned from SR into LLR1 first, resulting in the left lung undergoing a considerable re-

duction in pulmonary aeration before cats were transitioned into RLR. Whether cats undergoing RLR first would have a different effect on pulmonary aeration warrants further investigation. It may also be that the larger overall volume of the right lung allows for greater overall hyperinflation. Inclusion of the accessory lung lobe in the ROI for the right lung may have also contributed to an overall greater nondependent right lung volume because the accessory lung lobe appears to be less commonly affected by pulmonary atelectasis or collapse,[16] compared with the other lung lobes. Although there was a significant increase in the percentage of hyperaerated lung tissue in the left lung during RLR, compared with findings when cats were in SR and during LLR1, and in the right lung during LLR2, compared with the percentage when cats were in SR, the magnitude of these changes was small and a concurrent significant decrease in overall attenuation was not noted.

In the present study, acquisition of diagnostic-quality helical CT scans during the expiratory pause and without breath-hold techniques was crucial to maximize the potential for atelectasis formation in the study cats. To attain this goal, experimental requirements included short CT scan times, slow respiratory rates in the cats, and accurate coordination of the timing of the CT scan with the expiratory pause. To achieve the short scan times, a high collimator pitch (1.438) and slice thickness (2 mm) were used, which resulted in scan times of 3.045 to 3.494 seconds. Slower respiratory rates were achieved by maintaining the cats under a deep plane of anesthesia. Mainstream capnography was used to remotely monitor the respiratory rate and breathing phases of the cats to achieve accurate coordination of the CT scan with the expiratory pause. Control of these factors resulted in diagnostic-quality CT scans of the thorax in the expiratory pause without notable motion artifact.

Although potentially confusing, the quantitative HU classification scheme used in the present study defines nonaerated lung tissue as areas with attenuation of –100 to +100 HU, which implies that there is retained air within the lung tissue. However, previous studies[27–37] that used the same classification scheme indicated that the voxels within the nonaerated lung compartment are not strictly gas free because they have a gas-to-tissue ratio of between 1:10 and 0. This takes into account that even in complete small airway collapse, some gas remains in the pulmonary unit behind the collapsed bronchioles.[27] This method of quantitative classification has been used extensively in human medical research[27–36] and some veterinary medical investigations.[11,12] In humans, the classification scheme has been widely used in the assessment of pulmonary function and disease as a separate and sometimes complementary tool to morphological subjective assessment. It is this quantitative classification that derives the most functional information in pulmonary pathophysiologic studies.[32–37]

The changes in pulmonary volume and attenuation in the dependent lung of the cats of the present study may reflect normal pulmonary collapsibility in healthy animals. This has potential future applications, particularly in research of COPD and emphysema because these conditions result in a reduction of pulmonary collapsibility.[30] Studies[31–37] in humans have revealed that quantitative CT indices of lung collapsibility are correlated with pulmonary function test results in patients with COPD; in those studies, lower lung collapsibility suggested more severe COPD and higher lung collapsibility suggested less severe COPD. This field of research into airway collapsibility and atelectasis of lungs with quantitative CT indices and correlation with pulmonary function tests in humans with COPD is particularly interesting in its potential application to veterinary patients. In dogs and cats, COPD is a difficult syndrome to diagnose because its clinicopathologic features overlap with those of other lower airway diseases[7] and, in general, detection of any lower airway disease with conventional radiography is difficult.[38,39] Acquisition of expiratory thoracic CT scans from veterinary patients is challenging and could be considered similar to the challenges of acquisition of expiratory thoracic CT scans from young children.[20,21] Quantitative CT analysis of lung volume and attenuation in veterinary patients placed in LR could potentially replace the need to acquire expiratory scans to obtain information regarding pulmonary function and air trapping.[19–21,28–37] Results of the present study may provide a starting point for investigation of the value of quantitative thoracic CT scans obtained from patients in LR as a functional tool in cases of COPD and emphysema. Such functional information may prove useful for the diagnosis, prognosis, and treatment monitoring of feline lung diseases.

There were several limitations to the present study including the small number of cats, lack of evaluation of intra- or interobserver repeatability for lung segmentation, effect of positioning sequence, and a deep plane of anesthesia. Given the small number of animals used in the study, there was insufficient power in the statistical analysis to detect significant differences at some points where the raw data indicated differences. A repeated study with a larger number of animals may be able to elucidate these differences more clearly. Although it would have been interesting to extrapolate the degree of change in attenuation and volume of the lungs in each position, the small number of study cats yielded insufficient data from which to extend these results to the entire feline population. The CT lung segmentation was performed by only 1 observer and was not repeated. We attempted to minimize the effect of intraobserver discrepancies by the use of a semiautomated method for lung segmentation. However, a degree of manual segmentation by means of a brush tool was still required; therefore, possible intraobserver discrepancies could not be completely excluded. An additional phase of the

study wherein the cats were transitioned to RLR following the initial SR positioning might have revealed some differences in pulmonary aeration, compared with findings after transitioning from the SR positioning to LLR first. It is unlikely that there would have been any difference in the prevalence of atelectasis formation, given the low prevalence detected in the present study. For each study cat, morphological pulmonary disease was ruled out by means of an initial diagnostic CT scan; however, functional pulmonary studies were not performed. As such, the presence of subclinical functional pulmonary disease that may influence pulmonary aeration cannot be completely excluded. Lastly, the cats were assessed in a deep plane of anesthesia, which may not reflect the routine handling of clinical patients undergoing diagnostic CT. Therefore, care should be taken when extrapolating the results of the present study to such cases.

Results of the present study indicated that there was a rapid and significant reduction in lung volume and an increase in lung attenuation of the dependent lung lobes in healthy cats anesthetized in LR. These changes occurred immediately (at 0 minutes) after each cat's position was modified and the subsequent scan was initiated. The lung volume and attenuation changes remained static over time in each position. The attenuation change was predominantly due to an increase in the percentage of poorly aerated lung tissue (areas of attenuation of −500 to −101 HU). Additionally, data obtained in the present study indicated that the percentage of true atelectasis in the lungs (areas of attenuation of −100 to +100 HU) of the healthy cats in the present study was minimal. Therefore, increased attenuation within the dependent lungs observed in thoracic radiographic and CT images of anesthetized animals in LR may be attributable predominantly to an increase in the percentage of poorly aerated lung tissue rather than to an increase in the percentage of truly atelectic areas of tissue.

Acknowledgments

This manuscript represents a portion of a thesis submitted by Dr. Foo to the Faculty of Veterinary Science, University of Sydney, as partial fulfillment of the requirements of the Master of Veterinary Clinical Studies degree.

The authors declare that there were no conflicts of interest.

Presented in abstract form at the 2017 Australia and New Zealand College of Veterinary Scientists (ANZCVS) Science Week, Surfers Paradise, QLD, Australia, July 2017.

The authors thank Helen Laurendet for technical assistance.

Footnotes

a. Eurofins Agroscience Services Pty Ltd, Orange, NSW, Australia.
b. Alfaxan, Jurox Pty Ltd, Rutherford, NSW, Australia.
c. Acepromazine, Ceva Animal Health Pty Ltd, Glenorie, NSW, Australia.
d. Butorgesic, Troy Laboratories Pty Ltd, Smithfield, NSW, Australia.
e. Medetate Injection, Jurox Pty Ltd, Rutherford, NSW, Australia.
f. Lignocaine hydrochloride 2% Pfizer Australia Pty Ltd, West Ryde, NSW, Australia.
g. Isoflo, Abbott Australasia Pty Ltd, Botany, NSW, Australia.
h. Viaflex, Baxter Healthcare Pty Ltd, Toongabbie, NSW, Australia.
i. Phillips, 16-slice Brilliance CT V2.3, Phillips Medical Systems Netherlands, Eindohoven, the Netherlands.
j. ASUS PA238QR, Beitou District, Taipei, Taiwan.
k. Macbook Pro OS X 10.11, 1 Infinite Loop, Cupertino, Calif.
l. OsiriX v8.0.1 64-bit, Pixmeo SARL, Bernex, Switzerland.
m. Mango v4.0.1, Research Imaging Institute, University of Texas Health Science Center, San Antonio, Tex.
n. Microsoft Excel 2008 for Mac, Version 14.6.9, Microsoft Corp, Redmond, Wash.
o. GenStat, 17th edition, VSN International Ltd, Hemel Hempstead, England.

References

1. Verschakelen JA, van Fraeyenhoven L, Laureys G, et al. Differences in CT density between dependent and nondependent portions of the lung: influence of lung volume. *AJR Am J Roentgenol* 1993;161:713–717.
2. Ahlberg N, Hoppe F, Kelter U, et al. A computed tomographic study of volume and x-ray attenuation of the lungs of Beagles in various body positions. *Vet Radiol* 1985;22:43–47.
3. Duggan M, Kavanagh BO. Pulmonary atelectasis: a pathogenic perioperative entity. *Anesthesiology* 2005;102:838–854.
4. Magnusson L, Spahn DR. New concepts of atelectasis during general anesthesia. *Br J Anaesth* 2003;91:61–72.
5. Brismar B, Hedenstierna G, Lundquist H, et al. Pulmonary densities during anesthesia with muscular relaxation: a proposal of atelectasis. *Anesthesiology* 1985;62:422–428.
6. Woo SW, Berlin D, Hedley-White J. Surfactant function and anesthestic agents. *J Appl Physiol* 1969;26:571–577.
7. Trzil JE, Reinero CR. Update on feline asthma. *Vet Clin North Am Small Anim Pract* 2014;44:91–105.
8. Henao-Guerrero N, Ricco C, Jones JC, et al. Comparison of four ventilator protocols for computed tomography of the thorax in healthy cats. *Am J Vet Res* 2012;73:646–653.
9. Lundquist H, Hedenstierna G, Strandberg A, et al. CT-assessment of dependent lung densities in man during general anaesthesia. *Acta Radiol* 1995;36:626–632.
10. Joyce CJ, Baker AB. What is the role of absorption atelectasis in the genesis of perioperative pulmonary collapse? *Anaesth Intensive Care* 1995;23:691–696.
11. Staffieri F, De Monte V, De Marzo C, et al. Alveolar recruiting maneuver in dogs under general anesthesia: effects on alveolar ventilation, gas exchange, and respiratory mechanics. *Vet Res Commun* 2010;34:S131–S134.
12. Staffieri F, Franchini D, Carella GL, et al. Computed tomographic analysis of the effects of two inspired oxygen concentrations on pulmonary aeration in anesthetized and mechanically ventilated dogs. *Am J Vet Res* 2007;68:925–931.
13. Giglio RF, Winter MD, Reese DJ, et al. Radiographic characterization of presumed plate-like atelectasis in 75 nonanesthetized dogs and 15 cats. *Vet Radiol Ultrasound* 2013;54:326–331.
14. le Roux C, Cassel N, Fosgate GT, et al. Computed tomographic findings of pulmonary atelectasis in healthy anaesthetized Beagles. *Am J Vet Res* 2016;77:1082–1092.
15. Staffieri F, De Monte V, De Marzo C, et al. Effects of two fractions of inspired oxygen on lung aeration and gas exchange in cats under inhalant anaesthesia. *Vet Anaesth Analg* 2010;37:483–490.
16. Lamb CR, Jones ID. Associations between respiratory signs and abnormalities reported in thoracic CT scans of cats. *J Small Anim Pract* 2016;57:561–567.
17. Thrall DE. Principles of radiographic interpretation of the thorax. In: *Textbook of veterinary diagnostic radiology.* 6th ed. St Louis: Saunders Elsevier, 2013;474–488.
18. Morandi F, Mattoon JS, Lakritz J, et al. Correlation of helical and incremental high-resolution thin-section computed tomographic imaging with histomorphometric quantitative evaluation of lungs in dogs. *Am J Vet Res* 2003;64:935–944.
19. Franquet T, Stern EJ, Gimenez A, et al. Lateral decubitus

CT: a useful adjunct to standard inspiratory-expiratory CT for the detection of air trapping. *AJR Am J Roentgenol* 2000;174:528–530.
20. Choi SJ, Choi BK, Kim HJ, et al. Lateral decubitus HRCT: a simple technique to replace expiratory CT in children with air trapping. *Pediatr Radiol* 2002;32:179–182.
21. Lucaya J, Garcia-Pena P, Herrera L, et al. Expiratory chest CT in children. *AJR Am J Roentgenol* 2000;174:235–241.
22. Morandi F, Mattoon JS, Kakritz J, et al. Correlation of helical and incremental high-resolution thin-section computed tomographic and histomorphometric quantitative evaluation of an acute inflammatory response of lungs in dogs. *Am J Vet Res* 2004;65:1114–1123.
23. Oliveira CR, Mitchell MA, O'Brien RT. Thoracic computed tomography in feline patients without use of chemical restraint. *Vet Radiol Ultrasound* 2011;52:368–376.
24. Lee SK, Park S, Cheon B, et al. Effect of position and time held in that position on ground-glass opacity in computed tomographic images of dogs. *Am J Vet Res* 2017;78:279–288.
25. Kim T, Chang D, Chang J, et al. Assessment of computed tomographic lung density in Beagle and Shih Tzu dogs. *J Vet Clin* 2010:273–283.
26. Rozanski EA, Bedenice D, Lofgren J, et al. The effect of body position, sedation, and thoracic bandaging on functional residual capacity in healthy deep-chested dogs. *Can J Vet Res* 2010;74:34–39.
27. Gattinoni L, Caironi P, Pelosi P, et al. What has computed tomography taught us about the acute respiratory distress syndrome? *Am J Respir Crit Care Med* 2001;164:1701–1711.
28. Vieira SR, Puybasset L, Richecoeur J, et al. A lung computed tomographic assessment of positive end-expiratory pressure-induced lung overdistension. *Am J Respir Crit Care Med* 1998;158:1571–1577.
29. Mets OM, de Jong PA, van Ginneken B, et al. Quantitative computed tomography in COPD: possibilities and limitations. *Lung* 2012;190:133–145.
30. Yamashiro T, Matsuoka S, Bartholmai B, et al. Collapsibility of lung volume by paired inspiratory and expiratory CT scans: correlations with lung function and mean lung density. *Acad Radiol* 2010;17:489–495.
31. Arakawa A, Yamashita Y, Nakayama T, et al. Assessment of lung volumes in pulmonary emphysema using multidetector helical CT: comparison with pulmonary function tests. *Comput Med Imaging Graph* 2001;25:399–404.
32. Xie X, de Jong PA, Oudkerk M, et al. Morphological measurements in computed tomography correlate with airflow obstruction in chronic obstructive pulmonary disease: systematic review and meta-analysis. *Eur Radiol* 2012;22:2085–2093.
33. Akira M, Toyokawa K, Inoue Y, et al. Quantitative CT in chronic obstructive pulmonary disease: inspiratory and expiratory assessment. *AJR Am J Roentgenol* 2009;192:267–272.
34. Lee YK, Oh YM, Lee JH, et al. Quantitative assessment of emphysema, air trapping, and airway thickening on computed tomography. *Lung* 2008;186:157–165.
35. Matsuoka S, Kurihara Y, Yagihashi K, et al. Quantitative assessment of peripheral airway obstruction on paired expiratory/inspiratory thin-section computed tomography in chronic obstructive pulmonary disease with emphysema. *J Comput Assist Tomogr* 2007;31:384–389.
36. Kauczor HU, Hast J, Heussel CP, et al. CT attenuation of paired HRCT scans obtained at full inspiratory/expiratory position: comparison with pulmonary function tests. *Eur Radiol* 2002;12:2757–2763.
37. Newman KB, Lynch DA, Newman LS, et al. Quantitative computed tomography detects air trapping due to asthma. *Chest* 1994;106:105–109.
38. Adamama-Moraitou KK, Patsikas MN, Koutinas AF. Feline lower airway disease: a retrospective study of 22 naturally occurring cases from Greece. *J Feline Med Surg* 2004;6:227–233.
39. Gadbois J, d'Anjou MA, Dunn M, et al. Radiographic abnormalities in cats with feline bronchial disease and intra- and inter-observer variability in radiographic interpretation: 40 cases (1999–2006). *J Am Vet Med Assoc* 2009;234:367–375.

5 - Conclusion:

This thesis has improved our understanding of the use of lung and hepatic CT and cholangiography using CT therefore contributing to the field of knowledge of feline medicine to improve the health and welfare of cats. In particular, these experimental research studies documented the safe use of Gd-EOB-DTPA as a potential gadolinium-based hepatobiliary contrast medium in healthy cats at three different doses and improved our knowledge of the prevalence and timing of changes in lung density and volume under anaesthesia in different positions in healthy cats.

We documented the first use of Gd-EOB-DTPA in healthy cats at low (0.0125 mmol/kg), medium (0.1 mmol/kg), and high (0.3 mmol/kg) doses. No adverse contrast related effects were noted including on renal and liver parameters and the cardiovascular system and gastrointestinal tract. A positive relationship in contrast enhancement was found with increasing dose. Using Gd-EOB-DTPA as a positive contrast media with CT provided a clear objective homogenous hepatic parenchyma enhancement and only poor to moderate biliary enhancement by visual assessment. The timing of hepatobiliary enhancement was different in the cat, with the liver having a significantly higher attenuation at 45 mins, with homogenous enhancement at all doses of contrast medium. The contrast-enhanced cystic and bile duct HU were significantly higher and maximal at 65 mins with the contrast-enhanced gallbladder HU not plateauing by 85 mins. This timing is similar to dogs and is longer compared to humans, in which the scanning of the biliary tract is recommended at 20-30 minutes after injection, with improved image quality of the bile ducts after a scan delay of 50-60 mins in patients without hepatobiliary dysfunction. Despite the poor to moderate biliary CT enhancement by visual assessment in our study, consideration into further research could include a higher contrast dose, longer duration between injection of the contrast media and scanning, and use in cats with diffuse or focal hepatic disease. Despite the limitations of MRI, research could be considered evaluating Gd-EOB-DTPA in cats with hepatic MRI and cholangiography, since MRI may improve the conspicuity of gadolinium in the hepatobiliary tract at lower doses as a reduced molar dose is required in MRI compared to CT.

We demonstrated that the dependent lung lobes in healthy anaesthetised cats underwent a rapid reduction in lung volume and an associated increase in lung density in lateral recumbency due to an increase in poorly aerated lung tissue, rather than truly atelectatic lung. The lung density did not progress over time with the dependent lung quickly recovering in density and volume when it became the non-dependent lung. There was also less poorly aerated lung in sternal recumbency than lateral recumbency.

Despite a lack of standardised thoracic CT protocol in cats to evaluate the lung, from this research we can recommend patients being placed in sternal recumbency for morphologic lung assessment, similar to other research in dogs, as this recumbency has a lower overall lung density in thoracic CT scans and is therefore least likely to mask pulmonary pathology. Following this, we can also recommend sternal recumbency for abdominal CT scans. In particular, it is desirable to have the least overall increase in lung density during

hepatic imaging and cholangiography using Gd-EOB-DTPA because of the longer duration of anaesthesia required for the recommended scan times. Since the dependent lung rapidly recovers when placed non dependently, in cases of concern wherein dependent poorly aerated or non-aerated is masking true pulmonary pathology, the patient can be positioned in the contralateral recumbency and the healthy lung should rapidly recover, therefore potentially increasing reducing the poorly or non aerated lung and increasing visualisation of possible pathologic lung changes.

Finally since lung density increases and volume reduction occur rapidly and remain static, we can recommend that prompt thoracic imaging, although desirable, is not essential and time can be taken to ensure ideal patient positioning to obtain optimal image quality using anaesthesia to avoid motion artefact. From this research, we can suspect that a delayed thoracic scan will likely not contribute to progressive masking of pulmonary pathology due to true atelectasis and that the longer duration of scan time required for hepatobiliary imaging is not contributing to true atelectasis which has been shown to be associated with post anaesthetic complications.

This thesis used positive (Gd-EOB-DTPA) and negative (gas) contrast to examine the relationship of attenuation (HU) over time in both studies. Further investigations in cats into the effect of hepatobiliary disease on the contrast attenuation over time in the hepatobiliary tract and the effect of reduced lung function and compliance on lung density and volume using different body positions and CT could be considered.

CT provided clear visualisation of the anatomy without motion artefact in all scans across both studies. Both studies confirmed that anaesthesia was sufficient to reduce patient motion and therefore motion artefact, thereby providing diagnostic scans that provided cross-sectional visualisation of the respective anatomic structures, with hyperventilation induced apnea in the hepatobiliary study and by use of an expiratory pause in the lung study. Further research could consider similar studies under sedation to evaluate their usefulness in multiple clinical scenarios, particularly if patients are not able to be safely anaesthetised.

The results from these studies demonstrate that there are unique considerations in veterinary patients, with regard to developing diagnostic tests that are relevant for each species, anatomy, size, shape and drug metabolism, in particular in cats. The impact of these considerations can affect the drug dose, timing of imaging studies and positioning when developing standardised protocols. The minimal difference in size and shape of cats, compared to dogs, means that the data from these studies can potentially be extrapolated for use in the majority of cat breeds.

This thesis has contributed to and advanced the field of knowledge in feline health by investigating two novel applications in lung and hepatic CT imaging and cholangiography. There are certainly motivations for further research in these fields to develop non-invasive morphologic and functional tests to rapidly diagnose pathology in cats with non-specific clinical signs. In particular, it would be desirable to develop a standardised protocol using a CT and one which provides a global view both of the abdomen, given the co-morbidities

often found in cats with hepatobiliary disease; and to develop a standardised protocol using CT for thoracic imaging to evaluate structural and functional pulmonary pathology in cats.

Further research in cats could investigate the effect of recumbency on cats with pulmonary pathology and evaluate the conspicuity of pulmonary pathology despite increases in lung density due to recumbency. Assessing the value of quantitative thoracic CT scans in lateral recumbency as a functional diagnostic tool in cats with feline asthma and air trapping, COPD and emphysema may prove useful for the diagnosis, prognosis, and treatment monitoring of feline lung diseases. Particularly in cats with bronchial disease since hyperaerated lung is also seen in air trapping in people, for example with COPD, and CT lung changes related to recumbency may also provide functional information, such as bronchial spasm induced trapping air and reducing lung density in cats (Foo et al., 2018).

List of Abbreviations:

CT	Computed tomography
Gd-EOB-DTPA	Gadoxetic acid
Min/s	Minutes
IV	Intravenous
Mmol	Millimole
Kg	Kilogram
HU	Hounsfield units
%	Percentage
COPD	Chronic Obstructive Pulmonary Disease
USA	United States of America
MDCT	Multidetector Computed Tomography
3D	Three dimensional
MRI	Magnetic Resonance Imaging
T	Telsa
ERCP	Endoscopic retrograde cholangiopancreatography
NM	Nuclear Medicine
2D	Two dimensional
FNA	Fine Needle Aspirate
MRC	Magnetic resonance cholangiography
MRCP	Magnetic resonance cholangiopancreatography
DIC-CT	Drip infusion cholangiography
ROI	Region of Interest
CBD	Common Bile duct
ml	Millilitre
MDP	Major duodenal papilla
WSAVA	World Small Animal Veterinary Association
EHBO	Extra hepatic biliary obstruction
ERP	Endoscopic retrograde pancreatography
CECT	Contrast enhanced computed tomography
CEUS	Contrast enhanced Ultrasonography
h	Hours
EU	European Union
I	Iodine
KV	Kilovolts
KeV	Kiloelectronvolt
S	Second
Gd	Gadolinium
Gd-BOPTA	Gadobenate Dimeglumine
MnDpDp	Mangafodipir trisodium
Mm	Millimeter
Kg	Kilogram

µmol	Micromole
µL	Microlitre
L	Litre
e.g.	For example
ROI	Region of Interest

References:

1. Adler, R., & Wilson, D. W. (1995). Biliary cystadenoma of cats. *Veterinary pathology*, *32*(4), 415–418.
2. Allison, A., Huizing, X., Jolliffe, C., & Schaafsma, I. (2017). Effect of fixed value positive end expiratory pressure valves on canine thoracic volume and atelectasis. *The Journal of small animal practice*, *58*(11), 645–651.
3. Amersham Health (2003, April) Material safety data sheet #1097 Teslascan pp 1-4. https://www.gehealthcare.co.uk/-/media/abccf7574a5d432d9cbd84614d80ace3.pdf
4. Anderson, S. W., Rho, E., & Soto, J. A. (2008). Detection of biliary duct narrowing and choledocholithiasis: accuracy of portal venous phase multidetector CT. *Radiology*, *247*(2), 418–427.
5. Arruda Bergamaschi, N., Huber, L., Ludewig, E., Böhler, A., Gumpenberger, M., Hittmair, K. M., Strohmayer, C., Folkertsma, R., & Rowan, C. (2023). Association between clinical history in the radiographic request and diagnostic accuracy of thorax radiographs in dogs: A retrospective case-control study. *Journal of veterinary internal medicine*, *37*(6), 2453–2459. .
6. Assefa, A. (2018). Diagnostic imaging techniques in veterinary practice: a review. Global Scientific Journal. Volume 6, Issue 9, September.
7. Balakrishnan, S., Singhal, T., Grandy-Smith, S., & El-Hasani, S. (2006). Agenesis of the gallbladder: lessons to learn. *JSLS : Journal of the Society of Laparoendoscopic Surgeons*, *10*(4), 517–519.
8. Banzato, T., Burti, S., Rubini, G., Orlandi, R., Bargellini, P., Bonsembiante, F., & Zotti, A. (2020). Contrast-enhanced ultrasonography features of hepatobiliary neoplasms in cats. *The Veterinary record*, *186*(10), 320.
9. Baralf, R.M. (2011). Lower respiratory tract diseases. In Little, S (Ed), *The cat, clinical medicine and management* (pp 861-891). Elsevier Health Sciences. Missouri, USA.
10. Bargellini, P., Orlandi, R., Paloni, C., Rubini, G., Fonti, P., Righi, C., Peterson, M. E., Rishniw, M., & Boiti, C. (2018). Contrast-enhanced *ultrasounds* complements two-dimensional ultrasonography in diagnosing gallbladder diseases in dogs. *Veterinary radiology & ultrasound*, *59*(3), 345–356.
11. Bayer Group. (2018, June). Australian Product Information for Biliscopin. https://resources.bayer.com.au/resources/uploads/PI/file9317.pdf
12. Bayer New Zealand Limited (2012, July) Data Sheet Primovist(TM). https://resources.bayer.com.au/resources/uploads/DataSheet/file10226.pdf
13. Bentley, C., Fouriez-Lablée, V., & Rossanese, M. (2024). Intra- and interobserver agreement in computed tomography localization of primary nonhematopoietic hepatic masses and comparison with surgical and histopathological outcomes in 21 cats. *Veterinary radiology & ultrasound*, *65*(5), 469–476.
14. Berent, A., Weisse, C., Schattner, M., Gerdes, H., Chapman, P., & Kochman, M. (2015). Initial experience with endoscopic retrograde cholangiography and endoscopic retrograde biliary stenting for treatment of extrahepatic bile duct

obstruction in dogs. *Journal of the American Veterinary Medical Association*, *246*(4), 436–446.
15. Berk, R. N., Barnhart, J. L., Nazareno, G., & Witt, B. L. (1981). The potential of iosulamide meglumine as a contrast material for intravenous cholangiography: an experimental study in dogs. *Investigative radiology*, *16*(3), 240–244.
16. Best, E. J., Bush, D. J., & Dye, C. (2010). Suspected choledochal cyst in a domestic shorthair cat. *Journal of feline medicine and surgery*, *12*(10), 814–817.
17. Bertolini, G., & Prokop, M. (2011). Multidetector-row computed tomography: technical basics and preliminary clinical applications in small animals. *Veterinary journal (London, England : 1997)*, *189*(1), 15–26.
18. Boland, L., & Beatty, J. (2017). Feline Cholangitis. The Veterinary clinics of North America. Small animal practice, 47(3), 703–724.
19. Bracco Diagnostics.(2017) Cholografin Meglumine Package Insert. https://www.accessdata.fda.gov/drugsatfda_docs/label/2017/009321s030lbl.pdf.
20. Brain, P. H., Barrs, V. R., Martin, P., Baralf, R., White, J. D., & Beatty, J. A. (2006). Feline cholecystitis and acute neutrophilic cholangitis: clinical findings, bacterial isolates and response to treatment in six cases. *Journal of feline medicine and surgery*, *8*(2), 91–103.
21. Briola, C. (2022). Magnetic Resonance Imaging and Magnetic Resonance Imaging Cholangiopancreatography of the Pancreas in Small Animals. *Veterinary Sciences*, *9*(8), 378.
22. Buote, N. J., Mitchell, S. L., Penninck, D., Freeman, L. M., & Webster, C. R. (2006). Cholecystoenterostomy for treatment of extrahepatic biliary tract obstruction in cats: 22 cases (1994-2003). *Journal of the American Veterinary Medical Association*, *228*(9), 1376–1382.
23. Burke, C., Alexander Grant, L., Goh, V., & Griffin, N. (2013). The role of hepatocyte-specific contrast agents in hepatobiliary magnetic resonance imaging. *Seminars in ultrasound, CT, and MR*, *34*(1), 44–53.
24. Caccamo, R., Twedt, D. C., Buracco, P., & McKiernan, B. C. (2007). Endoscopic bronchial anatomy in the cat. *Journal of feline medicine and surgery*, *9*(2), 140–149.
25. Campos, M. A., & Diaz, A. A. (2018). The Role of Computed Tomography for the Evaluation of Lung Disease in Alpha-1 Antitrypsin Deficiency. *Chest,* 153(5), 1240–1248.
26. Caoili, E. M., Paulson, E. K., Heyneman, L. E., Branch, M. S., Eubanks, W. S., & Nelson, R. C. (2000). Helical CT cholangiography with three-dimensional volume rendering using an oral biliary contrast agent: feasibility of a novel technique. *AJR. American journal of roentgenology*, *174*(2), 487–492.
27. Carlisle, C. (1977) A comparison of technics for cholecystography in the cat. *Veterinary Radiology,* 18(6):173-176
28. Center S. A. (2009). Diseases of the gallbladder and biliary tree. *The Veterinary clinics of North America. Small animal practice*, *39*(3), 543–598.

29. Chau, J., Podadera, J. M., Young, A. C., & Makara, M. A. (2017). Use of gadoxetic acid for computed tomographic cholangiography in healthy dogs. *American journal of veterinary research*, *78*(7), 828–839.
30. Cher, T., M.D., & Szklaruk, Janio,M.D. PhD. (2010). MR contrast agents: Applications in hepatobiliary imaging. *Applied Radiology*, 39(11), 26-31,34-36,38-40,42.
31. Choi, S-Y., Lee,I., Jeong, W-C., Heng, H.G., Lee, Y-W. and Choi, H-J. (2014). Quantitative CT evaluation for lung volume and density in dogs *J Vet Clinic,* 31(5):376-381.
32. Constant, C., Hecht, S., Craig, L.E., Lux, C. N., Cannon, C. M., & Conklin, G. A. (2016). Gadoxetate disodium (Gd-EOB-DTPA) contrast enhanced magnetic resonance imaging characteristics of hepatocellular carcinoma in dogs. *Vet Radiol ultrasound,* 57:594–600.
33. Cullen J. M. (2009). Summary of the World Small Animal Veterinary Association standardization committee guide to classification of liver disease in dogs and cats. *The Veterinary clinics of North America. Small animal practice*, *39*(3), 395–418.
34. Day M. J. (2016). Cats are not small dogs: is there an immunological explanation for why cats are less affected by arthropod-borne disease than dogs?. *Parasites & vectors*, *9*(1), 507.
35. Döhr, O., Hofmeister, R., Treher, M., & Schweinfurth, H. (2007). Preclinical safety evaluation of Gd-EOB-DTPA (Primovist). *Investigative radiology*, *42*(12), 830–841.
36. Duggan, M., & Kavanagh, B. P. (2005). Pulmonary atelectasis: a pathogenic perioperative entity. *Anesthesiology*, *102*(4), 838–854.
37. Eich, C. S., & Ludwig, L. L. (2002). The surgical treatment of cholelithiasis in cats: a study of nine cases. *Journal of the American Animal Hospital Association*, *38*(3), 290–296.
38. Ettinger, S.J. and Feldman, E.C. (2010). Section XVI Chapter 281 Aguirre A. *Textbook of Veterinary Internal Medicine,* Saunders Elsevier
39. Foo, T. S., Pilton, J. L., Hall, E. J., Martinez-Taboada, F., & Makara, M. (2018). Effect of body position and time on quantitative computed tomographic measurements of lung volume and attenuation in healthy anesthetized cats. *American journal of veterinary research*, *79*(8), 874–883.
40. Fujita, M., & Orima, H. (1994). Effect and safety of meglumine iotroxate for cholangiocystography in normal cats. *Veterinary Radiology & ultrasound,* 35: 79-82.
41. Fukuda, S., Reetz, J. A., Hamamoto, K., Griffin, L., & Schaffer, P. A. (2023). Diagnostic imaging and histopathologic features of rounded atelectasis in four cats and one dog: A descriptive case series study. *Veterinary radiology & ultrasound*, *64*(3), 411–419.
42. Gagne, J. M., Weiss, D. J., & Armstrong, P. J. (1996). Histopathologic evaluation of feline inflammatory liver disease. *Veterinary pathology*, *33*(5), 521–526.
43. Gaillot, H. A., Penninck, D. G., Webster, C. R., & Crawford, S. (2007). Ultrasonographic features of extrahepatic biliary obstruction in 30 cats. Veterinary radiology & *ultrasound*, 48(5), 439–447.

44. Gaschen L. (2009). Update on hepatobiliary imaging. The Veterinary clinics of North America. Small animal practice, 39(3), 439–467.
45. Gaschen, L. (2016). Imaging in dogs and cats with respiratory distress: The lung, *WSAVA Conference Proceedings*. https://www.vin.com/apputil/content/defaultadv1.aspx?pId=19840&catId=105878&id=8249670&ind=372&objTypeID=17
46. GE Healthcare Australia PTY LTD (2021, Nov). Iohexol Product information. https://www.ebs.tga.gov.au/ebs/picmi/picmirepository.nsf/pdf?OpenAgent=&id=CP-2010-PI-01628-3&d=20241227172310101
47. Gobbo, O. L., Zurek, M., Tewes, F., Ehrhardt, C., & Crémillieux, Y. (2012). Manganese: a new contrast agent for lung imaging?. *Contrast media & molecular imaging*, *7*(6), 542–546.
48. Gold, J. A., Zeman, R. K., & Schwartz, A. (1979). Computed tomographic cholangiography in a canine model of biliary obstruction. *Investigative radiology*, *14*(6), 498–501.
49. Grand, J. G., Doucet, M., Albaric, O., & Bureau, S. (2010). Cyst of the common bile duct in a cat. *Australian veterinary journal*, *88*(7), 268–271.
50. Greco, A., Meomartino, L., Gnudi, G., Brunetti, A., & Di Giancamillo, M. (2022). Imaging techniques in veterinary medicine. Part II: Computed tomography, magnetic resonance imaging, nuclear medicine. *European journal of radiology open*, *10*, 100467.
51. Gulati, A., & Balasubramanya, R. (2024). Lung Imaging. *In: StatPearls [internet].* Treasure Island, Florida: StatPearls Publishing. Available from: https://www.ncbi.nlm.nih.gov/sites/books/NBK558976/
52. Hamm, B., Staks, T., Mühler, A., Bollow, M., Taupitz, M., Frenzel, T., Wolf, K. J., Weinmann, H. J., & Lange, L. (1995). Phase I clinical evaluation of Gd-EOB-DTPA as a hepatobiliary MR contrast agent: safety, pharmacokinetics, and MR imaging. *Radiology*, *195*(3), 785–792.
53. Hampson, E.C.G.M., Filippich, L.J., Kelly, W.R. and Evans, K. (1987). Congenital biliary atresia in a cat: a case report. *Journal of Small Animal Practice*, 28: 39-48.
54. Hashimoto, M., Itoh, K., Takeda, K., Shibata, T., Okada, T., Okuno, Y., & Hino, M. (2008). Evaluation of biliary abnormalities with 64-channel multidetector CT. *Radiographics : a review publication of the Radiological Society of North America, Inc*, *28*(1), 119–134.
55. Hayakawa, S., Sato, K., Sakai, M., Kutara, K., Asano, K., & Watari, T. (2018). CT cholangiography in dogs with gallbladder mucocoele. *The Journal of small animal practice*, 10.1111/jsap.12832.
56. Heller, S. L., & Lee, V. S. (2005). MR imaging of the gallbladder and biliary system. *Magnetic resonance imaging clinics of North America*, *13*(2), 295–311.
57. Henninger W. (2003). Use of computed tomography in the diseased feline thorax. *The Journal of small animal practice*, *44*(2), 56–64.
58. Henao-Guerrero, N., Ricco, C., Jones, J. C., Buechner-Maxwell, V., & Daniel, G. B. (2012). Comparison of four ventilatory protocols for computed tomography of the thorax in healthy cats. *American journal of veterinary research*, *73*(5), 646–653.

59. Hirose, N., Uchida, K., Kanemoto, H., Ohno, K., Chambers, J. K., & Nakayama, H. (2014). A retrospective histopathological survey on canine and feline liver diseases at the University of Tokyo between 2006 and 2012. *The Journal of veterinary medical science*, *76*(7), 1015–1020.
60. Hittmair, K. M., Vielgrader, H. D., & Loupal, G. (2001). Ultrasonographic evaluation of gallbladder wall thickness in cats. Veterinary radiology & *ultrasound* : the official journal of the American College of Veterinary Radiology and the International Veterinary Radiology Association, 42(2), 149–155.
61. Hoeffel, C., Azizi, L., Lewin, M., Laurent, V., Aubé, C., Arrivé, L., & Tubiana, J. M. (2006). Normal and pathologic features of the postoperative biliary tract at 3D MR cholangiopancreatography and MR imaging. *Radiographics : a review publication of the Radiological Society of North America, Inc*, *26*(6), 1603–1620.
62. Horton, K.M., Johnson, P.T., Fishman, E.K. and Megibow, A.J. (2009). Applications of computed tomography to the gastrointestinal tract. In Yamada T. (Ed). *Textbook of gastroenterology.* 5th Ed pp 3140-3172, Wiley-Blackwell, UK.
63. Hunt TD, Wallack ST. Minimal atelectasis and poorly aerated lung on thoracic CT images of normal dogs acquired under sedation. Veterinary radiology and *ultrasound*. 2021; 62: 647–656.
64. Ibrahim, A., Rashwan, A., El Sharaby, A., Abumandour, M., & Nomir, A. (2024). Thoracic cavity of the Shirazi cats: New insights using computed tomography and magnetic resonance imaging. Anatomia, Histologia, Embryologia, 53, e13005.
65. Jaffey J. A. (2022). Feline cholangitis/cholangiohepatitis complex. *The Journal of small animal practice*, *63*(8), 573–589.
66. Jaffey J. A. (2022a). Canine hepatobiliary anatomy, physiology and congenital disorders. *The Journal of small animal practice*, *63*(2), 95–103.
67. Ji, S., Jung, S., Kim, B., Jung, J., Yoon, J., & Choi, M. (2015). Feasibility of percutaneous contrast *ultrasound*-guided cholecystography in dogs. Veterinary radiology & *ultrasound*, 56(3), 296–300.
68. Johnson EG, Wisner ER. Advances in respiratory imaging. Vet Clin North Am Small Anim Pract. 2007 Sep;37(5):879-900, vi.
69. Kim, D., Park, S., Kim, C., Yoon, S., & Choi, J. (2019). U*ltrasound*-guided transhepatic computed tomography cholecystography in beagle dogs. *Journal of veterinary science*, *20*(4), e37.
70. Klaengkaew, A., Sutthigran, S., Thammasiri, N. et al. The evaluation of non-anesthetic computed tomography for detection of pulmonary parenchyma in feline mammary gland carcinoma: a preliminary study. BMC Vet Res 17, 237 (2021).
71. Lamb, C. R., & Jones, I. D. (2016). Associations between respiratory signs and abnormalities reported in thoracic CT scans of cats. *The Journal of small animal practice*, *57*(10), 561–567.
72. Larson, M.M. (2020). Feline Pulmonary Disease. In *Feline Diagnostic Imaging,* (eds M. Holland and J. Hudson. Wiley and Sons, Inc. New Jersey, USA.
73. Larson and Berry, (2023). Ch 19. Feline thorax in *Atlas of small animal diagnostic imaging. Wiley and Sons, Inc. New Jersey, USA.*

74. Lee, N. K., Kim, S., Lee, J. W., Lee, S. H., Kang, D. H., Kim, G. H., & Seo, H. I. (2009). Biliary MR imaging with Gd-EOB-DTPA and its clinical applications. *Radiographics : a review publication of the Radiological Society of North America, Inc*, *29*(6), 1707–1724.
75. Lee, S. K., Park, S., Cheon, B., Moon, S., Hong, S., Cho, H., Chang, D., & Choi, J. (2017). Effect of position and time held in that position on ground-glass opacity in computed tomography images of dogs. *American journal of veterinary research*, *78*(3), 279–288. https://doi.org/10.2460/ajvr.78.3.279
76. Léveillé, R., Biller, D. S., & Shiroma, J. T. (1996). Sonographic evaluation of the common bile duct in cats. *Journal of veterinary internal medicine*, *10*(5), 296–299.
77. le Roux, C., Cassel, N., Fosgate, G. T., Zwingenberger, A. L., & Kirberger, R. M. (2016). Computed tomographic findings of pulmonary atelectasis in healthy anesthetized Beagles. *American Journal of Veterinary Research*, *77*(10), 1082-1092.
78. Lin, C., & Lo, P. (2018). Simple technique for aiding thoracic CT scanning of cats without general anaesthesia. *The Veterinary Record, 182*(7), 197.
79. Linta, N., Baron Toaldo, M., Bettini, G., Cordella, A., Quinci, M., Pey, P., Galli, V., Cipone, M., & Diana, A. (2017). The feasibility of contrast enhanced ultrasonography (CEUS) in the diagnosis of non-cardiac thoracic disorders of dogs and cats. *BMC veterinary research*, *13*(1), 141.
80. Linton, M., Buffa, E., Simon, A., Ashton, J., McGregor, R., & Foster, D. J. (2015). Extrahepatic biliary duct obstruction as a result of involuntary transcavitary implantation of hair in a cat. *JFMS open reports*, *1*(2), 2055116915610359.
81. Lorusso, V., Arbughi, T., Tirone, P., & de Haën, C. (1999).Pharmacokinetics and tissue distribution in animals of gadobenate ion, the magnetic resonance imaging contrast enhancing component of gadobenate dimeglumine 0.5 M solution for injection (MultiHance). *Journal of computer assisted tomography*, *23 Suppl 1*, S181–S194.
82. Louvet, A., & Duconseille, A. C. (2015). Feasibility for detecting liver metastases in dogs using gadobenate dimeglumine-enhanced magnetic resonance imaging. Veterinary radiology & *ultrasound* : the official journal of the American College of Veterinary Radiology and the International Veterinary Radiology Association, 56(3), 286–295.
83. Low D, Williams J. Surgical Management Of Feline Biliary Tract Disease: Decision-making and techniques. J Feline Med Surg. 2023 Nov;25(11):1098612X231206846.
84. Lusic, H., & Grinstaff, M. W. (2013). X-ray-computed tomography contrast agents. *Chemical reviews*, *113*(3), 1641–1666.
85. Lux, C. N., Sula, M. M., Sun, X., & Hecht, S. (2024). Gadoxetate disodium (Gd-EOB-DTPA) contrast-enhanced magnetic resonance imaging for differentiation between benign and malignant splenic lesions in dogs. *Veterinary radiology & ultrasound*, *65*(5), 556–566.

86. Mai, W., O'Brien, R., Scrivani, P., Porat-Mosenco, Y., Tobin, E., Seiler, G., McConnell, F., Schwarz, T. And Zwingenberger, A. (2008). The lung parenchyma. In Schwarz, T., & Johnson, V. (Eds.), *BSAVA Manual of Canine and Feline Thoracic Imaging* (pp 242-320). British Small Animal Veterinary Association. UK.
87. Maiti, S. K., Ajith, P., Dutta, A., Kumar, N., & Sharma, A. K. (2011). Laparoscopic-assisted cholecystocentesis and cholecystocholangiography in canines. Journal of Applied Animal Research, 39(1), 29–32.
88. Mantis, P., Johnson, V. And Morandi, F. (2008). The bronchial tree. In Schwarz, T., & Johnson, V. (Eds.), *BSAVA Manual of Canine and Feline Thoracic Imaging* (pp 228 - 241). British Small Animal Veterinary Association. UK.
89. Marks, A. L., Hecht, S., Stokes, J. E., Conklin, G. A., & Deanna, K. H. (2014). Effects of gadoxetate disodium (Eovist(®)) contrast on magnetic resonance imaging characteristics of the liver in clinically healthy dogs. *Veterinary radiology & ultrasound*, *55*(3), 286–291.
90. Marolf, A. J., Leach, L., Gibbons, D. S., Bachand, A., & Twedt, D. (2012). Ultrasonographic findings of feline cholangitis. *Journal of the American Animal Hospital Association*, *48*(1), 36–42.
91. Marolf, A. J., Kraft, S. L., Dunphy, T. R., & Twedt, D. C. (2013). Magnetic resonance (MR) imaging and MR cholangiopancreatography findings in cats with cholangitis and pancreatitis. *Journal of feline medicine and surgery*, *15*(4), 285–294.
92. Marolf A. J. (2017). Diagnostic Imaging of the Hepatobiliary System: An Update. *The Veterinary clinics of North America. Small animal practice*, *47*(3), 555–568.
93. Masseau, I., & Reinero, C. R. (2019). Thoracic computed tomographic interpretation for clinicians to aid in the diagnosis of dogs and cats with respiratory disease. *Veterinary journal (London, England : 1997)*, *253*, 105388.
94. Mayhew, P. D., Holt, D. E., McLear, R. C., & Washabau, R. J. (2002). Pathogenesis and outcome of extrahepatic biliary obstruction in cats. *The Journal of small animal practice*, *43*(6), 247–253.
95. In McDonough, S.P. and Southard, T. (Eds) (2017). The Respiratory System. In *Necropsy Guide for Dogs, Cats, and Small Mammals*. Wiley-Blackwell.
96. Meomartino, L., Greco, A., Di Giancamillo, M., Brunetti, A., & Gnudi, G. (2021). Imaging techniques in Veterinary Medicine. Part I: Radiography and Ultrasonography. *European journal of radiology open*, *8*, 100382.
97. Miller, J. (2014). Cholangiography using 64-multi-detector row computed tomography in the normal dog. [Masters Thesis, Mississippi State University]. United States.
98. Morandi, F. (2008) Basics of thoracic nuclear medicine. In Schwarz, T., & Johnson, V. (Eds.), *BSAVA Manual of Canine and Feline Thoracic Imaging* (pp 75-81). British Small Animal Veterinary Association. UK.
99. Morcos S. K. (2003). Review article: Effects of radiographic contrast media on the lung. *The British journal of radiology*, *76*(905), 290–295.
100. Morandi, F., Mattoon, J. S., Lakritz, J., Turk, J. R., & Wisner, E. R. (2003). Correlation of helical and incremental high-resolution thin-section computed

tomographic imaging with histomorphometric quantitative evaluation of lungs in dogs. *American Journal of Veterinary Research*, *64*(7), 935-944.

101. Neer T. M. (1992). A review of disorders of the gallbladder and extrahepatic biliary tract in the dog and cat. *Journal of veterinary internal medicine*, *6*(3), 186–192.
102. Newell, S.M., Graham, J.P., Roberts, G.D., Ginn, P.E., Chewning, C.L., Harrison, J.M. and Andrzejewski, C. (2000), Quantitative magnetic resonance imaging of the normal feline cranial abdomen. *Veterinary Radiology & ultrasound*, 41: 27-34.
103. Newell, S. M., Selcer, B. A., Roberts, R. E., Cornelius, L. M., & Mahaffey, E. A. (1996). Hepatobiliary scintigraphy in the evaluation of feline liver disease. *Journal of veterinary internal medicine*, *10*(5), 308–315.
104. Noguchi, A., Iwanaga, T., Miura, N., Sogawa, T., & Fujiki, M. (2023). Common bile duct perforation due to choledocholithiasis in a cat with gallbladder agenesis. *JFMS open reports*, *9*(1), 20551169221146513.
105. Nyland, T. G., Koblik, P. D., & Tellyer, S. E. (1999). Ultrasonographic evaluation of biliary cystadenomas in cats. Veterinary radiology & *ultrasound*, 40(3), 300–306.
106. O'Brien, R.T. (2016) Radiographic and Computed Tomography Imaging of the Feline Thorax, In Little (Ed). *Augusts consultations in feline internal medicine* (pp 425 - 432). Vol 7. Elsevier, USA.
107. Oliveira, C. R., Mitchell, M. A., & O'Brien, R. T. (2011a). Thoracic computed tomography in feline patients without use of chemical restraint. Veterinary radiology & *ultrasound*, 52(4), 368–376.
108. Oliveira, C. R., Ranallo, F. N., Pijanowski, G. J., Mitchell, M. A., O'Brien, M. A., McMichael, M., Hartman, S. K., Matheson, J. S., & O'Brien, R. T. (2011b). The VetMousetrap: a device for computed tomographic imaging of the thorax of awake cats. *Veterinary radiology & ultrasound*, *52*(1), 41–52.
109. Otte, C. M., Penning, L. C., & Rothuizen, J. (2017). Feline biliary tree and gallbladder disease: Aetiology, diagnosis and treatment. *Journal of feline medicine and surgery*, *19*(5), 514–528.
110. Pasanen, P., Partanen, K., Pikkarainen, P., Alhava, E., Pirinen, A., & Janatuinen, E. (1992). Ultrasonography, CT, and ERCP in the diagnosis of choledochal stones. *Acta radiologica (Stockholm, Sweden : 1987)*, *33*(1), 53–56.
111. Persson, A., Dahlström, N., Smedby, O., & Brismar, T. B. (2006). Three-dimensional drip infusion CT cholangiography in patients with suspected obstructive biliary disease: a retrospective analysis of feasibility and adverse reaction to contrast material. *BMC medical imaging*, *6*, 1.
112. Pollard, R. And Puchalski, S. (2011). CT Contrast and Applications. In Schwarz and Saunders (Eds). *Veterinary Computed Tomography*. (pp 57-65.) Wiley and Sons, UK.
113. Prather, A. B., Berry, C. R., & Thrall, D. E. (2005). Use of radiography in combination with computed tomography for the assessment of noncardiac thoracic disease in the dog and cat. *Veterinary radiology & ultrasound*, *46*(2), 114–121.
114. Rahmani, V., Peltonen, J., Amarilla, S. P., Spillmann, T., & Ruohoniemi, M. (2023). Cholangiopancreatography in cats: a post-mortem comparison of MRI with

fluoroscopy, corrosion casting and histopathology. *Veterinary radiology & ultrasound*, *64*(4), 713–723.

115. Rahmani, V., Peltonen, J., Amarilla, S. P., Hmelnikov, D., Ruohoniemi, M., & Spillmann, T. (2023b). Feasibility of Magnetic Resonance Cholangiopancreatography in Dogs-A Post-Mortem Study. *Animals : an open access journal from MDPI*, *13*(15), 2517.
116. Rahmani, V., Peltonen, J., Hmelnikov, D., Uosyte, R., Männikkö, S., Spillmann, T., & Ruohoniemi, M. (2024). Three-dimensional magnetic resonance cholangiography is superior to two-dimensional single-shot magnetic resonance cholangiography for visualization and image quality of the feline and canine biliary tract: A postmortem study. *Veterinary radiology & ultrasound*, *65*(4), 377–384. https://doi.org/10.1111/vru.13372.
117. Reimegård, E., Lee, H.T.N. & Westgren, F. Prevalence of lung atelectasis in sedated dogs examined with computed tomography. Acta Vet Scand 64, 25 (2022).
118. Regional Health Limited (2005, February). Multihance(TM) (dimeglumine gadobenate). New Zealand datasheet https://www.medsafe.govt.nz/profs/datasheet/m/MultiHanceinj.pdf
119. Rojo Ríos, D., Ramírez Zarzosa, G., Soler Laguía, M., Kilroy, D., Martínez Gomariz, F., Sánchez Collado, C., Gil Cano, F., García García, M. I., Jáber, J. R., & Arencibia Espinosa, A. (2023). Creation of Three-Dimensional Anatomical Vascular and Biliary Models for the Study of the Feline Liver (*Felis silvestris catus* L.): A Comparative CT, Volume Rendering (Vr), Cast and 3D Printing Study. *Animals : an open access journal from MDPI*, *13*(10), 1573.
120. Rozanski, E. A., Bedenice, D., Lofgren, J., Abrams, J., Bach, J., & Hoffman, A. M. (2010). The effect of body position, sedation, and thoracic bandaging on functional residual capacity in healthy deep-chested dogs. Canadian journal of veterinary research = Revue canadienne de recherche veterinaire, 74(1), 34–39.
121. Rivero, M.A., Arencibia, A., Latorre, R., Gil, F., Vilar, J.M. and Vázquez, J.M. (2005), Magnetic Resonance Imaging and Cross Section Images of the Cat Thorax. Anatomia, Histologia, Embryologia, 34: 43-44.
122. Rodan, I. and Sparkes, A. (2011).Preventative health care for cats. In Little, S (Ed), *The cat, clinical medicine and management* (pp151-180). Elsevier Health Sciences. Missouri, USA.
123. Rosenberg, F. J., Ackerman, J. H., & Nickel, A. R. (1980). Iosulamide: a new intravenous cholangiocholecystographic medium. *Investigative radiology*, *15*(6 Suppl), S142–S147.
124. Rudorf, H. Taeymans, O. & Johnson, V. (2008). Basics of thoracic radiography and radiology. In Schwarz, T., & Johnson, V. (Eds.), *BSAVA Manual of Canine and Feline Thoracic Imaging* (242-320). British Small Animal Veterinary Association. UK.
125. Samii, V. F., Biller, D. S., & Koblik, P. D. (1998). Normal cross-sectional anatomy of the feline thorax and abdomen: comparison of computed tomography and cadaver anatomy. *Veterinary radiology & ultrasound*, *39*(6), 504–511.

126. Schmitz, S. A., Wagner, S., Schuhmann-Giampieri, G., Krause, W., & Wolf, K. J. (1997a). A prototype liver-specific contrast medium for CT: preclinical evaluation of gadoxetic acid disodium, or Gd-EOB-DTPA. *Radiology*, *202*(2), 407–412.
127. Schmitz, S. A., Häberle, J. H., Balzer, T., Shamsi, K., Boese-Landgraf, J., & Wolf, K. J. (1997b). Detection of focal liver lesions: CT of the hepatobiliary system with gadoxetic acid disodium, or Gd-EOB-DTPA. *Radiology*, *202*(2), 399–405.
128. Schwarz, T. (2008). Basics of thoracic computed tomography. In Schwarz, T., & Johnson, V. (Eds.), *BSAVA Manual of Canine and Feline Thoracic Imaging* (pp 66-70). British Small Animal Veterinary Association. UK.
129. Seale, M. K., Catalano, O. A., Saini, S., Hahn, P. F., & Sahani, D. V. (2009). Hepatobiliary-specific MR contrast agents: role in imaging the liver and biliary tree. *Radiographics : a review publication of the Radiological Society of North America, Inc*, *29*(6), 1725–1748.
130. Shanaman, M. M., Hartman, S. K., & O'Brien, R. T. (2012). Feasibility for using dual-phase contrast-enhanced multi-detector helical computed tomography to evaluate awake and sedated dogs with acute abdominal signs. *Veterinary radiology & ultrasonography*, *53*(6), 605–612.
131. Simon, B. A., Christensen, G. E., Low, D. A., & Reinhardt, J. M. (2005). Computed tomography studies of lung mechanics. *Proceedings of the American Thoracic Society*, *2*(6), 517–507.
132. Soto, J. A., Alvarez, O., Múnera, F., Velez, S. M., Valencia, J., & Ramírez, N. (2000). Diagnosing bile duct stones: comparison of unenhanced helical CT, oral contrast-enhanced CT cholangiography, and MR cholangiography. *AJR. American journal of roentgenology*, *175*(4), 1127–1134.
133. Spain, H. N., Penninck, D. G., Webster, C. R., Daure, E., & Jennings, S. H. (2017). Ultrasonographic and clinicopathologic features of segmental dilatations of the common bile duct in four cats. *JFMS open reports*, *3*(1), 2055116917716881.
134. Spillmann, T., Happonen, I., Kähkönen, T., Fyhr, T., & Westermarck, E. (2005). Endoscopic retrograde cholangio-pancreatography in healthy Beagles. Veterinary radiology & ultrasonography, 46(2), 97–104.
135. Spillmann, T., Willard, M. D., Ruhnke, I., Suchodolski, J. S., & Steiner, J. M. (2014). Feasibility of endoscopic retrograde cholangiopancreatography in healthy cats. *Veterinary radiology & ultrasonography*, *55*(1), 85–91.
136. Staffieri, F., De Monte, V., De Marzo, C., Grasso, S., & Crovace, A. (2010). Effects of two fractions of inspired oxygen on lung aeration and gas exchange in cats under inhalant anaesthesia. *Veterinary anaesthesia and analgesia*, *37*(6), 483–490.
137. Staffieri, F., Franchini, D., Carella, G. L., Montanaro, M. G., Valentini, V., Driessen, B., Grasso, S., & Crovace, A. (2007). Computed tomographic analysis of the effects of two inspired oxygen concentrations on pulmonary aeration in anesthetized and mechanically ventilated dogs. *American journal of veterinary research*, *68*(9), 925–931.

138. Taenzer, V., & Volkhardt, V. (1979). Double blind comparison of meglumine iotroxate (Biliscopin), meglumine iodoxamate (Endobil), and meglumine ioglycamate (Biligram). *AJR. American journal of roentgenology*, *132*(1), 55–58.
139. Tanaka, T., Akiyoshi, H., Mie, K., Shimazaki, H., & Ohashi, F. (2018). Drip infusion cholangiography with CT in cats. *Journal of feline medicine and surgery*, *20*(12), 1173–1176.
140. Toft, K. G., Hustvedt, S. O., Grant, D., Friisk, G. A., & Skotland, T. (1997). Metabolism of mangafodipir trisodium (MnDPDP), a new contrast medium for magnetic resonance imaging, in beagle dogs. *European journal of drug metabolism and pharmacokinetics*, *22*(1), 65–72.
141. Uno, T., Hamati, K., Okamoto, K., Onaka, C., Fujita, K., Yamamura, H. (2009). . Iotroxate meglumine dose vs. CT values over time and visualization in the biliary duct system in CT imaging using cholangiography in dogs. *Journal of the Japan Veterinary Medical Association*;62(11): 875-881.
142. Van Beers, B. E., Pastor, C. M., & Hussain, H. K. (2012). Primovist, Eovist: what to expect?. *Journal of hepatology*, *57*(2), 421–429.
143. Van den Ingh, T.S.G.A.M., Cullen, J. M., Twedt, D.C., Van Winkle, T., Desmet, V.J., Rothuizen, J. (2006) Morphological classification of biliary disorders of the canine and feline liver. In Rothuizen, J., Bunch, S.E., Charles, J.A., Cullen, J.M., Desmet, V.J., Szatmári, V., Twedt, D.C., Van den Ingh, T.S.G.A.M., Van Winkle, T., Washabau, R.J. (Eds). *WSAVA Standards for Clinical and Histological Diagnosis of Canine and Feline Liver Diseases* (pp61-76), W.B. Saunders. USA.
144. Wandtke, J. C., Hyde, R. W., Fahey, P. J., Utell, M. J., Plewes, D. B., Goske, M. J., & Fischer, H. W. (1986). Measurement of lung gas volume and regional density by computed tomography in dogs. *Investigative radiology*, *21*(2), 108–117.
145. Woods, K. S., Brisson, B. A., Defarges, A. M., & Oblak, M. L. (2012). Congenital duplex gallbladder and biliary mucocele associated with partial hepatic cholestasis and cholelithiasis in a cat. *The Canadian veterinary journal = La revue veterinaire canadienne*, *53*(3), 269–273.
146. Yasaka, K., Saigusa, H., & Abe, O. (2024). Effects of Intravenous Infusion of Iodine Contrast Media on the Tracheal Diameter and Lung Volume Measured with Deep Learning-Based Algorithm. *Journal of imaging informatics in medicine*, *37*(4), 1609–1617.
147. Yeh, B. M., Liu, P. S., Soto, J. A., Corvera, C. A., & Hussain, H. K. (2009). MR imaging and CT of the biliary tract. *Radiographics : a review publication of the Radiological Society of North America, Inc*, *29*(6), 1669–1688.
148. Yonetomi, D., Kadosawa, T., Miyoshi, K., Nakao, Y., Homma, E., Hanazono, K., Yamada, E., Nakamura, K., Ijiri, A., Minegishi, N., Maetani, S., Hirayama, K., Taniyama, H., & Nakade, T. (2012). Contrast agent Gd-EOB-DTPA (EOB·Primovist®) for low-field magnetic resonance imaging of canine focal liver lesions. *Veterinary radiology & ultrasound*, *53*(4), 371–380.
149. Zoran, D.L. (2012) Diseases of the Liver in The Cat Clinical Medicine and Management Ed. Susan E Little Saunders Missouri pp 522